A Neural Network Model of Frog Retina: A Discrete Time-Space Approach

Yillbyung Lee

Department of Computer and Information Science
University of Massachusetts
Amherst, Masschusetts 01003

COINS Technical Report 86-39

A Neural Network Model of Frog Retina: A Discrete Time-Space Approach

A Dissertation Presented

By

Yillbyung Lee

Submitted to the Graduate School of the
University of Massachusetts in partial fulfillment
of the requirements for the degree of

Doctor of Philosophy

September 1986

Department of Computer and Information Science

Yillbyung Lee
© 1986
All Rights Reserved

This research was supported in part by:
The National Institutes of Health
Grant Numbers NS14971-04/05/07 (M. A. Arbib, Principal Investigator)

A NEURAL NETWORK MODEL OF FROG RETINA:
A DISCRETE TIME-SPACE APPROACH

A Dissertation Presented

By

YILLBYUNG LEE

Approved as to style and content by:

Michael A. Arbib, Chairperson of Committee

Andrew G. Barto, Member

Stephen A. George, Outside Member

Conrad A. Wogrin, Department Chair
Computer and Information Science

DEDICATED TO

MY PARENTS: KI-EUL LEE AND KEUM-BONG-A KANG

ACKNOWLEDGEMENTS

There are many people to whom heartfelt thanks are due in relation to the completion of my doctoral work of which this dissertation is the final product. I would like to take this opportunity to express my sincere appreciation to at least some of them.

I thank my parents, first of all, for the unbounded love and support they have always given me, even at times when I was undeserving. I just hope I could provided to my child what they have provided me.

Second, I would like to thank my wife and our daughter for their patience and understanding.

Third, I would like to thank my sisters and Dr. K. W. Min for the moral support and care they have given me during the many years.

Fourth, I would like to thank the members of my dissertation committee for their help and guidance. Prof. M. Arbib for suggesting the problem and guiding me through the whole thesis research as well as providing me with moral and financial supports. He has been and will be an inspirational model of a teacher and scholar to me. I also would like to thank for the considerate and appropriate advices he has given me when I needed them. I am most grateful that I had the

chance to know him and work with him.

Prof. A. Barto for the excellent lectures on adaptation and learning and the influence he had on me through the connectionist idea, both directly, and indirectly through his group of research people.

Prof. S. George for providing a right experimental perspective to compare the model with, thus providing an invaluable feedback to my research from an experimental neuroscientist, and for the help and support he has given me especially during the last days of my writing this thesis.

Fifth, I thank Prof. D. Waltz for introducing me to the exciting world of A.I. and *The Metaphorical Brain*; Profs. K. Fite, N. Spinelli, and G. Wyse for their illuminating lectures, discussion and guidance in neuroscience and visual brain studies.

Sixth, I thank Jeff Teeters for providing an excellent graphics driver and a data compaction algorithm, and for the help in preparing the diagrams; Drs. D. House, F. Cervantes and C. Anderson for their friendship and help during our stay in Amherst; Jae W. Choe for the rigorous editorial help and friendship, Hong G. Kim and Tack D. Han for their help in preparing this thesis; and Youngsik Kim for sharing the joy of high fidelity.

Finally, I would like to thank the people in Amherst and the Korean community at Umass for making my stay a pleasant one, and the faculty, staff and students in the COINS department for providing an enjoyable learning/working environment.

ABSTRACT

A NEURAL NETWORK MODEL OF FROG RETINA:
A DISCRETE TIME-SPACE APPROACH

September 1986

Yillbyung Lee

B.S., Yonsei University

M.S., University of Illinois

Ph.D., University of Massachusetts

Directed by: Professor Michael A. Arbib

Most computational models of the nervous systems in the past have been developed at the level of a single cell or at the level of a population of uniform elements. But neither the absolute temporal activity of a single neuron nor some steady state of a population of neurons seems to be of utmost importance. A spatio-temporal pattern of activities of neurons and the way they interact through various connections appear to matter most in the neuronal computations of the vertebrate retina.

A population of neurons are modelled based on a connectionist scheme and on experimental data to provide a spatio-temporal pattern of activities for every cell involved in the cone-pathways for a patch of frog's retina. The model has discrete

representations for both space and time. The density of each type/subtype of neuron and the existence and the size of the connections are based on anatomical data. Individual neurons are modelled as variations of a leaky-capacitor model of neurons. Parameters for each type of model neuron are set so that their temporal activities approximate the typical intracellular recording for the corresponding neurons given the known visual/electrical stimulus patterns. Connectivity was thought the single most important factor for network computation. Computer simulation results of the model are compared with well-known physiological data.

The results show that a network model of coarse individual neuronal models based on known structures of the vertebrate retina approximates the overall system behaviour successfully reproducing the observed functions of many of the cell types, thus showing that the connectionist approach can be applied successfully to neural network modelling and provide an organizing theory of how individual neurons interact in a population of neurons.

TABLE OF CONTENTS

List of Tables

List of Figures

CHAPTER I

INTRODUCTION

Brain, (Frog) Retina, and Modelling

The study of the brain or of the nervous system has progressed substantially during the last few decades and is now moving towards explaining the micro-mechanisms of how our minds work.

Within the nervous system, sensory subsystems have been extensively studied because we can control the environment which acts as the stimulus to the sensory nerve cells. Likewise, the motor subsystems have been studied extensively because we can observe what the nerve cells command related motor parts to do. Among the sensory subsystems, the visual system has received most attention because it is, in many cases, including our own, the single most important sense used for its owner's survival. And for studying any visual system we cannot exclude the study of how the retina works because that is where the early visual processing occurs on which later visual processing depends. This is why the study of retina is so important. Yet, most important to us is that the vertebrate retina is well suited for studies of local interactions which appear to play a central role in the workings of central nervous systems:

> *...the vertebrate retina is an ideal system in which to seek insights into the local circuit mechanisms underlying information processing [in the vertebrate brain]. The retina is rich in local circuits and is amenable to detailed extracellular and intracellular recordings. The analysis of how its synaptic interactions mediated by local circuits has progressed well beyond similar efforts in other parts of the vertebrate brain [Dowling, 1979: 163].*

Besides, all vertebrate retinas share the same basic layered architecture as well as similar functional organizations, thus much information about the retina of one species can be inferred from that of others which can help to form a relatively coherent framework.

The visual system of amphibians, including the frog retina, has been an object of intense study, resulting in a large amount of anatomical and physiological data. The retina of the mudpuppy, *Necturus maculosus* , and that of the (tiger) salamander have often been used because of their large cell size [Werblin and Dowling, 1969; Dowling and Werblin, 1969] which allows for easier cellular recording and subsequent staining. Those of the toad and the frog have been a subject of extensive study in anatomy [Dowling, 1968, 1976; Shantz, 1976; Carey, 1975; Cajal, 1893] and in physiology [Dowling, 1968, 1976; Schürg-Pfeiffer and Ewert, 1982; Grüsser and Grüsser-Cornehls, 1976; Grüsser-Cornehls and Saunders, 1981a, 1981b; Maturana et al., 1960; Lettvin et al., 1959, 1961; Keating and Gaze, 1970; Morrison, 1975] partly because these animals display interesting yet easily identified behaviors towards certain types of stimuli and partly because of their wide availability as experimental animals.

There is a rich set of both anatomical and physiological data for the visual system and in particular for the retinas of these animals. However, our partial understanding of neural mechanisms for a particular nervous system makes it difficult to integrate essential data into a consistent framework. Modelling a neural system can aid us in developing such a framework, which can increase insights into the substantive phenomena under investigation. Especially, mathematical or computational models as compared to qualititative ones require more consideration for causal connections in model making. Such models can be checked for their validity and can be used to make predictions about the outcome of experiments either through interpretation of the analytical conclusions drawn from a given model or through a set of simulations. Furthermore, a computationally efficient version of the model may be used as a front-end for an overall model of the

frog/toad visual system [Arbib, 1982; Lara et al., 1983; House, 1984; Cervantes, 1985].

Neural Network Modelling Approach

According to Grüsser and Grüsser-Cornehls [1976], there are following classes of models in neurobiology: global functional models, qualitative parametric models, descriptive mathematical models, system-theoretic models, quantitative neuronal network models, and interpretive models and development of new global models.

Most of the vertebrate retina modelling in the past dealt with the temporal activity of a single cell or single unit modelling, in the sense of accounting for the phenomena that affect the concerned cell [Rodieck, 1965; Baylor et al., 1974a; Moreno-Diaz, 1965; Richter and Ullman, 1982; an der Heiden and Roth, 1983]. There are many neural models at the level of individual cells or of perceptive units and also at the overall neural network level where their main concern is the property of the whole network such as stability. But there is a big gap between these two levels of what I call "micro-" and "macro-" neural models, of relating how these micro-neural models can account for the global activity of the macro-neural models.

It should be emphasized that it is not the absolute temporal activity of a single neuron but the spatio-temporal activity of a population of neurons that is important in the neuronal computations of the vertebrate visual system. Moreover, it is imperative that the theoretical approaches in neuroscience should provide a theory as to how and/or whether these spatio-temporal patterns of activity really stem from those micro-level neural models, i.e., the theory of how neural connections bring about the competition and cooperation within a population of neurons. So, the current modelling approach situates itself between the connectionist approach [McCulloch and Pitts, 1943] where the nervous-system-like

network structure was emphasized but the detailed neuron-like function was ignored, and the traditional neuromodelling approach where functions of individual neurons [Richter and Ullman, 1982] and sometimes their internal structures are emphasized but the overall organization of interactions with other neurons were mostly ignored. The current model starts out, as in the connectionist paradigm, from the idea of a network of rather simple individual units and the relative importance of connections between them as a fundamental factor of information processing in the neural network. The approach is appropriate at least in the modelling of the retina because, as mentioned, that is where local interaction appears to dominate the interesting aspects of the visual information processing performed by the underlying structure. And then we try to change the types of connections and adjust the connectivities between individual elements following the guidelines suggested/restricted by the anatomy for the detailed functional modelling of individual elements.

Although neural network modelling and simulation does not necessarily preclude a hardware one, in the sense of using digital/analog computers and electronic modules, the mathematico-software computer simulation method is used because hardware models are in general not flexible enough for such changes as in the weight of the connectivity or the types of connectivity. The whole knowledge surrounding the vertebrate retina is far from complete, and the study of such changes becomes very significant. On the other hand, a software solution has the advantage of being easily modifiable as empirical knowledge becomes obsolete or more extensive, and has the added advantage of being readily adaptable to represent other neural systems with similar overall structure.

Current study models of a network of neurons rather than a single output neuron. In order to compute the patterns of activities for all cells involved in visual

processing, the model adopts discrete representations for both time [1] and space, falling into the category of *discrete model with continuous states* following an der Heiden's [1980] classification. Individual neurons are represented by variations of the leaky-capacitor model [Holden, 1976]. Different types of connections between cells are modelled based on their synaptic specializations [Dowling, 1968, 1976, 1979; Miller, 1979; Shepherd, 1979; Werblin and Dowling, 1969]. The overall synaptic connectivities are based on the shape and diameter of their dendritic trees and supplemented with reasonable assumptions about their nature with a concern for the logical completeness of functions exhibitied by the retina. Unlike the real retina, the model assumes spatial homogeneity within each cell layer [Carey, 1975; Rodieck, 1973].

The model described in this dissertation also falls into the class of *quantitative neuronal network model* where the structural conditions of the network, especially the types and the degrees of the connections are considered to be of fundamental importance. In essence, the current approach fills the gap between those who are interested in the level of behavior or perceptual primitives in the connectionist framework and those who are interested in low-level detailed responses for individual neurons or a small number of neurons. The current neural network modelling is trying to provide an organizing theory of how to make connections between simple neuronal models by relating perceptual primitives to individual neurons.

Simulations of Single Cone Pathways

Like other vertebrate retinas, the frog retina has five major types of neurons: photoreceptors, horizontal cells, bipolar cells, amacrine cells and ganglion cells

[1] This is not a discrete-time simulation in the conventional sense, it is rather a continuous-time simulation approach, where time is a multiple of a discrete time and every cell state is updated simultaneously after each discrete time passage [an der Heiden, 1980].

[Cajal, 1893; Dowling, 1968, 1976, 1979]. In addition, there are the Müller cells, which are glial elements, and another type of neuron called interplexiform cells, which will not be included in the present model. There are four types of photoreceptors in the frog retina: single cone, double cone, red rod, and green rod. Only single cone pathways are modelled here in order to restrict the scope of the dissertation while keeping the generality of the modelling, allowing a later addition of the rod and double cone pathways. The single cone pathways are chosen since most of the interesting responses of the ganglion cells and of frog behaviour are observed under photopic or mesophotopic conditions when most of the initial visual signals are processed by the cones, and since the single cone has one color pigment while the less populous double cone has two color pigments which makes matters more complicated.

Simulation was chosen over mathematical analysis for investigating the model mainly because of the strong motivation to better model the individual responses rather than concentrate on overall network behavior. The hierarchical structure of retinal organization lends itself to partial simulations of the individual layers involved. Moreover, the mathematical complexity of the analysis appears to be immense.

Although the simulation will be presented according to the different major cell types with the related layers, there are two main aspects in the present set of computer simulations. The first concerns the duplication of the temporal characteristics of the individual neurons under typical experimental settings such as how amacrine cells respond to the change in the illumination upon their receptive fields [Werblin and Dowling, 1969; Matsumoto and Naka, 1972]. The second concerns duplicating the well-known quantitative data on frog retinal cells such as area functions for the horizontal cells or velocity functions for the ganglion cells.

By modelling neural networks emphasizing their overall structure of connections and simulating a spatio-temporal pattern of individual cell activities, we hope to show that the resulting functional outputs of the retinal cells which can

be directly or indirectly related to perceptual primitives can be obtained from simple functional assumptions about individual neurons and from anatomical constraints derived from the anatomy, thus advancing the notion of the fundamental relationship of function and struture within a nervous system which acts as a (visual) information processor. Furthermore, the model may predict how neighboring cells respond under known situations and how certain cells react under as yet untried circumstances. Also, and just as important, the validation of functional responses under a given set of structural assumptions such as the distribution of weights and the type of connections may enable us to predict the existence of unidentified structures which are vaguely assumed in experimental situations but which in most cases cannot yet be rigorously verified.

Organisation of the Dissertation

The dissertation is divided into the following chapters and an appendix. In this chapter, we have discussed the rationale for our choice of the frog retina as the subject nervous system as well as for our approach to modelling.

In chapter 2, a literature review is done on the following two areas. First, anatomical and physiological findings concerning vertebrate retinas, especially of amphibians including the frog, will be discussed. This part will familiarize the reader with the experimental data as well as the conceptual models relevant to the style of information processing in the vertebrate/frog retina. The relationship between the function of the retina and the underlying structures will be emphasized. Important aspects of vertebrate retina which will not be modelled in this thesis, such as adaptation, color processing, and Müller cells, will also be noted. Second, existing diverse models of vertebrate retina will be critically reviewed with respect to their strength and weakness.

In chapter 3, an overview of the modelling and the simulation is described as well as the description of the mathematical notations to represent our model.

The first section of the chapter deals with the modelling and some of the choices we made in the model, the second with the notations that will be used to describe the model with an example, and the third with the simulation details.

In chapter 4, stimulus pattern generation and retinal image formation are described. It shows how various stimulus patterns are represented in the model and the inherent limit of the employed representation. Then it shows the model of the frog eye optics and the simulated retinal images in comparison to the stimulus patterns.

In chapter 5, the modelling and the corresponding simulations of the single cone, horizontal cell and bipolar cell models are presented. It describes how certain parameters for the individual models are chosen and compares the simulated results with the experimental data by the cell layers.

In chapter 6, the modelling of the amacrine cell and ganglion cell models are presented. It describes how certain parameters for the individual models are chosen and compares the resulting simulations with the experimental data for the amacrine cell layer. It also briefly describes the current stage of modelling for the ganglion cell layer and the preliminary results available.

Chapter 7, the conclusion, discusses the extent to which the function of a nervous system can be derived from its connective structures. Suggestions are also made for future research.

Appendix describes the software system used to represent the retina model and to run the computer simulations. It provides an overview of the software to assist those who want to use/modify this system for their own simulations.

CHAPTER II

LITERATURE REVIEW

Introduction

This chapter discusses the anatomical/physiological background materials upon which the current retinal model is based and reviews other existing retinal models. This is not intended to be a comprehensive literature review on the frog retina. Rather it shows a minimum knowledge that is required to understand and build a model of frog retina.

The nature and characteristics of the frog and other vertebrate retina are discussed first, as they form the foundation upon which retinal models, including the present one are based. This background material is discussed in the following order. First, the optics of the frog eye will be discussed since the optics provides the retinal image of the world surrounding the animal to its retina. Of course, in order to simulate experiments that are done with the retina only (without the lens and the vitreous humor parts of the eye, as was done by Werblin and Dowling [1969]), a discussion of optics would be unnecessary. However, most of the experiments are concerned with observing the electrical potentials of optic fibers during the presentation of different types of stimuli, and are performed with the intact eye as a whole [Grüsser and Grüsser-Cornehls, 1976; Maturana et al., 1960; Schürg-Pfeiffer and Ewert, 1981]. Therefore, eye optics becomes a necessary part of efforts to model and simulate experimental findings. Second, the frog retina will be discussed along with those of other amphibians and vertebrates, based upon findings of existing anatomical and physiological research.

The last section in this chapter will be a review of existing models on the frog or other vertebrate retina. They will be briefly reviewed in terms of the underlying approaches and their strength as well as weakness.

Background Material

Frog Eye Optics and its Retinal Image

Although there are many different processes that go on in the vertebrate eye, we are mainly concerned here with the way optics blurs the projection of images to the retina. While the notion of blurring (or worsening of resolution) intuitively suggests counterproductiveness in the overall visual information process, it is important to remember that the real world image consists of much (spatially random) noise that the smoothing process – another expression for blurring – can reduce and thereby prepare the visual image that is projected on to the photoreceptor cells of the retina for further processing [Duda and Hart, 1973].

Size Relationship between an Object and the Image. The strongest refractive surface in the (vertebrate) eye is the anterior surface of the cornea. Essentially all of the remaining refraction occurs at the surfaces and within the internal stria of the crystalline lens. The interacting effects of these various refractive elements are complex, but for a normal eye and a distant object, a good first order approximation to the optical behaviour can be made by substituting for all those refractive elements a single thin lens, for example in the case of *Rana esculenta* [du Pont and de Groot, 1976a], with a focal length of 5.46 mm and located 5.46 mm in front of the retina, or about 2.73 mm behind the anterior surface of the cornea. Figure 1 from du Pont and de Groot [1976a] shows the idealized schematic eye of the frog. The center of the equivalent lens in the diagram is called the nodal point of the simplified eye.

To find the location of any given object point of a scene in the retinal image,

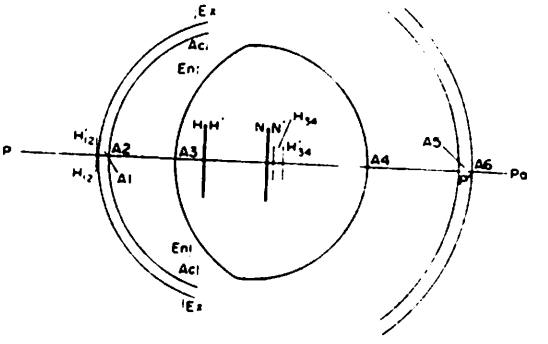

Figure 1: Schematic eye of the paralysed frog. A_1: anterior surface of the cornea; A_5: retina; A_6 sclera; N: anterior nodal plane of the eye. From du Pont and de Groot [1976a].

one draws a straight line from the point through the nodal point of the eye: the intersection of that line so drawn with the retina is the location of the region in the retinal image that corresponds to the object point. Because the distance from the nodal point of the eye to the retina is about 5.46 mm, the size of the image of any object in the plane perpendicular to the line of sight, or as projected onto that plane, is given by the following relationship: $S_i/S_o = 5.46/D_o$ where S_o is the size of the object, or its projection on the perpendicular plane, S_i that of the image, and D_o is the distance from the nodal point of the eye to the object, in mm. Therefore, with a fixed distance to the object D_o and a measureable size of the object S_o, we can readily calculate the size of the retinal image S_i.

In many experiments in which frogs are used for studies of the visual system, the animal is placed so that the eye is at the centre of a hemisphere of radius 25 or 30 cm [Gaze, 1958; Maturana et al., 1960; Pickering, 1968]. It is believed that photic stimuli at that distance from its eye will give a sharp image on the retina of the animal.

Point Spread Function and Modulation Transfer Function. There are several optical effects – such as focus error, aberration (spherical, chromatic, astigmatism, etc.), diffraction and scattering – within the retina, that blur the

retinal image.

As a result of all of these factors, the retinal image of each point of an object is distributed over a region, rather than focused at one point, of the retinal surface. *Retinal image* refers to the image that is formed at the outer segment layer of photoreceptors, rather than the one at the vitreal surface of the retina. The two dimensional function that describes the image distribution for a single object point is called the *point spread function.* If the point spread function is known for a given eye, the actual light distribution in the retinal image of any scene can be obtained by convolving the light distribution in the scene with the point spread function. In fact the point spread function varies with the distance from the center of fovea, and so in principle the entire set of point spread functions must be known in order to derive the retinal image.

In practice, direct measurement of the point spread function of an eye is very difficult. But this function can be calculated from measurements of the *line spread function*, which is somewhat easier to obtain. An alternative procedure for deriving a point spread function is to measure the *modulation transfer function* (MTF), which is a measure of the available contrast in an image. Once the line spread function or the MTF of an optical system is known, its point spread function can be calculated by Fourier analytic methods [Krüger and Moser, 1973]. Further details for obtaining the point spread function can be obtained from Yellott et al. [1984]. Figure 2 from Krüger and Moser [1972] shows the course of MTF for frog *R. Esculenta* compared to the superior MTF of the human eye.

The Visual Field. Optical and neurophysiological techniques have been used to measure the anuran visual field. Fite [1973] used the direct optical method, based upon the fact that from all points from which one can see the entrance pupil of the eye, light can also reach the posterior part of the eye through the real pupil. The total field-of-view of a frog excludes only the area beneath its body [Fite, 1973].

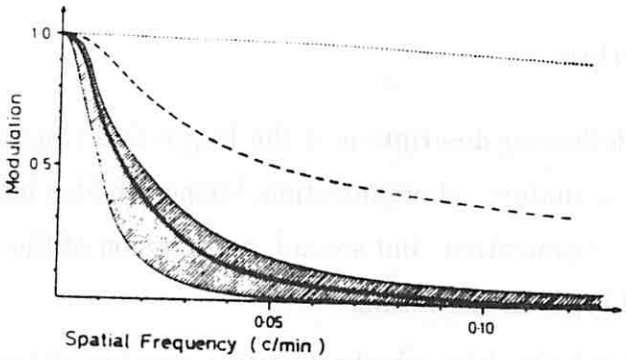

Figure 2: The course of the MTF of a frog's eye (—) compared to the suprior MTF of the human eye (- - -). The hatching gives the range in which the MTF's of several specimen were situated. From Krüger and Moser [1972].

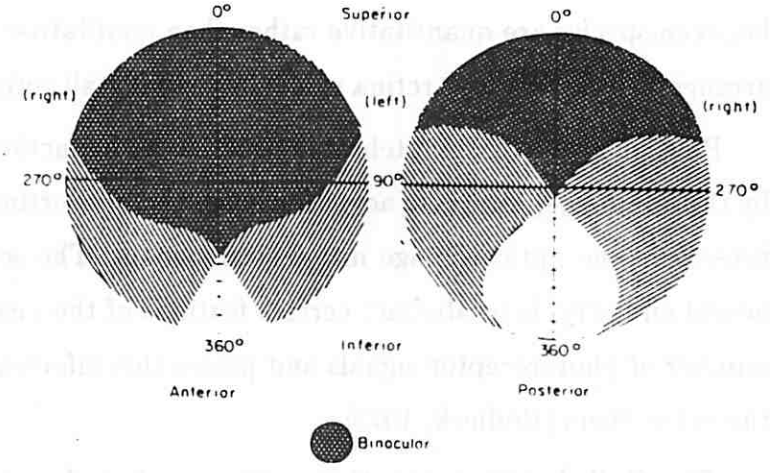

Figure 3: Perimetric maps of anterior and posterior field-of-view as measured for *R. pipiens* and *R. palustris*, showing right and left eye's visual field and region of binocular overlap. From Fite [1973].

The Retina

The following description of the frog retina consists of: first, a discussion of the overall anatomical organization, further divided into cellular organization and synaptic organization, and second, a discussion of the five functionally differentiated cell types in the retina.

Anatomically, the vertebrate retina consists of two major divisions: a single layer of columnar neuroepithelial cells, termed ***retinal epithelium***; and the major part of the retina, consisting of neurons and glia, termed ***sensory retina***. We will concern ourselves only with the latter part since that is where visual information is processed. The most striking feature of the retinal organizaiton is the separation of cell bodies and processes into distinct layers. The gross structure of the vertebrate retina varies little across the different species, and the differences between species are quantitative rather than qualitative; that is, all the synaptic arrangement in the frog retina exists in virtually all retinas.

Physiologically, the vertebrate retina has two functions. The first, performed by the photoreceptors, is to act as a transducer, converting part of the information present in the optical image into neural signals. The second, performed by the neural circuitry, is to abstract certain features of the visual world from the large number of photoreceptor signals and passes this information on to the brain via the optic fibers [Rodieck, 1973].

The Cellular Organization. Figure 4 from Dowling [1968] shows a drawing showing typical cells in a frog retina stained by Golgi method. Like other vertebrate retinas, the frog retina viewed in longitudinal section displays three nuclear/cell layers and two plexiform layers. The most distal[1] cellular layer, the outer nuclear layer (ONL), consists of the perikarya of the receptor cells.

[1] *Distal* as well as *outer*, *upper*, and *ascendant* refers to either away from the center of the eye ball or away from the central nervous system, while *proximal* as well as *inner*, *lower*, *descendant* indicates the opposite direction.

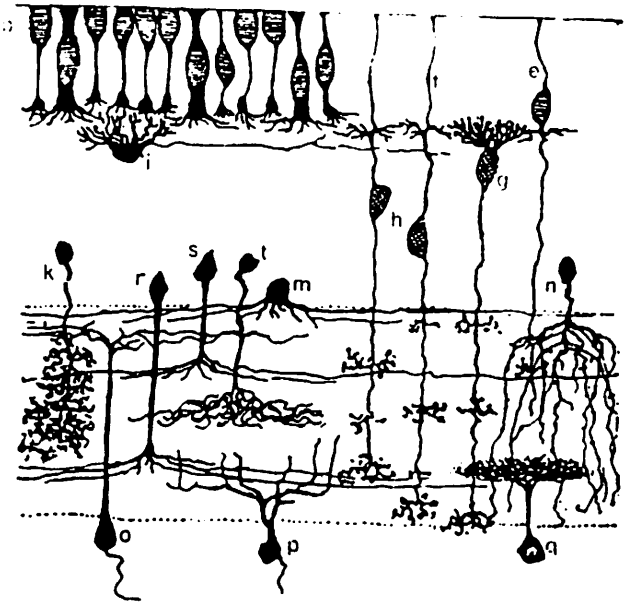

Figure 4: Drawing showing typical cells in a frog retina stained by Golgi method. Receptors (b); horizontal cell (i); bipolar cells (h, g); amacrine cells (k, r, s, t, m, m); ganglion cells (o, p). From Dowling [1968].

The inner nuclear layer (INL) contains the perikarya of the horizontal, bipolar, and amacrine cells. The most proximal cellular layer contains the ganglion-cell perikarya. In addition, there are glial elements, the Müller cells, which extend vertically through the entire retina; their nuclei are usually situated in the INL, and there are interplexiform cells, that appear to transmit information centrifugally.

Most of the present knowledge about interplexiform cells comes from two groups of animals, teleost fish and the monkeys. These cells receive input from amacrine cells in the IPL and make synapses on other amacrine processes in the IPL and bipolar cell dendrites and horizontal cell processes in the OPL. Even though they appear to be a general feature of the vertebrate retina, we will not cover this cell type any further since sufficient information is not available. For further discussion, see Dowling [1979].

So far no synaptic connection between neurons and Müller cells has been reported. Since Müller cells are not neurons nor do they have any connections

with other neurons in the retina, they do not participate in visual information processing in the retina. So, we will not be concerned with them here. For further information relating the Müller cells with the electroretinogram (ERG), see Dowling [1970].

Most of what we know about the cell types in the vertebrate retina, in terms of the extent and distribution of their processes, has come from light microscope (LM) examination of retinal tissue processed by the methods of Golgi [Cajal, 1893; Boycott and Dowling, 1969]. Cajal [1893], in particular, laid the groundwork in the anatomy of the frog retina.

It was noted that there are on the average about 35 receptor cells for every square degree in *R. Esculenta*, and about 100 in the area centralis [Grüsser and Grüsser-Cornehls, 1976]. And it can be estimated that about one fourth of the receptor cells for various frogs are cones [Donner and Reuter, 1976]. Carey [1975] provides the densities of different photoreceptor types and the spatial distribution of these cells for the retinas of several different species of frogs and toads.

The gross ratio of 2 to 3 receptor cells to 5 to 7 bipolar and horizontal cells per ganglion cells in the frog retina is reported by Walls [1942]. There are at least three functional types of receptor cells: single cone, red rod, green rod, and double cone which consists of two components that are morphologically similar to two of the other three types [Bäckström and Reuter, 1975; Rodieck, 1973]. And there appears to be several separate retinal pathways depending on light intensity and color [Stell et al., 1977; Faminglietti et al., 1977; Grüsser-Cornehls and Saunders, 1981a]. Also, two morphologically different types of horizontal cells (inner and outer, or large dendritic field and smaller dendritic field horizontal cells) and bipolar cells(inner and outer, or larger dendritic field and smaller dendritic field bipolar cells) in the frog retina are reported in the literature [Cajal 1893; Rodieck 1973].

And there are at least five different functional types of ganglion cells [Maturana et al., 1960; Grüsser and Grüsser-Cornehls, 1976] and many more anatomical

types [Cajal, 1893; Grüsser and Grüsser-Cornehls, 1976].

The Synaptic Organization and Pathways. Observation of synaptic junctions between retinal neurons requires the high-power resolution of electron microscopy (EM). Two principal types of synaptic contacts have been described in vertebrate retinas, both of which are found in each plexiform layer. First, ribbon synapses are characterized by a dense ribbon or bar in the presynaptic cytoplasm. Ribbon synapses of the OPL are found exclusively in the receptor terminals; in the IPL, synaptic ribbons have been found only in the bipolar terminals. Second, conventional synaptic contacts in the retina are similar to synaptic contacts described as existing throughout the vertebrate nervous system [Dowling, 1976].

In the OPL, processes from both bipolar and horizontal cells penetrate into invaginations at the bases of the receptor terminals and come to lie in close proximity to the synaptic ribbons of the terminal. In addition, other processes make superficial contacts on the base of the receptor terminals. Elsewhere in the OPL, knobs originating from the horizontal cells (or interplexiform cells) make conventional contacts with horizontal cell processes and with bipolar cell dendrites. All the types and arrangements of contacts seen in the OPL of frog have been seen in the OPL of other vertebrates, and it does not appear that the OPL in frog is much different from that of other vertebrates.

In the IPL, both ribbon and conventional synapses are observed. As in other species, it is generally believed that ribbon synapses are made only by bipolar terminals and conventional synapses mainly by amacrine cells. *Serial synapses* between morphologically identical, presumably amacrine processes, are observed frequently in the frog and represent one of the most striking and probably significant differences between the IPL of frogs and other species. The incidence of ribbon synapses in the IPL is roughly similar in all species, but the number of conventional and serial synapses varies considerably between animals; the frog retina has four times more conventional synapses per unit area than the human retina [Dubin, 1970]. These data indicate that amacrine cells are involved in me-

diating the complex visual transformation in frog retina. Another characteristics of the frog retina is the small number of synapses observed between bipolar cells and ganglion cells compared to those observed between amacrine cells to ganglion cells.

Figure 5 from Dowling [1970] shows a summary diagram correlating the synaptic organization of the retina with intracellularly recorded responses of the neurons. It shows how visual signals are propagated though the retina.

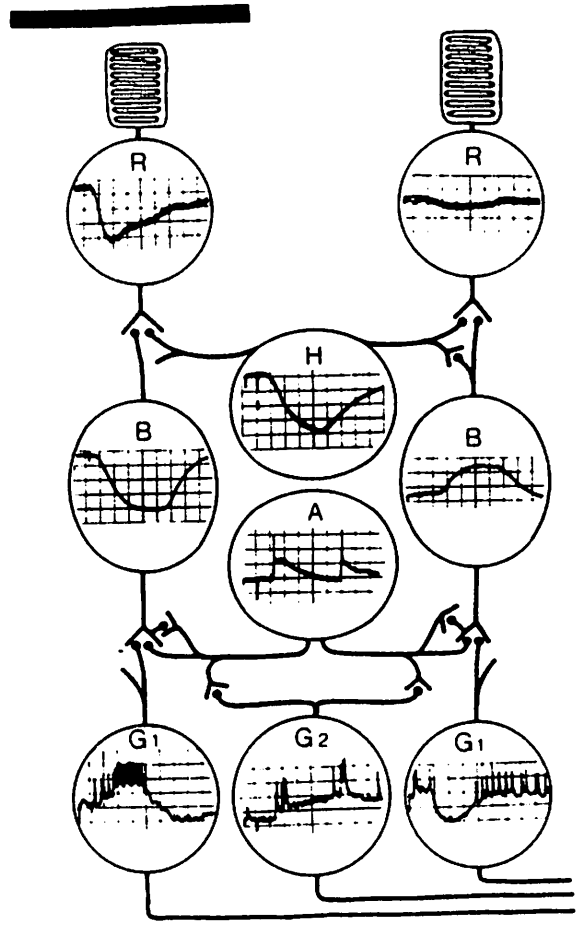

Figure 5: Summary figure correlating the synaptic organization of retina with intracellularly recorded responses of the neurons. Receptors R; horizontal cells H; bipolar cells B; amacrine cells A; ganglion cells G_1, G_2. From Dowling [1970].

Intracellular recordings of the vertebrate retina. Figure 6 from Werblin and Dowling [1969] shows a summary diagram showing intracellularly recorded responses of the major types of neurons in the mudpuppy retina. It shows how different visual stimuli are processed in the amphibian retina. Matsumoto and Naka [1972] shows similar intracellular recordings for the major cell types except photoreceptors for a frog retina.

Photoreceptors. The frog has four receptor types; red rods, green rods, single cones, and double cones. The cone terminals tend to be somewhat larger than rod terminals, but in other respect resemble the rod terminals closely.

In turtles [Baylor et al., 1971] and in marine toads [Fain, 1975], it has been shown that adjacent receptor cells summate their activities, probably via electric junctions between them. In the case of the turtle cone, the diameter of summation was about $50\mu m$ while in the toad rod it was about $800\mu m$. In mudpuppies, intracellular recording from a receptor cell [Werblin and Dowling, 1969] showed no difference between a small spot illumination and a spot with added annulus illumination as shown in Figure 7. An electrical coupling interaction has been found at the level of the photoreceptors [Baylor et al., 1971; Fain, 1975; Fain et al., 1976]. This interaction appears to be mediated by low resistence gap junctions, which allow currents to spread directly between cell interiors. Wilson et al. [1983] measured the electrical coupling between photoreceptors using pairs of intracellular microelectrodes under visual control in the tiger salamander retina. Their data combined with voltage-clamp data obtained previously from isolated cones and rods in order to come up with a quantitative model of the receptor network. Their model is consistent with the review and conclusion by Dowling [1976] that the degree of coupling between rods fair, between cones is little, and between rods and cones are medium.

The role of these electrical couplings between the receptors is not entirely clear. Some conjecture that the electrical couplings between cones are necessary in order to reduce random noise that arises primarily from random variations in

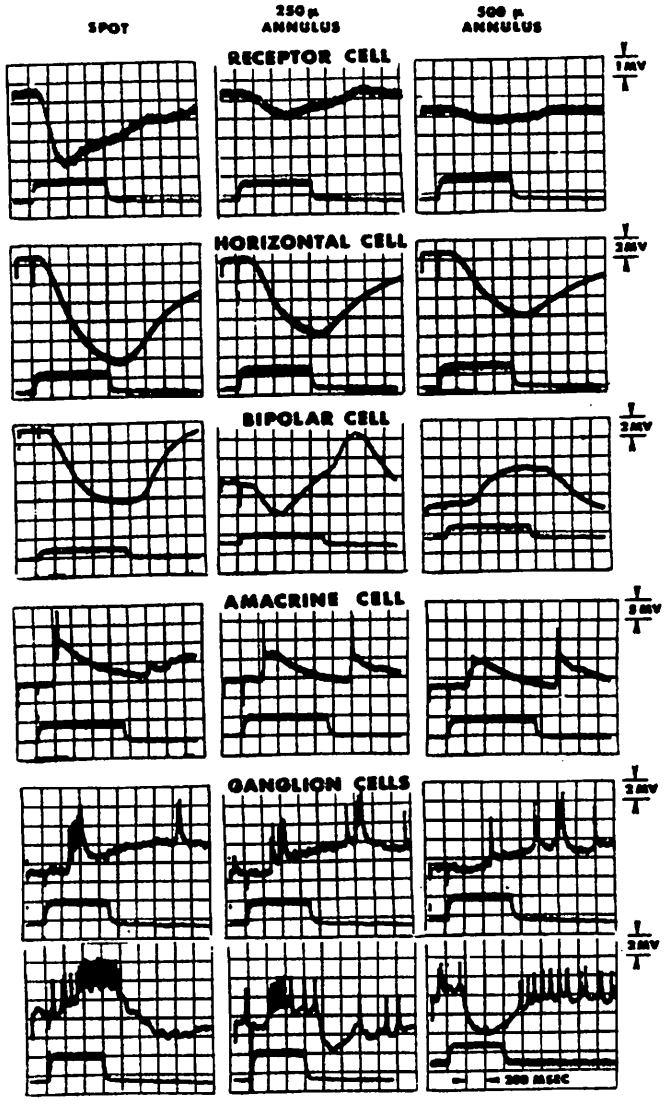

Figure 6: Intracellular recordings from neurons in a mudpuppy retina. First column shows responses of various neurons to a spot of light as stimulus, while the second and third column show responses to annuli of different sizes. From Werblin and Dowling [1969].

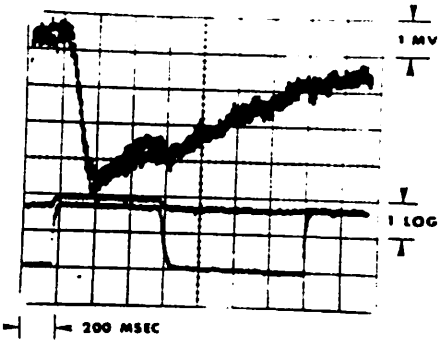

Figure 7: The autonomy of the receptor response is illustrated by two superimposed records. One record was obtained with spot illumination while the other with extra annulus illumination. From Werblin and Dowling [1969].

a number of blocking particles in the outer segment of the photoreceptors.

The functional relationship between the amplitude of a light flash and the magnitude of the photoreceptor hyperpolarization was investigated in turtle cones [Baylor and Fuortes, 1970], rat rods, and carp cones [Tomita, 1970].

This relation is represented by the equation: $\Delta V/\Delta V_m = I/(I + I_{half})$, where ΔV is the change in membrane voltage, ΔV_m the maximum observed change, I the intensity of the light flash, and I_{half} a constant equal to the intensity of the light flash for which $\Delta V = \frac{1}{2}\Delta V_m$. The dynamic range of photoreceptors is reported to be 4.2 log units for human rods and 2.7 log units for rat rods [Rodieck, 1973].

Compared to rods, cones respond faster to changes of illumination and recover from bleaching quicker [Tomita, 1970]. Hood and Grover [1974] shows cellular recordings for frog cone responses to different intensities and durations of light illuminations.

The biochemistry of signal processing inside receptor cells is not well understood, but it appears that heavy catenary chemical reactions are carried out to allow high sensitivity (e.g. in rat rods, a photon elicits about 3 percent of its

peak response) and a high amplification factor for light changes onto their outer segment. Most of the existing investigation on the excitation of photoreceptors has dealt with rod cells. The rod cells are sensitive to light because they contain a visual pigment, called *rhodopsin*, which is capable of trapping photons.

The conformational changes resulting from the breakdown of rhodopsin ultimately produce a change in the permeability of the outer segment plasma membrane, specifically a decrease in Na^{++} conductance. The biophysical and biochemcial mechanisms which link photon absorption by rhodopsin with this decreased Na^{++} conductance remain unclear. There are two current hypotheses for the molecular events that may underlie transduction of rod cells. According to one hypothesis, a cyclic nucleotide, cGMP, achieves signal amplification enzymatically. The other hypothesis suggests a role for Ca^{++} in receptor transduction. Strong and weak points of both hypotheses are extensively discussed by Fein and Szuts [1982].

Horizontal Cells. Cajal [1893] described outer and inner horizontal cells in frog, which differ principally in the position and size of their perikarya. The outer horizontal cell perikarya are smaller and are more distally positioned in the INL. The inner horizontal cells, although having a larger cell perikaryon, appear to have shorter dendrites, i.e., they have a smaller diameter dendritic field. Cajal claimed that both types of horizontal cell in the frog have a thin axon-like process. He stated that both types of horizontal cells should be classified as short-axon neurons.

Horizontal cell response has been called *S-potential*, which is an intracellularly recorded graded response to retinal illumination. There are two types of S-potential: the *L-potential* and the *C-potential*. The C-potential hyperpolarizes or depolarize depending on the spectrum of light illumination and is observed only in fishes [Svaetichin and MacNicholl, 1958]. The L-potential hyperpolarizes only in response to light illumination and is observed in all vertebrate retina.

Werblin and Dowling [1969] shows the temporal responses of horizontal cell to

various light pattern, while Matsumoto and Naka [1972] shows similar responses in frog retina. These observations show that horizontal cells respond to light illuminations which are far from them. It is believed that there is a propagation of electrical signals within the horizontal cell layer through *gap junctions* even though these were observed only in fish retinas. Naka [1972] compares the horizontal dendrite size and the much larger distance the horizontal cell signals propagate within the layer as well as the resulting *area effects.*

Bipolar Cells. Cajal describes two varieties of bipolar cells in frogs. Larger or outer bipolar cells have a distally-placed cell body and bushy ascending dendritic processes, whereas the small or inner bipolar cell perikarya are more proximally positioned, are about a third smaller, and have thinner dendritic branches. In many species, the larger bipolar cells appear to be related mainly to the rods and the smaller bipolars to the cones.

Werblin and Dowling [1969] shows intracellular recordings of bipolar cells in mudpuppy retina in response to various stimuli, while Matsumoto and Naka [1972] shows those in frog retina. There are two functional subtypes of bipolar cells: A hyperpolarizing type which hyperpolarizes in response to light illuminations in the central part of its receptive field and a depolarizing type which depolarizes to the same stimulus. Both have wider antagonistic surround receptive fields. The central receptive field is mediated by the direct local photoreceptor signals, while the surround receptive field is mediated by the horizontal cells. Rodieck [1965] provides a rigorous analysis of the center/surround receptive fields for a cat retina. Nye and Naka [1971] demonstrates the relative delay for the signals mediated through horizontal cells compared to those received directly from photoreceptor cells in frog retina.

Amacrine Cells. The amacrine cells in the frog retina are varied in their dendritic morphology and difficult to classify into discrete sub-types. Cajal [1893] divided these into two large groups, stratified and diffuse cells. Stratified cells have processes that extend to one, two or sometimes three discrete levels in the IPL

while diffuse cells extend processes through several levels of the IPL. Stratified cells tend to have larger diameter dendritic fields as compared to diffuse cells. Cajal considered his description of amacrine cells in the frog to be incomplete, yet he described at least 13 varieties.

Amacrine cells vary in the form of their dendritic fields in terms of size, diffuse versus stratified, and monostratified versus bistratified and multistratified [Cajal, 1893; Shantz, 1976]. There are two functionally different subtypes of amacrine cells: transient and sustained.

Tansient amacrine cells have been observed to display large amplitude excitatory postsynaptic potentials, so it is plausible that amacrine cells function in one of two different states: when stimuli are below somatic spike threshold, dendrites may function independently of each other through dendrodendritic synapses; and when stimuli reach above somatic spike threshold, the operation of dendrites may be much more uniform as they are invaded by the somatic spikes [Miller, 1979]. The idea of local feedback between bipolar cells and amacrine cells through reciprocal synapses seems to explain fairly well the spiking characteristic of transient amacrine cell responses [Sheperd, 1978]. We can conceptualize transient type amacrine cells essentially acting as local temporal differentiators of bipolar cell signals, which detect the temporal change of local light intensity before passing them onto ganglion cells.

Sustained type amacrine cells are reported in catfish retina by Chan and Naka [1976]. Unlike transient types they tend to be depolarized for a duration of light stimulus while exhibiting small spikes. Even though they are observed in a small number of vertebrate retina, they appear to be a general one in the vertebrate retina [Grüsser, 1979].

Ganglion Cells. The ganglion cells in the frog retina, like the amacrine cells, are very varied in their dendritic morphology and difficult to classify into discrete sub-types. As with amacrine cells, Cajal divided ganglion cells into two large groups, stratified and diffuse cells. Stratified cells have processes that ex-

tend to one, two or sometimes three discrete levels in the IPL while diffuse cells extend processes through several levels of the IPL. Stratified cells tend to have larger diameter dendritic field as compared to diffuse cells. Cajal suggests eleven subtypes of these cells using similar criteria to those used with amacrine cells.

From the work of Cajal [1893], many morphological details are known about the retinal receptors and nerve cells, which can be used for a morphological classification of different ganglion cells. Such a scheme might help to understand the different *functional classes* of ganglion cells found by neurophysiologists. More details on the frog ganglion cell anatomy can be found in Shantz [1976]. Further possible criteria for classification not included in Grüsser and Grüsser-Cornehls [1976] is the the type of branching of the main dendrites (*E*- and *H*-type ganglion cells of Lettvin et al. [1961]; Pomeranz [1972]).

Cajal differentiated five substrata of the inner plexiform layer of frog retina. The dendrites of the ganglion cells are frequently restricted to one, two, or three different substrata; the same is true for the synaptic endings of the bipolar cells. Cajal found that different receptors (single cones, double cones, red rods, green rods) had dendritic fields of different sizes (e.g. red rod bipolar cells with wide dendritic fields, cone bipolar cells with small dendritic fields). Therefore, the restriction of the dendritic terminals of a ganglion cell to certain substrata of the inner plexiform layer probably constitutes a functional difference in the perceptive unit. In contrast to the mammalian retina, the dominant signal flow in the frog retina is processed by a four neuron chain [Dowling, 1968, 1970]:

receptors $\longrightarrow$ bipolar cells $\longrightarrow$ amacrine cells $\longrightarrow$ ganglion cells.

The number of functional classes of retinal ganglion cells found in physiological experiments is smaller than that of anatomical classes. This, however, is not surprising at all because the physiological classification to date is based mainly on the responses to achromatic stationary or moving stimuli of rather simple configurations. If the presently known data about chromatic responses of frog retinal ganglion cells are extended, a more precise correlation between morphological and

physiological data might be possible.

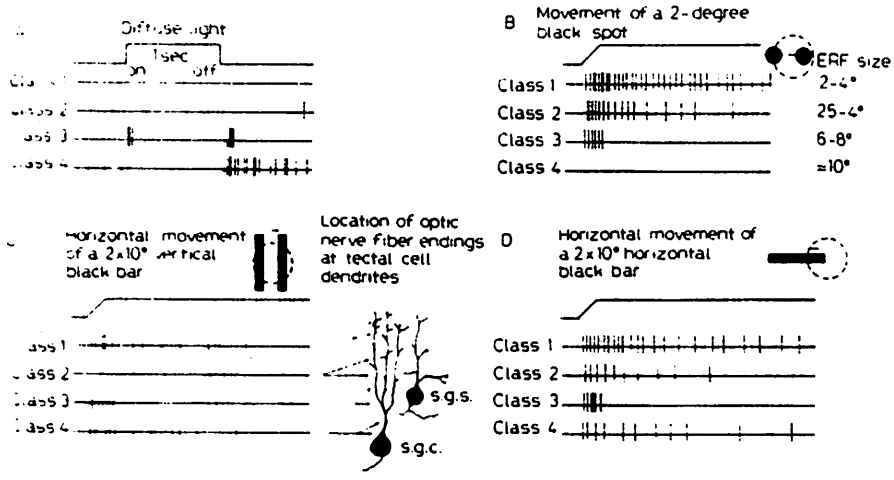

Figure 8: Scheme of the neuronal response type of four different classes of ganglion cells in the retina of *R. esculenta*. The responses to diffuse light, movement of a 2° black spot, and black bars. From Grüsser and Grüsser-Cornehls [1976].

The following is a brief summary description of the six classes of ganglion cells found in Grüsser and Grüsser-Cornehl's [1976] functional classification, which is a modification of Lettvin et al.'s original typology. Figure 8 from Grüsser and Grüsser-Cornehls [1976] shows typical responses for four different types of retinal ganglion cells in the frog. See Grüsser and Grüsser-Cornehls [1976] for the details of the ganglion cell responses.

Class 0 Neurons (*On*-Neurons):

These units correspond to probably to Hartine's [1938] *on* cells. These units exhibit an on-activation response to diffuse light. Stimulation in the inhibitory receptive field (IRF), where such a surround exists, evokes transient hyperpolarization of the cell membrane; simultaneous stimulation of the excitatory receptive field (ERF) and IRF causes a weak depolarization. Receptive field size is 10°-17° of visual angle.

Class 1 Neurons:

Class 1 ganglion cells are Maturana et al.'s [1960] *sustained edge detectors.* These units do not respond to changes in diffuse illumination, but a small spot projected onto the ERF produces a sustained *on* response, as do moving or stationary edges. The ERF is approximately 2°-3° and is surrounded by a weak inhibitory receptive field of 5°-6°. White-on-black and black-on-white stimuli of equal contrast produce equivalent responses. The sustained response to stationary stimuli is slightly decreased but still extant after darkening and relightening of the field.

Some Class 1 units receive input from 432nm rods and 575nm cones in opponent-process fashion; Grüsser and Grüsser-Cornehls [1976] suggests that these correspond to Cajal's AII cells, which are stratified ganglion cells terminating in layers 2 and 4 of the IPL, and that non-opponent Class 1 units correspnd to Cajal's AI cells terminating in IPL layer 4 only.

Class 2 Neurons:

Maturana et al. [1960] refer to these as *convex edge detectors.* A large (6°-20°) IRF surrounds their 2.5°-4° ERF. A small stationary spot illumination or a moving contrast stimulus causes maximal response from this cell. Rapid habituation with a 10-30 sec recovery period is observed for successive small light stimuli in local areas of the ERF; this occurs regardless of background illumination and is not solely due to photochemical effects. These show on-, off- or on-off activation in response to a small spots of light. Grüsser and Grüsser-Cornehls [1976] demonstrates convincingly that these units are not at all selective for convex edges but rather respond equally well to all stimuli of equal size and contrast for images restricted to their ERF. Grüsser and Grüsser-Cornehls further suggests that black-on-white stimuli are more effective than white-on-black, although there are differences between, for example, frog and toad responses to black-on-white stimuli.

When the stimulus illumination is suddenly removed, Class 2 units will im-

mediately cease their activity; however, unlike Class 1 units, Class 2 units do not resume firing when the stimulus illumination is restored. (This phenomenon was termed *erasability* by Maturana et al. [1960].)

Class 3 Neurons:

These are Maturana's ***changing contrast detectors*** and probably Hartline's *on-off* cells; they are also referred to as ***event detectors*** (cf. Moreno-Diaz [1965]). Their ERFs of 6°-8° have 10°-15° inhibitory surrounds somewhat weaker than those of Class 2 units; stimulation of the IRF can inhibit ERF activation, but will not itself evoke a response. These units spike both at onset and termination of the stimulus; in both cases the cell membrane is observed to depolarize, yielding a burst of axonal impulses which is sometimes preceded by a brief hyperpolarization in the case of the *on* phase. Maximal response occurs for stimuli centered in the ERF, and white-on-black and black-on-white stimuli are equally effective.

Class 4 Nurons:

Class 4 ganglion cells are Lettvin et al.'s [1959] ***dimming detectors***, so named because they respond to small spots of light centered in their (10°-15°) ERFs with *off* activation.

A 2 to 5 degrees moving object that dims the ERF evokes a response, as will any image in general that causes the ERF to dim, regardless of the image's size.

Class 5 Neurons:

Maturana et al. [1960] labelled Class 5 units ***dark detectors***; they ***are continuously active and this activity increases as ambient illumination decreases.*** Information on these units is scant, as they are rarely observed.

In addition to the above mentioned qualitative descriptions of frog retinal ganglion cells, there are well studied quantitative data of them. Among the functions that describe relations between a stimulus parameter and the response of various ganglion cells are ***area function***, ***velocity function***, ***contrast function*** and ***configuration factor***.

An area function [Butenandt and Grüsser, 1968; Butenandt, 1975] relates stimulus size/area to the activities of types 2, 3 and 4 ganglion cells in the frog retina.

A velocity function [Finkelstein and Grüsser, 1965] relates speed of a moving stimulus to the activities of type 1, 2, 3 and 4 ganglion cells.

A contrast function [Grüsser and Grüsser-Cornehls, 1976] relates the contrast between the stimulus and the background to the activities of type 1, 2 and 3 ganglion cells. These and other ganglion cell data of quantitative nature are well summarized in Grüsser and Grüsser-Cornehls [1976].

Also, there are configuration factors that are well studied by Ewert and his colleagues [Ewert, 1976, Schürg-Pfeiffer and Ewert, 1981]. It relates stimulus configuration of vertical, horizontal or square bar with the activities of type 1, 2 and 3 ganglion cells.

Review of Retinal Models

There are many different vertebrate retinal models which try to explain/predict various phenomena associated with the types of information processing that is being carried out. However, in this section we are limiting ourselves to a small class of these models where at least one of the following concerns are satisfied: Explanation of the neuronal functions performed in terms of their underlying structure; Anuran amphibian retinal output; And modelling approach which is of general importance.

There are several *quantitative neuronal network* models which are reviewed by Grüsser and Grüsser-Cornehls [1976], which are mostly their work with their colleagues. They were mostly developed as our interpretation for some qualitative or quantitative relations found in the dependency of the ganglion cell discharges on certain stimulus parameters. Common to all these models are the serial con-

nections of low pass and band pass filters, some non-linear threshold mechanism, and spatial summing properties at different levels. Even though they successfully reproduced such experimental data as velocity function of type 2 ganglion cells quite well basing their connections on the anatomical studies, their main interest lay in the functional duplication of the ganglion cells. Generally their models lack the detailed functional descriptions in the intervening layers/cells as well as how those intervening neuronal computations are performed, which resulted in the lack of explanation in the local, in the sense of intra-layer and inter-layer, computations that are performed by the vertebrate retina. They combine different approaches of analog, digital computer and hardware modellong and their expertises in neurophysioloy to come up with vary convincing models to replicate various properties of frog ganglion cells.

Of these, Butenant and Giesel [Grüsser and Grüsser-Cornehls , 1976] demonstrates the importance of the *spatio-temporal pattern* of activities like the current modelling approach even though it shares the common goal of functional duplication at the ganglion cell level with other models mentioned.

Another intersting model by Butenandt [1975] studies the movement-specific property of frog retinal ganglion cell. It varies its randomized spatial kernel, which represents the dendritic summation property, to come up with the optimal simulation data. It implies the evolutionary development of pattern recognition capability of the frog retinal information processing aspect. It also shows the concern for the importance of connectivity that is modulating the response of the neuron concerned. So, it shares with the current model the importance of *dendritic computation* as a way of achieving the computational task of the retina.

Another important line of modelling efforts was started by Moreno-Diaz [1965]. It is an analytical model of frog type 2 ganglion cell, which provides how a complicated system can be mathematically modelled and analysed under typical conditions even though some of the underlying anatomical/physiological assumptions, such as impulse generating bipolar cells, were not correct.

Moreno-Diaz and Rubio [1979] developed "a theoretical model for layered visual processing". The basic idea underlying the model is that retinal data processing is performed by layers of similar computational elements. But, each layer is functional and may not correspond to the actual anatomical layer. But it can perform any non-linear arbitray function on a three dimensional input space which consists of 2 spatial dimensions and a time dimension. So this is a model where *spatio-temporal pattern* of activitites are emphasized even though the computation carried out may not be a simulated computation of retinal structure. The fundamental point of view shared by both the above model and the current model is that the computation is performed by the layers of simple identical elements. There is another similarity that their individual computing elements/neuron models basically do not learn, which implies time invariance. The major difference is the concern or the lack of it for the underlying structure which eventually shares the same functional goal. Although the models by Moreno-Diaz and his colleagues removed correspondences to the structure of the retina, the *layered* nature of the local computations and the choice of functional channels whose combination functionally synthesizes ganglion cell responses of various vertebrate retinas [Moreno-Diaz and Rubio, 1979; Moreno-Diaz et al., 1980] demonstrate the novelty of the approach by Moreno-Diaz and his colleagues.

Siminoff [1983] presents an analog hardware model of the vertebrate retina. It is an extension of his previous cone retina model [1981], which mostly considered the organization of the vertebrate retina. Regardless of the validities of the underlying simplifying assumptions, the model is important in that it provides a theory of spatial organization and a way of testing it. But, due to its inflexibility to changes it had difficuties in extending the model further as other hardware models. And the model is now extended to a class of retinal models such that an instantiation of the model would be able to simulate any vertebrate retina [Siminoff, 1986]. But the real weakness of the model appears to stem from the very spatial organization it emphasized. It is too simplistic to think most vertebrate

retina shares the common structure of one central unit hexagon[2] and six unit hexagons. One of the unique features of Siminoff's model involves the use of the difference in two bipolar cell signals as a source of temporal contrast detection or phasic response.

Richter and Ullman [1982] proposed a model for the temporal characteristics of X- and Y-type reponses of ganglion cells in the primate retina. The model is based on detailed anatomical studies and plausible assumptions such as difference-of-Gaussian of receptive field organization. But overall the model is mainly interested in the ganglion cell responses and pays little attention to how different local interactions between cells in a layer or between cells in different layers would contribute to the overall retinal information processing. And, as most other models interested in the functional descriptions at the output level, it lacks the facility to study the spatio-temporal pattern of activity. This model is based on sound anatomical and physiological studies and it replicates the experimental data very well. It also provides numerous predictions about the structures and physiology of the retina which it can be tested upon.

[2]Six surrounding and one central cones defined to act as a functional unit to the subsequent layers, i.e., horizontal cells and bipolar cells.

CHAPTER III

OVERVIEW OF THE MODELLING AND THE SIMULATION

Modelling

As have been reviewed in Chapter 2, major efforts in modelling the vertebrate retina in the past dealt mostly with activities of a single cell or with the overall behavior of the network of neurons. The current model, however, deals with both temporal activities of single cells as well as the spatial activity patterns among a population of cells. It uses discrete time, discrete space and continuous states [an der Heiden, 1980], enabling the modeller to access the cell state dynamics of every cell involved in the visual field being modelled. It is formed in the following manner: first, individual neurons are modelled by variations of the *leaky-capacitor model* [Holden, 1976]; second, different types of connections between cells are modelled based on their *synaptic specializations* [Dowling, 1968; Shepherd, 1979]; third, the *overall synaptic connectivities* are then modelled based on the shape and size of their dendritic trees and are approximated with 2-D Gaussian functions [Rodieck, 1965]; and fourth, various *parameters* of the model are adjusted so that models of individual neurons reproduce the temporal characteristics of corresponding neurons, which are well known under various experimental conditions through intracellular or extracellular recordings. The intracellular recordings used to ground the present modelling effort are those of major types of cells in the mudpuppy and in the frog retina from Werblin and Dowling [1969] and Matsumoto and Naka [1972], respectively.

Once the model can reproduce the qualitative response characteristics of the frog's retina as found in physiological studies [Maturana et al., 1960], it may be expected to reproduce the well-known quantitative data on the frog retina as well [e.g., Grüsser and Grüsser-Cornehls, 1976; Schürg-Pfeiffer and Ewert, 1981]. Since the Model attempts to reproduce states of every cell involved in the visual processing at a given moment, it has the following strengths as well as weaknesses:

1. It enables the modeller to view the spatial patterns of concurrent activities among different types of retinal cells.

2. Results of computer simulation of the retinal process as represented in the model can be compared with intracellular or extracellular recordings of the corresponding cell types, making it easy to detect those parts of the model which have inadequate representations.

3. It may allow the modeller to emulate effects of forced cell potentials to arbitrary cells as in using the voltage clamp technique, as well as to emulate effects of certain retinal diseases.[1]

4. As is well understood, "*the advantage of a* continuous *representation compared with a* discrete *one consists in a more concise description and in a simplification of the mathematical analysis*" [an der Heiden, 1980], and it can be very expensive, both in term of CPU-time and memory requirements, to improve the quality of individual cell's temporal details under the current approach.

5. It can be readily implemented in hardware.

The present model of the frog retina consists of five major layers representing five major types of cells, as was reviewed in Chapter 2: Photoreceptors, horizontal

[1] Even though the model is well suited for these types of simulation, the curent version of the model has not implemented these features yet.

cells, bipolar cells, amacrine cells, and ganglion cells. Figure 9 shows the overall layered organization of the model retina.

The layered structure of the retina model consists of interacting layers, as visual information in the form of light energy transforms into an electro-chemical one at the photoreceptor layer and continues its cycle of transformation up to the ganglion cell layer.

Unlike the real retina which has varying distribution densities of cones, rods and ganglion cells in the area centralis and in the periphery in frog and toad [Carey, 1975], the model assumes spatial homogeneity within each cell layer. The Model allows for variation in the density of each layer below the upper bound of 6 cells per visual degree (36 cells per 1°x1°), i.e., an inter-cell distance of $\frac{1}{6}^{\circ}$, which is an approximate average density of single cone a little outside of the area centralis of the frog retina [Carey, 1975; Donner and Reuter, 1976].

Rationale for Modelling the Cone Pathway

It is well known that research on the vertebrate retina has typically concentrated upon its output functions through the ganglion cells. More specifically, movement detection and sharp boundary detection mechanisms are at the core of discussions about the various functions of several well documented types of ganglion cells' activities [Maturana, et al. 1960; Grüsser and Grüsser-Cornehls, 1976; Morrison, 1975].

However, since the degree of retinal cone sensitivity to changes in illumination (in photopic cases) is much greater than any output responses in the ganglion cells would suggest, and also since the retinal cone displays strong directional selectivity to light, the overall process of retinal pathways must be far more complex than can be inferred from their outputs. Therefore, more research attention must be given to looking at retinal pathways as a whole. In this context, the attempt in the present dissertation to provide a mathematical model as a basis for simu-

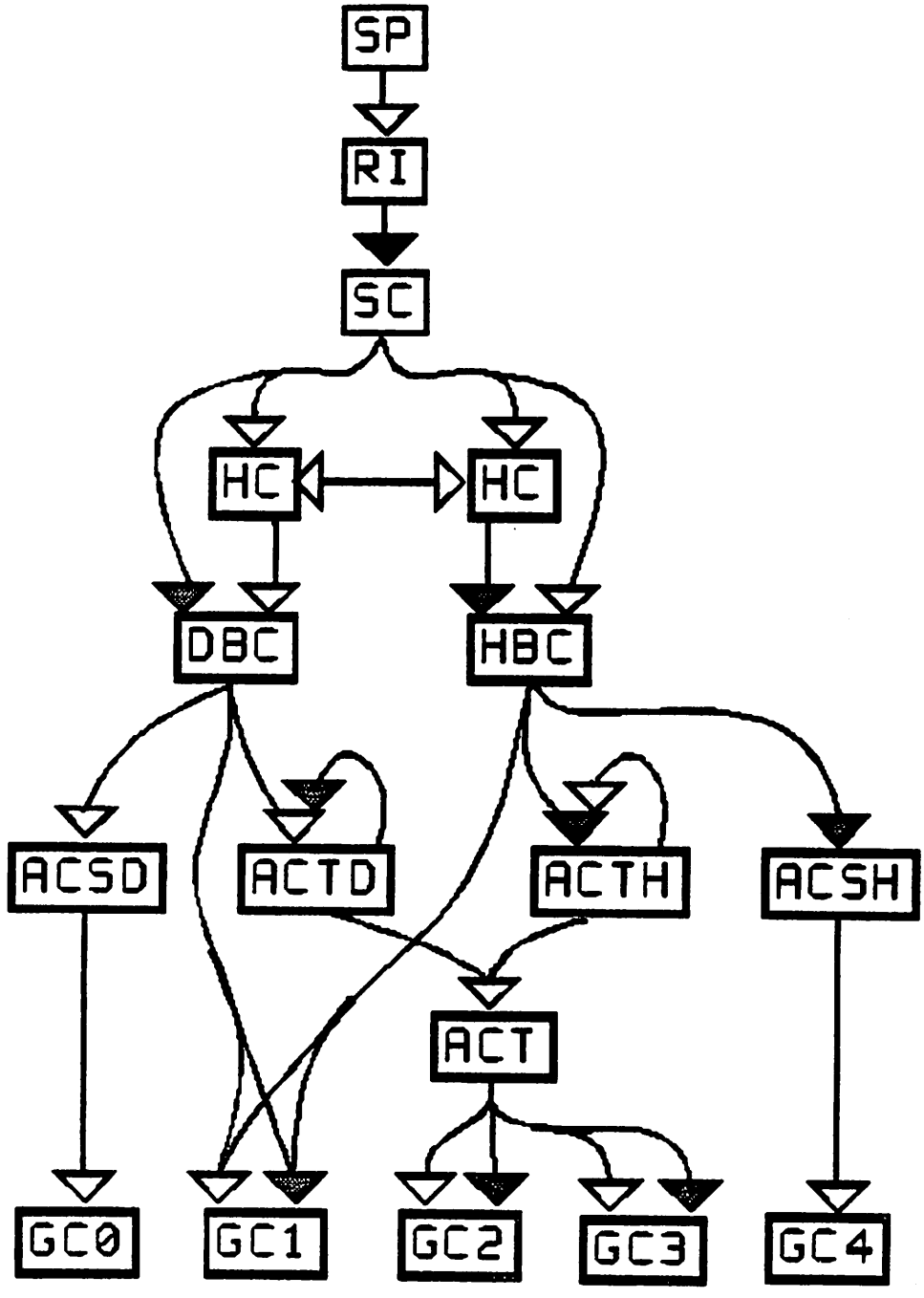

Figure 9: The overall organization of the model retina. Presence of a line symbolizes the existance of a connection, where an empty arrow head symbolzes a non-sign inverting connection and an filled arrow one a sign inverting connection.

lation of retinal processes represents a step toward filling the gap in our present knowledge about the frog retina as well as those of vertebrates in general.

Even though signals originating from red rods are known to mixed with those from cones [Grüsser-Cornehls and Saunders, 1981a], there appears to be enough support for a separate pathway for cone signals up to IPL not mentioning up to OPL. Specifically, it was observed that IPL sublamina are connected to functionally different subtypes of bipolar cells in the carp retina [Famiglietti et al., 1977; Rodieck 1973; Cajal 1894]. Most of the neuroethological data deals with photopic conditions [Maturana et al., 1960; Grüsser and Grüsser-Cornehls, 1976; Schürg-Pfeiffer and Ewert, 1981]. So, to test the model those experimental results requires us to model at least the cone pathways.

Why a 20 msec Time Step?

The most important consideration in deciding upon the fixed time step for the simulation of the frog retinal process using the current model has to do with the average propagation delay that is required for a signal to travel between two cells in the neighboring cell layers. It is impossible to account for the different rates of signal propagation that occur within a given neuron in the present model without becoming compartmental (which, of course, will present a tremendous burden in computing power) and/or using smaller time steps. We benefit from less computational requirements if we choose a bigger size time step but lose more details in temporal response, while the opposite would be true of smaller time step. We chose 20 msec as the fixed simulation time step based on our observations of the experimental data of Werblin and Dowling [1969] and Maturana and Naka [1972]. We think this time slot is also sufficiently small for most of the interesting analytic phenomena to occur in the retina except the fine details of ganglion cell spikes. For example, the latency of a mudpuppy receptor cell is about 50 msec while the peak time is about 300 msec [Werblin and Dowling 1969], and the peak time of the frog receptor cell (probably a cone [Tomita, 1970] because of its

relatively fast rise and fall time) is about 150 msec [Toyoda et al., 1969], and not more than one major spike is generated by amacrine cells within a 20 msec interval [Rodieck, 1973; Werblin and Dowling, 1969; Grüsser and Grüsser-Cornehls, 1976].

Algorithm Description Methods for the Model

The computations used to propagate light intensities and membrane potentials from distal to proximal layers in the Model are described[2] by two methods: *Connectivity diagrams* and *difference equations.* The connectivity diagram for a given layer gives a graphic illustration of where a typical cell in that layer receives its input from. They are easy to understand, but are not a complete description of the computations performed. The full details are given in the difference equations. We can illustrate both methods by considering a typical example, that of the hyperpolarizing bipolar cell (HBC).

Connectivity Diagram

The connectivity diagram for the HBCs is shown in figure 10. The lowest box represents a single HBC. The lines to boxes above it represent connections providing inputs from individual cells in more distal layers (single cones and horizontal cells). The width of the row of boxes on a given input layer is proportional to the diameter of the smallest circle enclosing all influencing cells in that layer. For example, the SC inputs to a given HBC are contained in a region more central to the HBC than the inputs provided by the HC layer as shown in the Figures 10 (b) and (c).

[2]Rewritten by permission from Teeters, Lee and Arbib [1986].

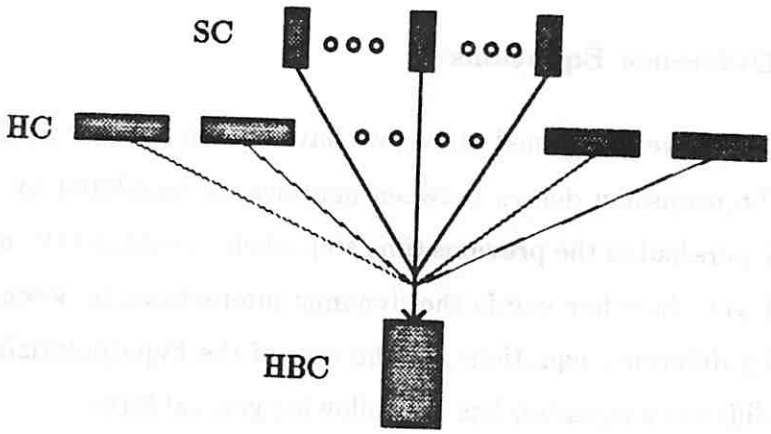

(a)

0	3	4	3	0
3	9	12	9	3
4	12	122	12	4
3	9	12	9	3
0	3	4	3	0

(b)

(c)

Figure 10: (a) Connectivity diagram for HBC, where SC stands for Single Cone, HC for Horizontal Cell and HBC for Hyperpolarizing Bipolar Cell. (b) Central excitatory spatial kernel for HBC. (c) Surround inhibitory spatial kernel for HBC.

Difference Equations

As we mentioned above, we have chosen 20 msec as the simulation time step. Transmission delays between neurons are simulated by using the potential the layers had in the previous time step when calculating the new state of a subsequent layer. In other words the dynamic interactions between the layers are specified by difference equations. In the case of the hyperpolarizing bipolar cell layer, the difference equation has the following general form:

$$HBC_t = f(HBC_{t-1}, SC_{t-1}, HC_{t-1})$$

HBC_t represents a matrix that contains potentials of the cells in the HBC layer at time step t. It is computed from the potential the layer had at the previous time step along with single cone and horizontal cell potentials at that time step.

Notation

The difference equations used to compute the new state of each layer are specified using a non-standard notation in which the primitive operations operate on matrices. The specific semantics are:

Identifier Names Examples: $MAT_t, MAT_{t-1}, K, W_{xx}$ are all identifiers with t or $t-1$ subscripts represent matrices that change dynamically during the simulation; the subscripts differentiate between the values at a given and previous time step. Identifiers consisting of the single letter K with a subscript represent constant(time independent) valued *mask* matrices which are used in the convolution operation ($*$) described below. All other identifiers are scalar constants.

Arithmetic Operators The operators $+$, $-$, $\cdot$, $/$ are semantically different from the normal scalar versions, because one or both of the operands may be a matrix. If both are matrices, the result will be a matrix, and it is

computed by applying the ordinary scalar operator to each pair of corresponding elements in the operand matrices. If one operand is a constant, we replace it by a matrix of appropriate size with all elements set equal to the constant; and the result matrix is found accordingly. We use the abbreviation $x^- = 1 - x$.

Convolution $(K * MAT)$. The asterisk "*" designates the two-dimensional convolution of a mask matrix (K) with matrix MAT. The result of the convolution is a matrix which has dimensions of the layer matrix minus the mask size.

Formally if MAT has dimensions $[-L : L, -W : W]$ (i.e., there are 2L+1 rows indexed from -L to L, and similarly 2W+1 columns), and K has dimensions $[-m : m, -m : m]$, then $K * MAT$ specifies a *Result* matrix of dimensions $[-L + m : L - m, -W + m : W - m]$ where each element at location (x,y) "$Result[x, y]$" is computed as follows:

$$Result[x, y] = \sum_{i=-m}^{m} \sum_{j=-m}^{m} K[i, j] \cdot Layer[x - i, y - j].$$

Conceptually each [x,y] element of the result matrix is generated by centering the *flipped* mask matrix on top of the corresponding [x,y] element of layer matrix, multiplying each pair of overlapping elements and adding the products. The entire result matrix is generated by repeating this operation over every position in the layer matrix. *Convolution* was chosen as the name of this operation because of the similarity to the one dimensional analog $\int g(t)h(t - \tau)d\tau$ which is better known in the time domain. The discrete version we use is two dimensional, and is only defined in those regions where all elements of the mask overlay elements of the layer matrix. (The mask does not go over the *edge* of the layer matrix.)

The weighted sum performed by the convolution corresponds to the fan-in of inputs from a dendritic tree. Synapses closer to the root of the tree have more influence than those far from the cell body. Neurons that have very large dendritic trees are assumed to not use inputs from every neuron that lies within their span, but instead to ***sample*** from the neurons within it. In the model this sampling is achieved by using the ***coarse*** masks which have non-zero elements only on their axis and main diagonals (See figure 10 (c)). *Dense* masks have all non-zero elements and are used when the dendritic span is small, and all neurons within it are assumed to contribute.

Data Shifts. (left, right, up, down). Functions which have a matrix as input and output. The output matrix is formed by shifting all elements of the input matrix in the specified direction. Elements which have no value to shift from, (elements on the edge upstream from the shift direction) retain their original, preshift, value.

Thresholding. The $LAYER\lfloor^{max}_{min}\,|^{new\_min}_{new\_max}\rceil$ form replaces all elements of $LAYER$ that have values above ***max*** or below ***min*** with ***new_max*** and ***new_min*** respectively. The $LAYER\lceil max \mid new\_max\rceil$ is similar, but only replaces values above ***max***, while $LAYER\lfloor min \mid new\_min\rfloor$ is similar, but only replaces values below ***min***.

In the case of the hyperpolarizing bipolar cell layer, the algorithm has the following form:

$$HBC_t = W_{hbc} \cdot HBC_{t-1} + W^{-}_{hbc}(K_{ch} * SC_{t-1} - \frac{1}{2}K_{oh} * HC^{-}_{t-1})$$

The difference equations in essence specify a ***family*** of models. The scalar and convolution mask constants are parameters that specify specific models within the family. In the case of the hyperpolarizing bipolar cell layer, these parameters

currently have the following values:

$$\begin{array}{ll} W_{hbc} & 1/4 \\ K_{ch} & Den(dia = 1°, \sigma = 1/4°) \\ K_{sh} & Cor(dia = 3°, \sigma = 4/3°) \end{array}$$

where the last two expressions will be explained shortly.

The convolution mask matrices (K identifiers) are normalized so that the sum of all their elements totals one. As mentioned earlier, there are two types: Coarse mask (designated *Cor*) have non-zero elements only on their two main diagonals and axes. Dense masks (desgnated *Des*) have the possibility of non-zero values in every element. The diameter of the matrix (*dia*) is specified in visual degrees which is translated into a matrix size using six elements per visual degree.

Formally $K_{den} = Den(dia = d°, \sigma = \sigma°)$ is a matrix of dimension $[-3d : 3d, -3d : 3d]$. Each element $[i, j]$ is defined (before normalizing) by:

$$K_{den}[i,j] = \begin{cases} e^{-(i^2+j^2)/(2\sigma^2)}, & \text{if } (i^2 + j^2 \leq (sd)^2); \\ 0, & \text{otherwise.} \end{cases}$$

$K_{cor} = Cor(dia = d°, \sigma = \sigma°)$ has the same dimensions, but before normalizing each element is defined by:

$$K_{den}[i,j] = \begin{cases} e^{-(i^2+j^2)/(2\sigma^2)}, & \text{if } (i^2 + j^2 \leq (sd)^2) \\ & \text{and } (i = 0 \text{ or } j = 0 \text{ or } i = -j) \text{ or } i = -j); \\ 0, & \text{otherwise.} \end{cases}$$

Simulation

In general, a mathematical model, an equation or a system of equations, by themselves may not contribute much to the understanding of a particular phenomenon. One way a mathematical model helps us understand the real world

phenomenon better is through mathematical conclusions followed by an interpretation process. The analysis will provide general conclusions about the nature of the phenomenon. But there are only a small class of mathematical models that yield to mathematical analysis. Most mathematical models of reasonable complexity do not fall into the above category. Some of these models can be readily analysed by making certain simplifying assumptions, whereas others can be divided into submodels that are then analysed and whose analyses are then combined to offer a reasonable conclusion for the whole model.

For these problems that resist mathematical analysis, simulation provides instantiations of the model in a given situation, i.e., the simulation process imitates the essential features of reality as captured by the model. So, in a simulation we try to copy the behavior of a process where the causes and outcomes are fairly well understood while the relationship among them may be quite complex and incapable of simple analytical description. But when simulation is used to study an actual system, the conclusions can only be "inferred" from the outcome of sample runs of the simulation.

In simulation, the effectiveness of any model is measured by how closely its predictions match those actions of the system that are observed in the world. Simulation permits experimental interaction with the model to produce verifiable responses, which can be compared with experimentally obtained data to validate the performance of the model. Simulation therefore provides a clear and unbiased test of the concepts involved in the formulation of the mathematical model and hence of the conceptual model. It also allows one to perform "experiments" on the model that lie outside the range of normal experimentation. For example, we can monitor the spatial patterns of cell potentials which represent thousands of cells, or we can fix the adaptational state while performing a prolonged simulation which otherwise might not be possible in a real situation.

Simulations are used in the following ways to help us understand better the real retina and the visual system in general. First, by simulations which attempt

to duplicate the intracellular recordings of individual cell responses under well known experimental conditions, we can modify/validate submodels of the retina model as well as the overall connectivities. This premits us to confirm or disconfirm conceptual models [Dowling, 1976; Naka and Rushton, 1966] of retinal processes on which the model is based. As an extension, we also simulate a parameterized sets of visual stimulus patterns such that the results can be compared with the generalizations of (parameterized) experimental data which were obtained under similar experimental conditions. Second, once we obtain satisfying results in the first stage of simulation, we can predict responses of any retinal neuron for any given input condition. Particularly, by using the model to simulate the ganglion cell activities, we can provide a spatio-temporal pattern of retinal outputs to models of higher visual brain areas [Cervantes, 1985].

Since we are dealing with a population model of rather simple individual neuron models, we do not expect each individual neuronal model to reproduce fine details of the response pattern. Rather, we are interested in getting as many essential features of the modelled neurons as possible while keeping the whole task of population modelling under control. Since the current approach emphasizes the importance of the interactions caused by connections, so we compromised on the details of individual responses to afford us the spatial activity patterns of the population.

This dissertation is limited mainly to the simulation's ability to validate/confirm the mathematical model and the conceptual model behind it. The simulation is presented according to the submodel layers. In each section, we first explain the experimental data and what we are trying to show in the corresponding simulations. We describe what might be called the essential functional features for each simulated experiments. Second, we compare the results of the simulation with the experimental data, noting and explainning the differences. Third, in the discussion subsection we discuss the points clarified by the Model and the difficulties encountered by it.

We then present simulations of a qualitative nature that we think are essential to assess the validity of any frog retinal model including ours: Simulations for the intensity versus response curve of a single photoreceptor [Fein and Szuts, 1982] and for a single cone temporal response under well-known experimental situations [Werblin and Dowling, 1969; Cervetto, 1976]; horizontal cell temporal response and the area effects including passive propagation of potential between horizontal cells as a function of distance [Naka, 1972; Werblin and Dowling, 1969; Matsumoto and Naka, 1972]; bipolar cell response patterns responding to a spot, annulus or both [Werblin and Dowling, 1969; Matsumoto and Naka, 1972]; transient amacrine cell responses in the IPL [Matsumoto and Naka, 1972]; and characteristic response patterns for major types of frog ganglion cells [Maturana et al., 1960; Grüsser and Grüsser-Cornehls, 1976].

Rigorous measurements of the effectiveness of the model[3] will have to wait until more extensive simulations are performed.

[3]The measurement of how closely the model fits the real world is, in general, a complicated problem that involves the full use of statistical techniques (cf. Sakuranaga and Naka [1985a]).

CHAPTER IV

STIMULUS PATTERN GENERATION AND RETINAL IMAGE FORMATION

Generation of Stimulus Patterns

The current spatial representation for the *stimulus pattern*(SP) which provides the simulated optical input pattern for the *eye optic model* is discrete, as is the *retinal image*(RI) which is the resulting output pattern from the eye optic model. This presents a problem as real optical images are continuous and we have to decide on the quantization size for the 2-D space. Of course, we can use an arbitrarily large array to represent a continuous SP, but that might mean an unacceptable waste of computer memory space and we have to still face a quantization when we provide RI to the *single cone*(SC) layer. Since there are about 36 receptor cells in a $degree^2$ in the retina, it seems reasonable that we provide at least that many light point sources, i.e. 6 light point image per degree. The model uses arrays of the same density to represent the SP and RI layers as the SC layer.[1] The above representation becomes a problem when the stimulus is a size that is not a multiple of 1/6° or moves with a speed that is not a multiple of inter-cellular distance per simulation time step, i.e., any speed except multiples of 8.5° per second in the current simulation setup of 36 single cones per square degrees and simulation time step of 20 msec. But, since stimulus movements in space are continuous and SPs of interest to us are relatively large compared to the inter-cellular distance, we can approximate the continuous representation of

[1] Actually, an array to represent SP is a little larger than both RI and SC since to convolve with a non-unit size RI spatial kernel to produce a given size RI means a bigger SP.

the SP with the current representation by interpreting a fraction in a cell of the SP-array to mean not the fraction of intensity of the local area, but a fraction of area with the same intensity as one of its four neighboring cell. So, you might think of those SP and RI representations as representing light intensities falling at the outer segment for a given photoreceptor with the corresponding spatial location. It will be more realistic if we use a variation of *sigmoidal* function rather than a linear mapping between the positional information and the fraction of light intensity because there are inter-call gaps where light illumination would not affect the phoreceptor responses.

The currently available types of SP are as follows:

1. a disc of variable diameter and intensity [Werblin and Dowling, 1969; Matsumoto and Naka, 1972];
2. an annulus of variable inner and outer diameters, and intensity [Werblin and Dowling, 1969; Matsumoto and Naka, 1972];
3. a disc surrounded by an annulus of any diameters and intensity [Werblin and Dowling, 1969; Matsumoto and Naka, 1972];
4. a rectangular bar of variable width, height and intensity [Schürg-Pfeiffer and Ewert, 1981]; and
5. two discs of variable size separated by a variable distance [Krüger and Moser, 1973].

Also, any value of the background illumination intensity can be specified as well as any level of random noise in the background [Ewert, 1980]. A frog's retina may receive an image up to 180° horizontally and 180° vertically [Fite, 1973]. Current implementation of SP generation allows any size SP to be generated. However, since the current implementation for the model represents a 16° by 16° SP and the related retinal patch, it would make no difference to have a static

SP which is larger than the limit. Figure 1 shows the types of stimulus patterns mentioned.

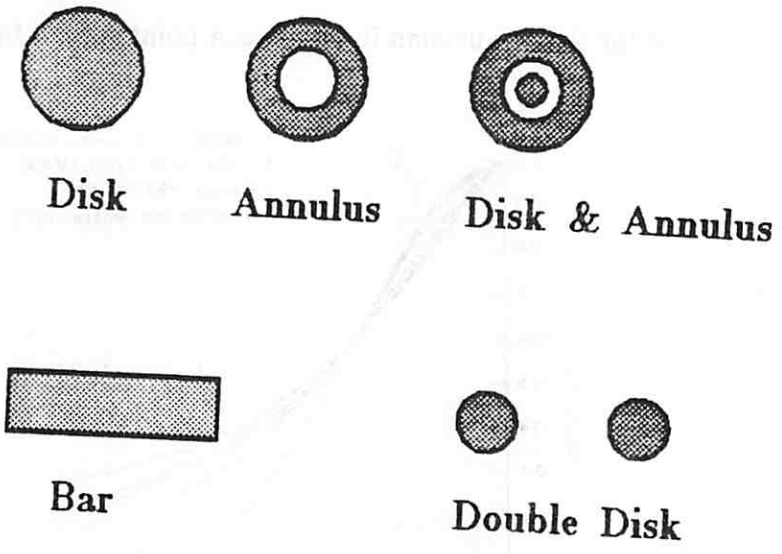

Figure 11: Types of Stimulus Pattern: Typical stimulus patterns projected to vertebrate retina during physiological and ethological experiments, which will be graphically generated for the model.

Model for the Optics and Retinal Image Formation

In this section, we are going to discuss first the model used to represent eye optics, and then the simulated results.

Model for the Optics

The point spread function of the frog optical apparatus can be approximated by a two dimensional Gaussian function [Krüger and Moser, 1973; du Pont and de Groot, 1976b]. The matching σ for the Gaussian function is approximately 0.5° [34' and 37' for spot and square stimuli respectively: du Pont and De Groot, 1976]

for the Modulation Transfer Function(MTF) for the eye of frog, *R. Esculenta.* We use the 2-D Gausssian function as a point spread function because its Fourier

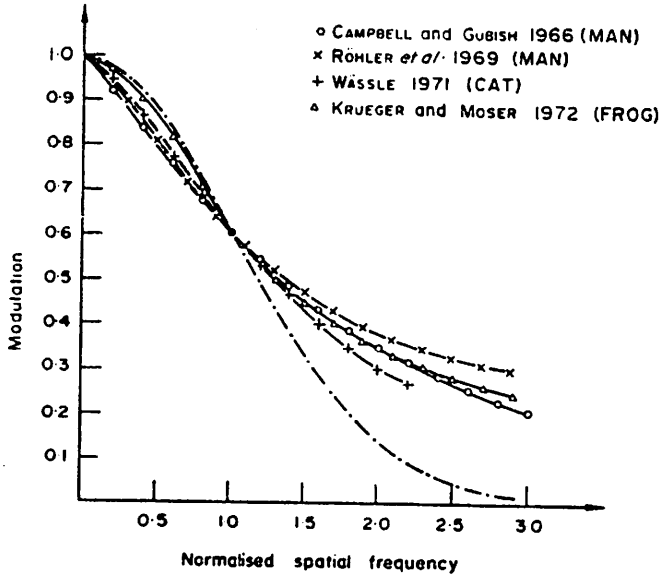

Figure 12: The MTF's of man, cat and frog, compared with Gaussian Function (·····). The individual parameter σ is the unit of the abscissa. Crosses, circles and triangles are characterizing signs. From Krüger and Moser [1973].

transform is also a Gaussian function which simplifies transfer of the measured parameter to the model parameter, and because it shares with other convolutions representing the dendritic influences the same form of functional computation. Figure 2 shows the MTF of frog compared with a Gaussian function.

In the Model, the retinal image is formed by convolving the stimulus pattern with a spatial kernel that is approximately a 2° by 2° two-dimensional discrete Gaussian function.[2] Figure 3 (a) shows a schematc diagram for the retinal image formation in the model, while Figure 3 (b) shows a dense spatial kernel and Figure 3 (c) shows a coarse spatial kernel. In the diagram, the light emanating from

[2]The 2° by 2° size of the kernel was chosen as an approximation. Considering the current value of σ, it appears to be a reasonable while efficient compromise.

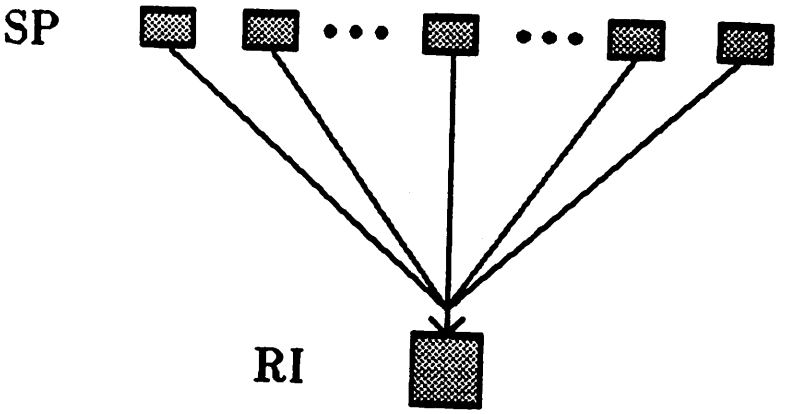

(a)

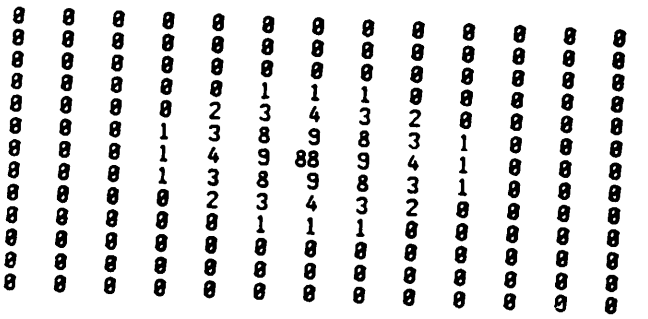

(b)

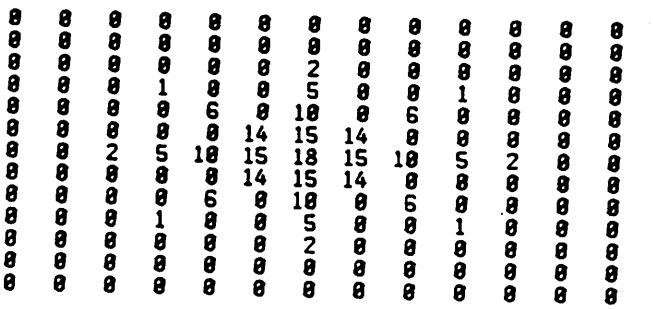

(c)

Figure 13: (a)Connectivity diagram for the retinal image formation. (b)Dense spatial kernel, the total of whose individual elements is multiplied by 256 and rounded for the purpose of display. (c)Coarse spatial kernel.

the external stimulus and its surroundings, represented by *SP[i,j,k]* – Stimulus Pattern at location *(i,j)* and at time k – passes through the optical apparatus of the eye and becomes the retinal image, represented by *RI[i,j,k]*, Retinal Image, at the outer segment layer (of the photoreceptors). Since minimal time delay exists between a stimulus pattern and the resulting retinal image, the algorithm to compute the retinal image from a stimulus pattern can be described as follows using the notation explained in chapter 3.

Algorithm

$$RI_t = K_{ri} * SP_t$$

$$K_{ri} : Cor(dia = 2°, \sigma = 1/3°)$$

$$\text{or } K_{ri} : Den(dia = 2°, \sigma = 1/3°)$$

Currently coarse sampling is used to improve the computational efficiency. The three parameters that govern the characteristics of the spatial-kernel of the point spread function are: (1) σ, (2) *dia* and (3) sample type (dense or coarse). Also, the Model includes a provision that allows skipping the retinal image formation process in order to replicate the experimental setup where light directly illuminates the retinal surface in cases when the ocular media of the eye has been cleared off for the purpose of experiments.

Simulations for Stimulation Pattern Generation and Retinal Image Formation

The major stimulus pattern types we will be using in the simulation are the typical stimulus patterns used in most of the neurophysiological and neuroethological experiments as shown in Figure 1: static disc, annulus and both of variable diameters; moving bar of variable speed; and two discs of varing distance.

Discrete stimulus pattern representation may cause problems when the stimulus pattern is not situated directly on top of a group of single cones, which is true almost always because we are dealing with stimuli of arbitrary size and speed. We use a linear mapping from partial illumination on top of a single photoreceptor with a partial illumination to that a whole cell gets. We initially thought a sigmoidal function to be a better alternative since the amount of light illuminated will change more abruptly around the edge of the cell rather than around its central portion. But we chose to use the computationally simpler linear mapping until further analysis is done, while testing the validity of the resulting retinal image using the current mapping. We then must see if the simulated stimulus patterns and the resulting retinal images meet the following questions:

1. Do the simulated stimulus patterns radically differ from stimulus patterns with the continuous representation, i.e., with real pictures or real things, and are the resulting retinal images a smoothed version of what we would expect from stimulus patterns of the continuous representation? These will check how reasonable the discrete stimulus pattern representation is.

2. Are dynamic stimulus patterns, e.g., a moving bar and the corresponding retinal images, simulated as in the real situation? This will give us a chance to check for the mapping since it moves the stimulus by a small amount in discrete time steps.

3. How do the resulting retinal images of two stimuli, for example discs, of decreasing distance appear? This should tell us about the resolution of the model dioptric apparatus.

4. How different are simulated retinal images from the different types of kernels of the same stimulus patterns? This would tell whether the computationally efficient *coarse* kernel is a reasonable substitute for the smoother *dense* kernel.

Results of simulation. Figure 4 shows stimulus patterns and the corresponding retinal images using both a dense and a coarse kernels. The first row shows stimulus patterns for a disc of diameter 1°, annulus of outer diameter of 3° and inner diameter of 1.5°, and superimposition of the above two stimulus patterns. The second row shows the resulting retinal image using a dense kernel, while the third row shows the resulting retinal image using a coarse kernel. This figure shows that the retinal images becomes much smoothed from the rather rough representation of stimulus patterns. The simulated retinal images using dense kernel are more faithful to the stimulus patterns displaying more angled edges, while those using coarse kernel display more rounded edges. The reason will be discussed in the next section.

Krüger and Moser[1972] calculated the influence of the MTF of the dioptric apparatus upon the retinal image in *Rana esculenta*. As shown in Figure 5, for a disc of 1° diameter, the maximum intensity is approximately 80 percent of the original stimulus. The current simulations shows it to be more than 80 percent, i.e., the model's optics is better than *R. esculenta*'s as calculated by Krüger and Moser [1972] at least in the central portion of the resulting image. Also, note that the single parameter 2-D Gaussian function approximation of a point-spread function of the eye optics would result in a rather peaky representation of the Point Spread Function (PSF) which can be inferred from 1-D Gaussian function compared with real eye optics shown in Figure 2.

In Figure 6 we see two 1° diameter discs separated by decreasing distances from the center of one disc to that of the other disc of 1.75°, 1.5°, 1.25° and 1°. As can be observed, two completely separate discs at a distance of 1.75° appears as one elongated object with two peaks at the top pair of stimulus pattern and retinal image. Here two discs in the stimulus pattern should not overlap, but the current stimulus pattern representation also includes positional information of SP and RI in relation to the photoreceptor locations. Our simulation results show that the maximum retinal illumination intensity at the 0° location is 0.9

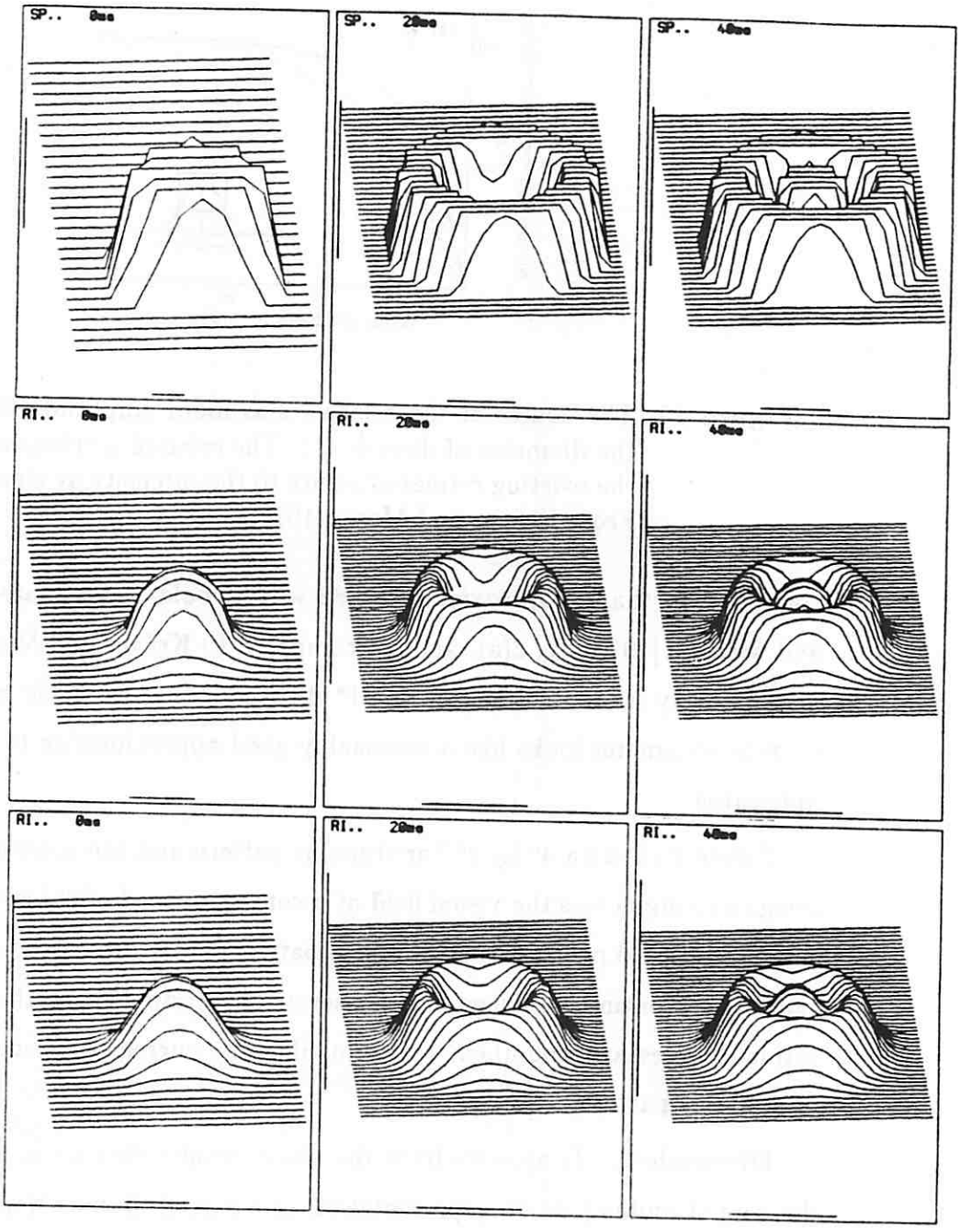

Figure 14: The top row shows stimulus patterns of a disc, an annulus and a superimposition of the two. The second and the third row show the simulated retinal image using a *dense* kernel and a *coarse* kernel respectively.

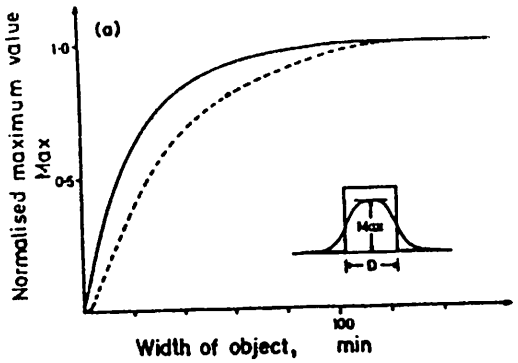

Figure 15: The course of the relative maximum amplitude depending on the diameter of discs (- - -). The relative amplitude is a ratio of the existing retinal intensity to the intensity at ideal conditions. From Krüger and Moser [1972].

compared to that of aprroximately 0.82 which could be estimated from Krüger and Moser's [1972] Fig.2(a), and 0.3 compared to Krüger and Moser's [1972] 0.3 at 0.5° away from the location for 1° disc. So, the eye optic model with the current parameter looks like a reasonably good approximation to a frog dioptric apparatus.

Figure 7 shows a 4° by 2° bar stimulus pattern and the corresponding retinal image moving across the visual field at a constant speed of 8°/sec. Note that the representational peculiarity of stimulus patterns which stems from the quantization of the continuous image into a discrete one disappears as the corresponding retinal images are smoothed, which justifies the current discrete representation of stimulus pattern.

Discussion. It appears from the above results that we can safely use the discrete stimulus pattern representation and partial illumination mapping with the coarse 2-D Gausssian kernel to simulate the real frog eye dioptric apparatus.

For the eye optics simulation of creating retinal images that would illuminate at the outer segment of photoreceptors, we use convolution of the stimulus pattern with a 2-D Gaussian filter with no time delay assummed. As mentioned in the last

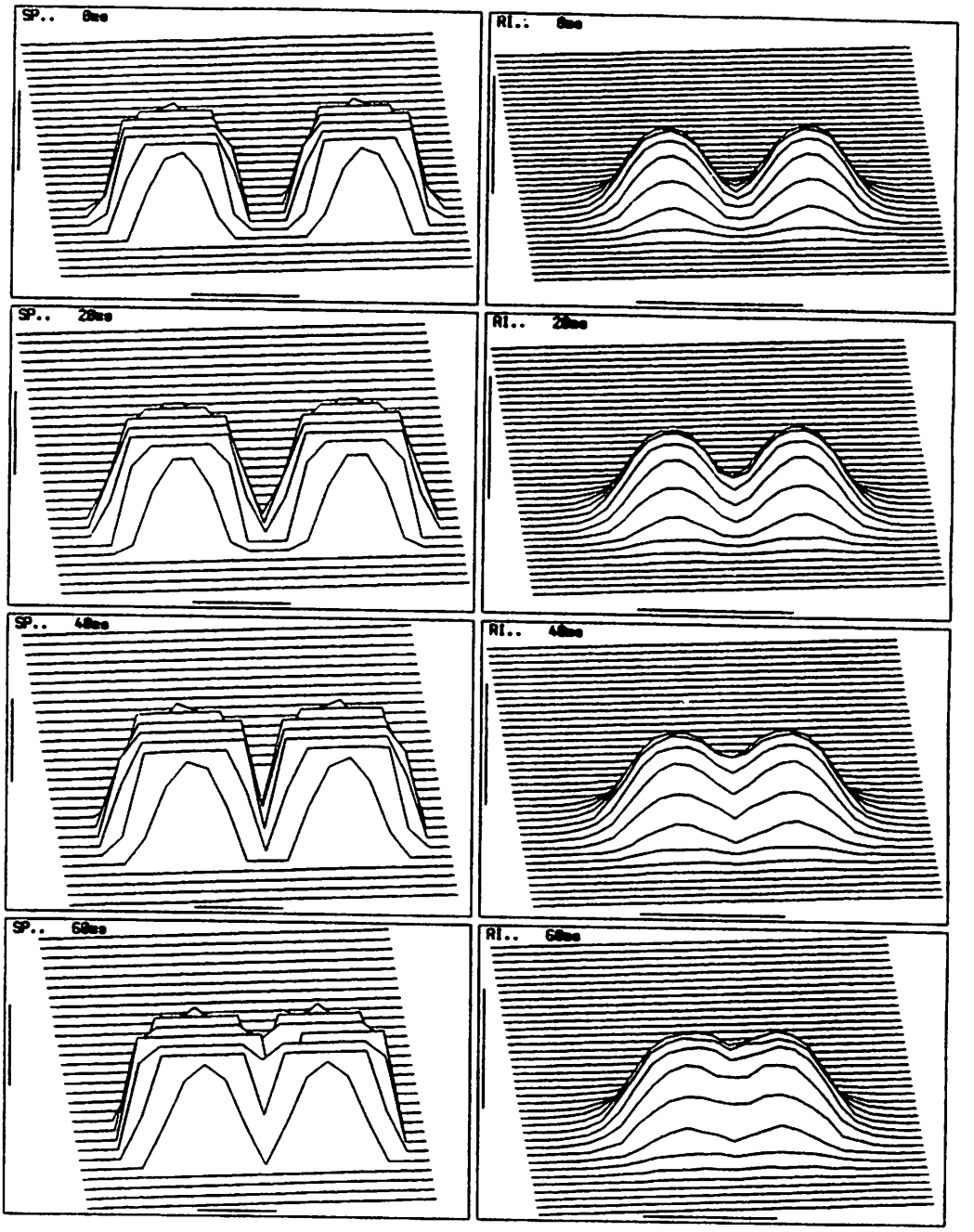

Figure 16: Two discs (1° diameter each) of decreasing separation and the corresponding retinal images. Note a vertical and a horizontal bar which shows a scale and relative location in the layer.

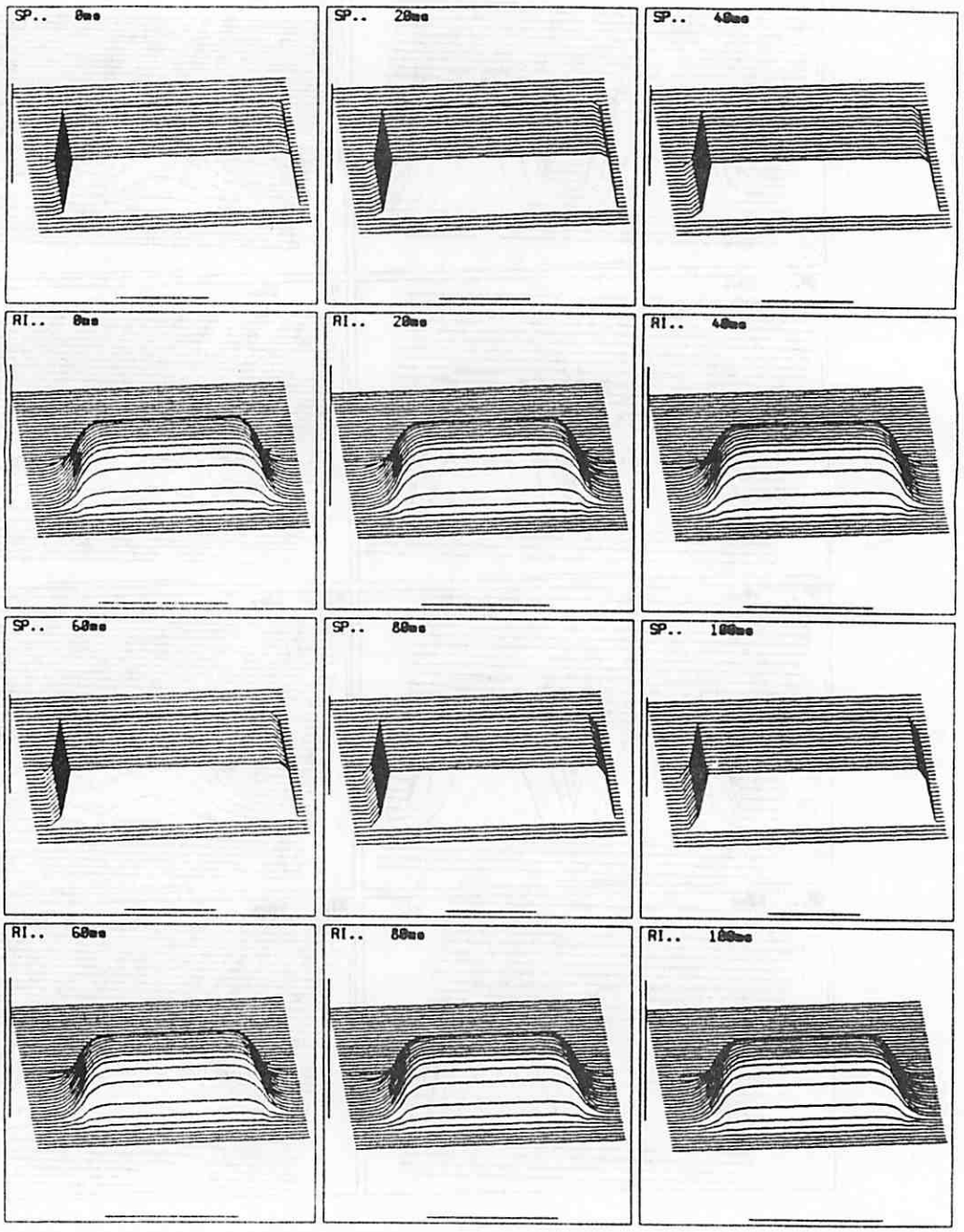

Figure 17: A moving bar (4°x2°) stimulus pattern moving across the visual field at a constant speed of 8°/sec from left to right and the corresponding retinal image.

chapter, we have two filters: one called a *dense* kernel and the other called a *sparse* kernel. We use a *sparse* kernel for most of the simulation because it produces a retinal image almost as good as the other while saving a lot of computation. So, unless otherwise mentioned all the following retinal images are simulated using the sparse kernel. Note that the two kernels could produce quite different results because of the way the distribution of the weights are set up. The central element in the dense kernel gets much greater weight than the corresponding one in a coarse kernel. This is the main reason why the retinal images simulated using a coarse kernel produced smoother image compared to those using a dense kernel as shown in Figure 4.

The small differences between the measured data and the simulated data are due to the Gaussian function approximation of the point spread function [Krüger and Moser, 1973]. For example, at value 2 in the normalized spatial frequency of figure 2 the theoretical difference becomes big enough to suspect that the Gaussian function is not suitable. This problem becomes worse as the spatial frequency gets higher, i.e., finer details have to be resolved. But, fortunately we are not concerned about minute details in the stimulus patterns or in the retinal images, but rather interested in stimulus patterns whose diameter or length is usually 1° or bigger. Also, the intensity-vs-response curve for photoreceptor(single cone) is characterized by a rather insensitive response at the extremities of the illumination intensities, therefore the current representation doesn't appear to cause any problem with the current simulation situations while offering an efficient method for computation.

CHAPTER V

SINGLE CONE, HORIZONTAL CELL AND BIPOLAR CELL LAYERS

Single Cone Layer

Modelling of the Single Cone Layer

The model assumes no coupling between cones. Support for the assumption comes from several studies as mentioned in chapter 2. The present model assumes no feedback loop between cones and horizontal cells, although others have suggested that feedback loops play an important functional role in the OPL and horizontal to photoreceptor synapses were found in the catfish retina [Sakai and Naka, 1983]. So, in the present model the single cone is regarded as affected only by its past history and the light incident upon it. Interaction with other cones

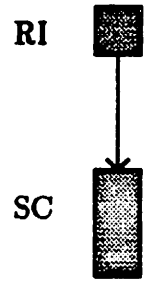

Figure 18: Connectivity diagram for the single cone model. Note that the single connection from RI to SC means that the only external factor that can change a single cone's response is the retinal image that illuminates it.

and feedback from horizontal cells are assumed to be nonexistent in the model.

Figure 18 shows a connectivity diagram for the model cone.

Cone adaptation is an important function and many have made it their focal research concern. For example, Baylor and Hodgkin [1974] and Baylor et al. [1974b] in their model of the turtle cone; Carpenter and Grossberg [1981] in their alternative model to Baylor et al. [1974b]; and Fein and Szuts [1982] in their discussion of photoreceptors. However, as mentioned before, these adaptational effects are not included in the current model in order to limit its scope so that more effort can be spent on the study of the connections with in a network organization rather than studies of individual cell reponse characteristics. By ignoring adaptational effects, any given simulation in its entire duration deals with only one intensity versus response curve for the peak and another for the steady state rather than a family of curves.

Figure 19 shows two intensity versus response curves for the model single cone [Rodieck, 1973; Fein and Szuts, 1982]. One curve is for the peak response potential and the other is for the steady state, and both are assumed to be sigmoidal functions of the following form:

$$\Delta V/\Delta V_{max} = I/(I + I_{half}),$$

where ΔV represents the potential change in the photoreceptor cell, ΔV_{max} the maximum potential change that is possible at the adaptational state which is assumed to be 1 in our case of no adaptation, I the illumination intensity, and I_{half} the light intensity which would cause the cell to hyperpolarize up to half the maximum amount.

The dynamics of the hyperpolarization involving the peak is algorithmically defined, and can be thought of as simulating the blocking of the putative Na^{++}-channels in the cell membrane of the outer segment of the single cone [Fein and Szuts, 1982; Rodieck, 1973]. Once overshoot to the peak hyperpolarization occurs, the cone is assumed to behave like a leaky capacitor to reach the steady state during illumination, and likewise to go from the steady hyperpolarization to the

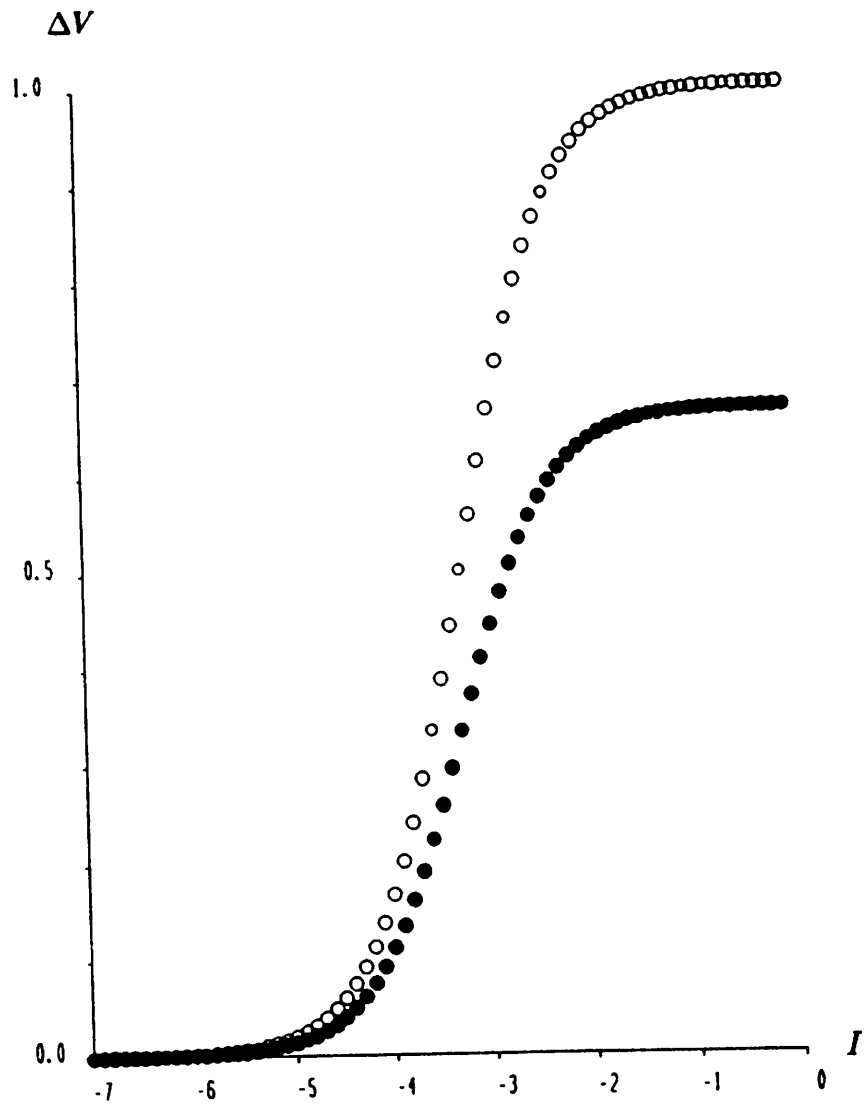

Figure 19: Intensity vs. response curves for the model single cone. Open circles represent the level of peak responses, while filled circles the level of steady state responses.

dark level upon the cessation of illumination.

Algorithm

$$SC_t = \begin{cases} W_{sc} \cdot SC_{t-1} + W_{sc}^{-} \cdot STDY_{t-1}^{-}, & \text{if } TSC_t = 0; \\ SC_{t-1} - SC_{t-1} \cdot PEAK_t^{-} \cdot (6 - TSC_t)/6, & \text{otherwise.} \end{cases}$$

$$STDY_t = \frac{2}{3} RI_{t-1}/(RI_{t-1} + RI_{half})$$

$$PEAK_t = RI_{t-1}/(RI_{t-1} + RI_{half})$$

$$TSC_t = \begin{cases} TSC_{t-1} - 1, & \text{if } TSC_{t-1} > 0; \\ 5, & \text{if } (TSC_{t-1} = 0) \text{ and } (RI_t > 10RI_{t-1}); \\ 0, & \text{otherwise.} \end{cases}$$

Currently $W_{sc} = 0.75$ is used. The decision is based upon the observation of the decaying (depolarizing) characteristics of intracellular recordings of photoreceptor cells [Werblin and Dowling, 1969; Cervetto, 1976]. TSC_t approximates the progress of photoisomerization subprocesses (of around seven in number) and its maximum value of 5 determines the number of time steps to peak. 10 is chosen as the value of the threshold of detection of changes in light illumination, since psychophysics indicates that it requires a difference of about one log unit for us to begin to perceive illumination changes.

The maximum value of the steady inhibition is assumed to be 2/3 of the peak hyperpolarization. Note that $PEAK_t$ and $STDY_t$ activities range from 0 up to 1 and 2/3, respectively (rather than from 1 down to 0 and 1/3, respectively) while the eventual cone cell potential ranges down from 1, i.e., it hyperpolarizes. RI_t is the light intensity in the model at time t and corresponds to I of the equation for the intensity versus response curve, while SC_t to ΔV, 1 to ΔV_{max} and RI_{half} to I_{half}, where RI_{half} is assumed to be 0.0075.[1]

[1] Presumably, frog single cones have their operating range of about six log units with their most

Simulations for Single Cone Layer

Since neither coupling between single cones nor feedback pathway from horizontal cells to single cone are assumed in the model, the only external stimulus to the single cone model is the light directly illuminating it and the only other influence on its current value is its past internal states.

We first would like to find out whether model single cone responses to different light intensities actually follow what are usually observed and characterized in the form of intensity versus response curves as examplified in the last subsection.

Secondly, we would like to check whether the simulated responses to the same light illumination with different duration approximate observed responses.

Thirdly, we would like to see how a single cone will respond to a surround illumination with or without a central illumination as compared to a central illumination.

Since no adaptation in the photoreceptor is modelled, we have to set the parameters of the individual single cone such that the simulation can be consistently performed under a given adaptational state. So, it is important to select I_{half} value consistent with the given simulation at hand. We assume that adaptational state does not change for the duration of our various simulations, which are relatively short for the substantial amount of adaptational processes to take place. In the following simulations, the I_{half} has been fixed to 0.00075 to simulate dark-adapted meso-photopic situations.

Result of simulations. In Figure 20 we use the temporal pattern for the stimulus pattern as the retinal image. This is because most intracellular record-

---

sensitive range changing according to their adaptational states. An arbitrary value of 0.0075 is currently chosen to signify the semi-photopic conditions under which the model is running for most of the quantitative data simulations for ganglion cells with lighted background, but that needs to be changed depending on the specific simulation environment to reflect the particular adaptational levels of the single cones involved in the experimental set up.

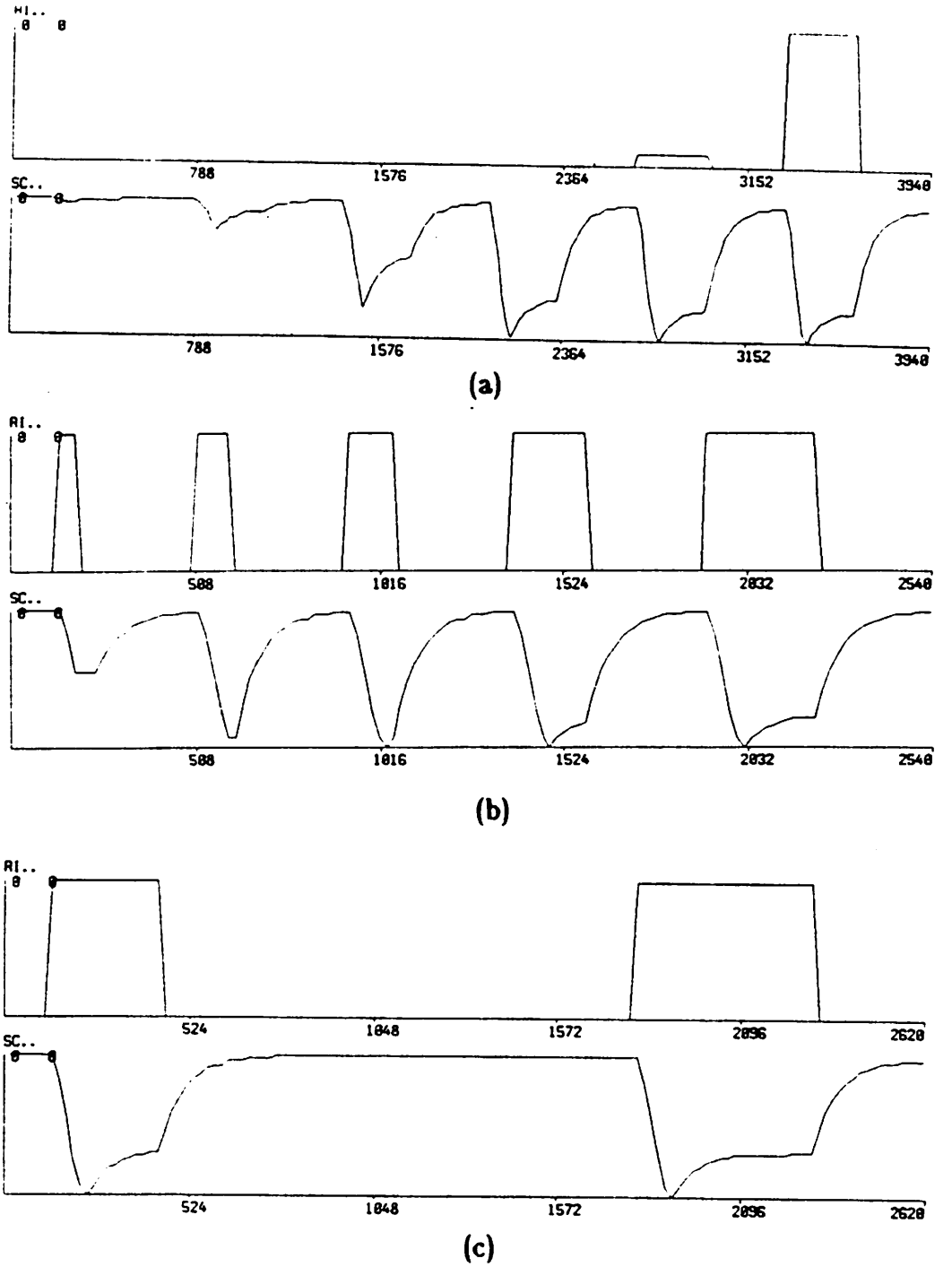

Figure 20: (a)Discs of increasing intensities with same duration. (b)Discs of increasing duration with same intensity. (c)Temporal pattern of SP, RI and SC.

ings of the photoreceptors are performed without the ocular media [Baylor et al., 1974b] or with it partially removed [Werblin and Dowling, 1969]. The model can be used with or without the formation of retinal image so that we can easily simulate both experimental situations. As can be observed, the typical single cone response to a sudden light illumination as can be seen in Figure 20 (c) follows almost immediately upon the retinal image (in the simulation, it appears our time step of 20 msec later). Then after about 80 msec of steep hyperpolarization, the response slows down to a peak hyperpolarization after about another 40 msec. After reaching the peak, it slowly depolarizes to the steady-state response of the photoreceptor that is determined by the illumination intensity. Once the illumination ceases, the photoreceptor slowly depolarizes towards the dark level of the photoreceptor.

Figure 20 (a) shows how a single cone model responds to a set of different normalized illumination intensities where 1.0 means the saturating light intensity for any adaptational state of the single cone whereas 0.0 means the other extreme: 0.00001 to 1.0 in step of 10 times brighter illuminations. Because of the high sensitivity of the single cone response, while we cannot detect and the graphics can not show the difference of magnitude in retinal image intensities other than 0.1 or 1.0, the single cone response to these stimulus with different intensities clearly show different responses. As expected I=0.00001 causes little reaction, while that of 0.0001 causes a substantial response. And the sudden change of the magnitude in single cone response between retinal image values of 0.0001 and 0.001 tell us that I_{half} is between these two numbers. Any illumination intensity greater than 0.001 will evoke an almost saturating response.

Figure 20 (b) shows how a single cone model responds to the same light illumination with a different set of durations before the cessation of the illumination. Here the durations are of 40, 80, 120, 200, 300 msec in sequence between uniform interval gaps of 300 msec for single cone recovery to the dark-level depolarization.

As can be observed in Figure 20 (a) and (b), the model doesn't show temporal

summation for short flashes of light illumination, which is well demonstrated by Hood and Grover [1974] in frog photoreceptors. But, at this stage in the model we are more interested in the neural network organization than in subtle details of an individual cell response characteristics.

Figure 20 (c) shows the model cone response to a spot illumination followed by an annulus illumination, and then a spot illumination with an added annulus illumination. The response shows that there is no response to an annulus illumination as expected from no coupling and no feedback assumptions, and the same response from a spot illumination with or without an added annulus illumination.

The temporal response characteristics were chosen instead of the exact replica of the available response pattern because most of the simulation follows the experiments of Werblin and Dowling [1969] and we didn't have single cone response under the same experimental conditions. The model's single cone response is much faster than that of mudpuppy rods since rod response is generally much slower than that of cones, and also because frog's cell response appears [Matsumoto and Naka, 1972] to be quite faster than those of mudpuppy cells. We chose to model the temporal pattern of the single cone as shown in Figure 21 (b) after that of a turtle cone as observed by Cervetto [1976] as shown in Figure 21 (a) mostly because it show essentially the same shape with much faster response which is characteristic of cone response.[2]

Discussion. Currently we use an algorithmic approach to curve-fitting the temporal response pattern of single cone. We use a time constant, which is currently 0.75, to control the decaying (depolarizing) slope of the model single cone response. The other constant to control the slope of the temporal curve is "TSC" in the model, whose current maximum value is 5, which determines how steep is the hyperpolarizing transient from the dark-level, which at the same time

[2]Of course, there are gap-junction mediated signal propagation between cones in the turtle, but not in the model. Figure 21 (a) is a response to a 100 μm spot illumination when coupling influence is negligible.

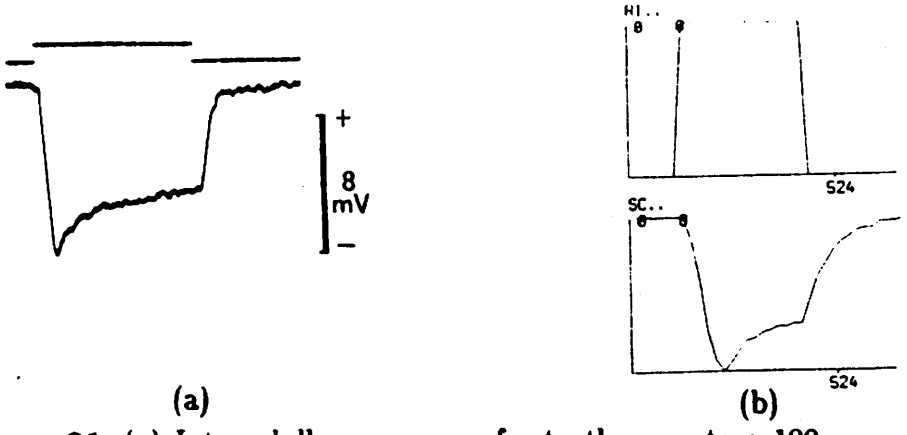

Figure 21: (a) Intracelullar response of a turtle cone to a 100 μm spot illumination when coupling influence is minimal. From Cervetto [1976]. (b) A sample single cone model reponse to a spot illumination.

determines the time-to-peak. It is determined mainly to have 120 msec of rise time to peak hyperpolarization. And by initializing I_{half} between 0 and 1, we can adjust the (fixed) sensitivity of the single cone. But note that for the most part of our simulation, any light intensity over 0.01 will in fact produce almost the same effect as the full saturating light intensity of 1. It means that for our purpose the exact value of I_{half} does not matter and with a given I_{half} and for most of cases small intensity variation will not influence the output of single cone model at all, which means that this single cone model is sensitive to only a range of medium light intensity values.

Another observation that should be noted is that Figure 21 (b) shows a very slow depolarizing characteristics at the final stage of the depolarization. This is an inherent of the basic leaky-capacitor model. Compared to these two in Figure 21, Figure 7 in chapter 2 shows a mudpuppy photoreceptor response, presumably a rod response, which is much slow.

For better single cone temporal response patterns including the adaptational effects, we can either devise or borrow a more elaborate adaptation model of the single cone/photoreceptor such as Baylor et al. [1974b] or Carpenter and

Grossberg's [1981], or we can improve upon the current single cone model by adding functions that change the values of I_{half} and ΔV_{max}, which are mentioned in the modelling subsection, as functions of time and intensities of past light absorption of the photoreceptor.

Horizontal Cell Layer

Modelling of the Horizontal Cell Layer

As has been been reviewed in Chapter 2, Cajal [1893] characterized the *inner* horizontal cell with its smaller dendritic tree from the *outer* horizontal cell. The former is assumed to be connected to cones in the model following the general principles of convergence in the rod-pathway and less-convergence in the cone-pathway [Kandel and Schwartz, 1981]. Flat mounts of frog horizontal cells [Shantz, 1976] suggests 60 μm (a little less than 1° in visual angle) as the approximate dendritic diameter of the horizontal cell.[3]

There seems to be at least one lateral interaction, direct or indirect, between horizontal cells, through presumed gap junctions, which we have to take into consideration as a proviso to the basic assumption on the nonexistence of inter-photoreceptor connections or horizontal cell to photoreceptor feedback circuitry [Sakai and Naka, 1983]. The physiological evidence for the lateral interaction between horizontal cells is that they react to a light stimulus several times beyond their dendritic reach [Naka, 1972]. Naka [1972] compared the size of a horizontal cell with its response range as shown in Figure 22. It is suggested that a row of horizontal cells behaves electrically as if it is equivalent to a laminar conducting medium bounded by a pair of parallel high resistance membranes, and this phenomenon is due to inter-horizontal cell gap junctions.

[3]Cajal's vertebrate retina diagrams do not have size specifications, and do not show the flat-mount view, which makes it difficult to read symmetry in the horizontal plane.

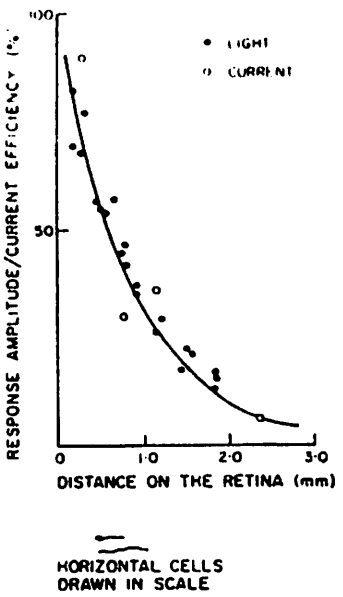

Figure 22: The decay of potential in the catfish S-space as a function of distance from the stimulus spot (closed circle), and approximate sizes of two classes of horizontal cells. From Naka [1972].

In the model, the spatial kernel for horizontal cells is approximated by a two-dimensional Gaussian function. We can roughly approximate the contribution that a synapse at one point in the dendritic branch makes to the soma potential by utilizing cable theory, but it is very difficult to determine all the quantitative synaptic densities for a given horizontal cell from the cells in the previous layer, i.e., single cones. Observations of synaptic contacts resulting from three dimensional reconstruction from EM studies appears to be the only reliable method to determine the quantitative synaptic densities, which could be applied to every major cell and their subtypes in the retina [Kolb, 1979]. Horizontal cells integrate local output signals from single cones and interact among themselves.

Figure 23 shows the connectivity diagram and its kernel for the horizontal cell model. The dynamics of the horizontal cell potential is modelled after a one-parameter leaky-capacitor with a slow time constant.

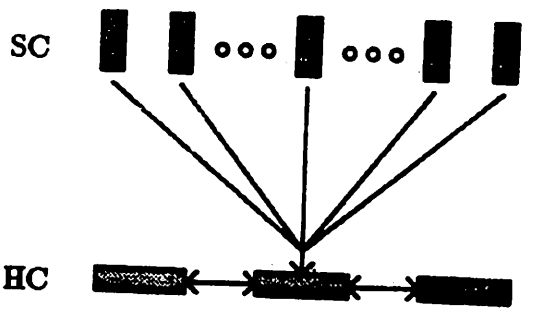

(a)

0	0	0	11	0	0	0
0	11	0	12	0	11	0
0	0	12	12	12	0	0
11	12	12	12	12	12	11
0	0	12	12	12	0	0
0	11	0	12	0	11	0
0	0	0	11	0	0	0

(b)

Figure 23: (a) Connectivity diagram for the horizontal cell model and (b) its spatial kernel. The weights are multiplied by 256 and rounded for diaplay as mentioned.

Algorithm

$$IND_{t-1} = W_{hc} \cdot HC_{t-1} + W_{hc}^{-} \cdot (K_{hc} * SC_{t-1})$$

$$MIN_{surr} = \begin{cases} MIN(left(IND_{t-1}), right(IND_{t-1}), \\ up(IND_{t-1}), down(IND_{t-1})) \end{cases} \quad \text{for cell at location}(i,j).$$

$$HC_t = \begin{cases} W_{conn} \cdot MIN_{surr} + W_{conn}^{-} \cdot IND_{t-1}, & \text{if } MIN_{surr} < IND_{t-1}; \\ IND_{t-1} + W_{conn}^{-} \cdot (MIN_{surr} - IND_{t-1}), & \text{otherwise.} \end{cases}$$

$$K_{hc} : Den(dia = 1°, \sigma = 6°)$$

The current value of 0.9 for W_{hc} signifies the slow rate of change horizontal cells respond to external changes, $dia = 1°$ represents the approximate dendritic tree diameter for an average *inner* horizontal cell, and $\sigma = 6°$ represents the relative ease of ion conduction to occur within the horizontal cell. In the equation, IND_{t-1} is used as a buffer to store an individual contribution to the cell's potential for

the next time step, whereas HC_t integrates this individual contribution with those from the four neighboring horizontal cells'. The summation with the four neighboring horizontal cells in the algorithm described above represents the gap junction effect where propagation of current occurs. The underlying assumption for this was that gap junctions exists between horizontal cell bodies rather than through dendritic junctions with a cell body or another dendrite. And the ease of the ionic flow between these gap junctions are represented by $W_{conn} = 0.95$ in the model.

Simulations for the Horizontal Cell Layer

Three simulations were performed for horizontal cells of the model in this section. The first simulation shows temporal responses of the horizontal cell compared to those of other cells to typical stimulus illumination such as disc, annulus or both.

The second simulation concerns the passive propagation property of the electrical potentials between horizontal cells. It is described quantitatively in Naka [1972] as: $V = V_0 e^{-x/a}$, where V_0 is the cell potential at the location of illumination, V the decayed potential x mm away from the location and a is the space constant which is approximately 0.25 mm for the tench and between 0.5 mm and 1.0 mm for the catfish. Figure 22 shows the decay of the potential in the catfish S-space as a function of distance from the site of the stimulus (closed spot). Note that a substantial amount of potential is detected in a location several times the size of the horizontal cell dendritic diameter away. Since the dendritic tree diameter of the model horizontal cell is 1°, we will assume the spot of light be 1° so that the horizontal cell directly under illumination will get the maximum activation from its single cone inputs. In this simulation a fixed light spot is illuminated while a row of cells at different distances are observed until their response reaches some steady-state. This is hard to do in a real experimental setup since the exact position of light in reference to the observed cell would be very

hard to identify. This approach has the advantage of getting rid of the residual effects such as adaptation of the moving light spots has upon cells illuminated compared to experimental approaches where a single cell is being recorded while the illumination has to be moved [Naka, 1972].

The third simulation duplicates the area effect which, according to Naka [1972], refers to the phenomenon where the amplitude of the S-potential increases as the retinal area illuminated increases up to a certain limit. It can be observed in the intracellular recordings of mudpuppy [Werblin and Dowling, 1969] and frog [Matsumoto and Naka, 1972] among others, and quantified by Naka [1972] by the following equation for small area: $V/V_{max} = I/(I+I_{half})$. And for larger areas the response includes the influence affected from the neighboring horizontal cells. At the present stage of the modelling, we are interested in the ability of the model to at least qualitatively reproduce the two area effects of the horizontal cell: Small and large area effects.

Result of Simulations. Figure 24 (a) shows a single horizontal cell's response to light illuminations of spot and two annuli of different sizes. Note the sluggish response characteristic of these responses. The simulated horizontal cell temporal characteristics to the spot and small annulus stimuli in Figure 24 (b) roughly approximate those observed in Werblin and Dowling [1969], which is shown in Figure 24 (a). But, the simulated horizontal cell response to both spot and annulus illumination does not agree with a similar experiment in that real horizontal cell will produce more hyperpolarization in the horizontal cell compared to a simulated response which is tha same as the response to a spot illumination only.

Figure 25 shows a 1° disc stimulus pattern and the corresponding spatial pattern activities for the horizontal cell layer at different sampled times: 300, 600, 900 msec. This shows that with the same stimulus pattern in place and corresponding single cones being stabilized to their respective steady-state values after a short transient peak, the horizontal cell signals slowly propagate within

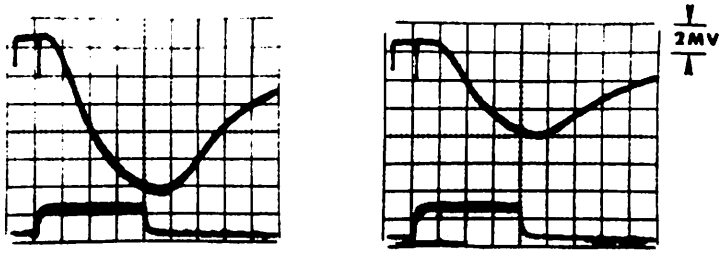

(a)

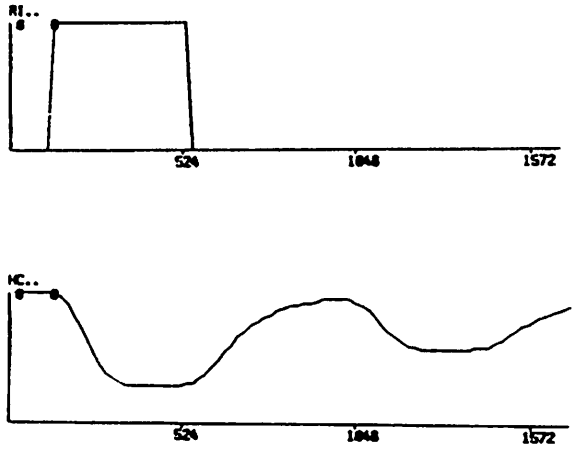

(b)

Figure 24: (a) Intracellular recordings of a horizontal cell response to a spot illumination and and annulus. Modified from Werblin and Dowling [1969]. (b) Temporal response of a model horizontal cell to a spot and an annulus illumination.

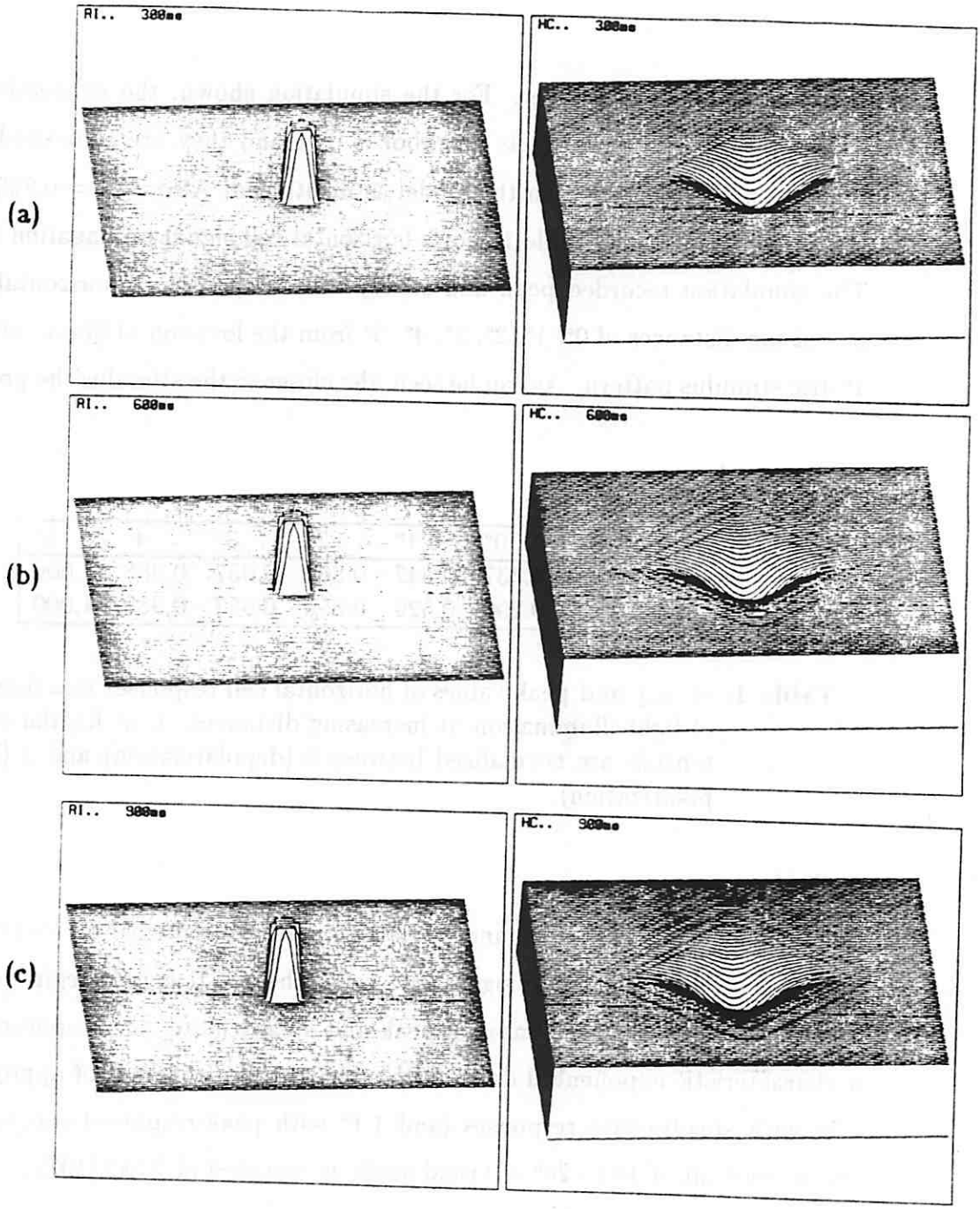

Figure 25: Spatial pattern of activities for a small disc in sequence of timesteps. (a) at time step 300 msec from the onset of spot of light, (b) at time step 600 msec and (c) at time step 900 msec.

the locality of its own layer. For the simulation shown, the connectivity of a horizontal cell W_{hc} towards its neighbor is 0.95 and they are connected only to the closest four neighbors in the model as mentioned. Also, $W_{hc} = 0.825$ was for the above simulation. Table 1 shows horizontal cell signal propagation at work. The simulation recorded peak and steady-state responses of horizontal cells at increasing distances of 0°, 1°, 2°, 3°, 4°, 5° from the location of illumination for a 1° disc stimulus pattern. As can be seen, the closer to the stimulus the greater the

location(h,v)	0°	1°	2°	3°	4°	5°
steady	0.337	0.547	0.867	0.957	0.988	1.000
peak	0.290	0.529	0.855	0.957	0.988	1.000

Table 1: Steady and peak values of horizontal cell responses to a fixed spot of light illumination at increasing distances. Unit for the cell potentials are normalized between 0 (depolarization) and 1 (hyperpolarization).

differences between the peak and the steady state responses and vice versa. It is natural since by the time the signal travels far, the initial signals begin to stabilize and smooth out. In both cases of peak and steady state, the responses display a characteristic exponential decay with a sharp space-constant of approximately 2.5° with steady-state responses (and 1.1° with peak-response) compared to a space constant of 10 to 20° of visual angle as reported in Naka [1972].

Figure 26 shows how a population of horizontal cells responds to a set of similar stimulus patterns of the same intensity but with different sizes. It is obvious that as the stimulus pattern becomes bigger more horizontal cells are affected and also most of the horizontal cells are proportionally more affected by stimulus pattern of the increasing sizes. Table 2 shows the resulting quantitative data about how horizontal cells at different locations respond to disc stimulus

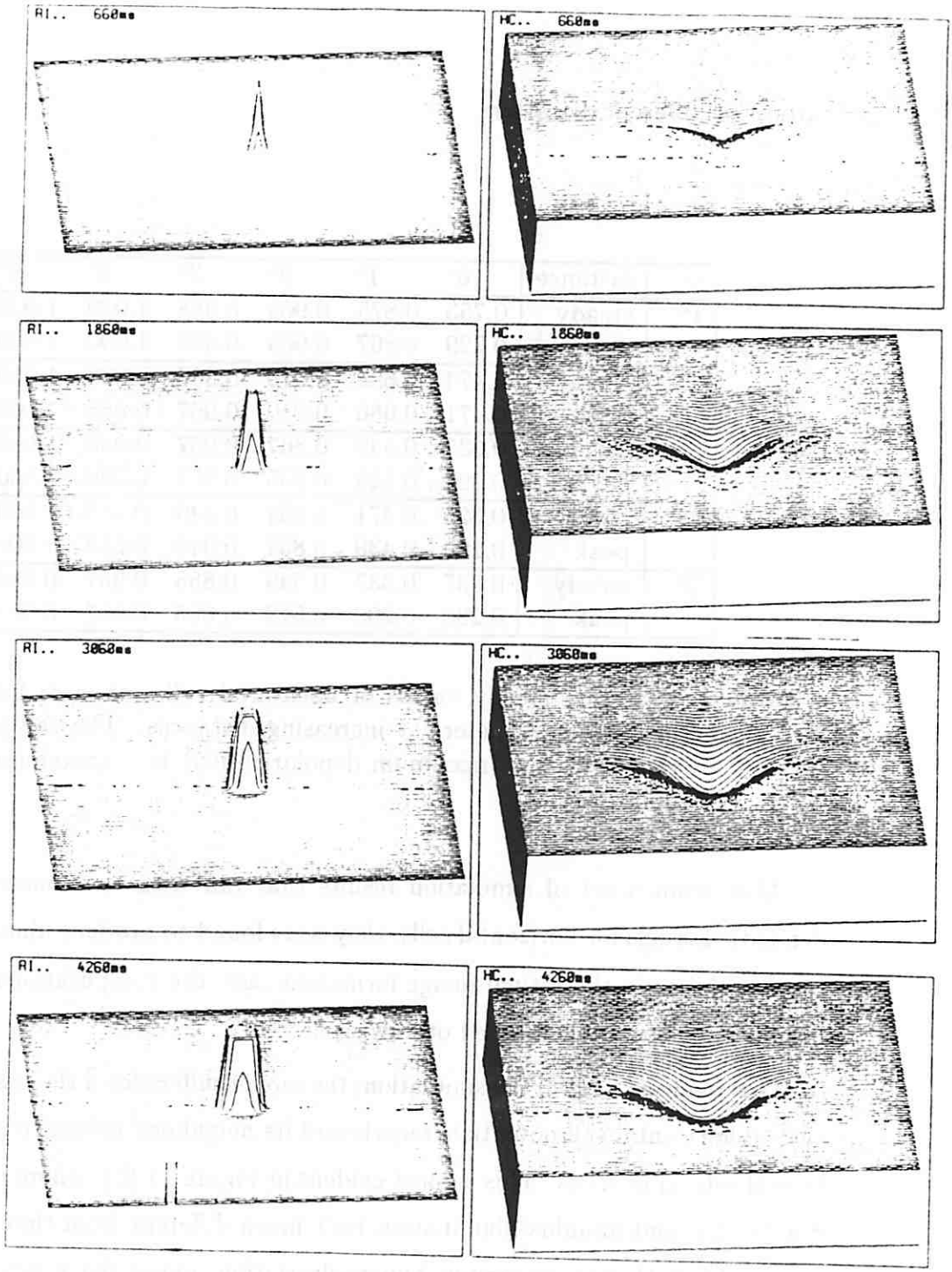

Figure 26: Spatial pattern of HC activities with increasing size.

pattern of different diameters.

size	distance	0°	1°	2°	3°	4°	5°
1°	steady	0.753	0.875	0.965	0.988	1.000	1.000
	peak	0.729	0.867	0.965	0.988	1.000	1.000
2°	steady	0.474	0.698	0.910	0.967	0.988	1.000
	peak	0.471	0.686	0.910	0.967	0.988	1.000
3°	steady	0.337	0.549	0.867	0.957	0.988	1.000
	peak	0.290	0.529	0.855	0.957	0.988	1.000
4°	steady	0.325	0.471	0.831	0.949	0.988	1.000
	peak	0.290	0.439	0.831	0.949	0.988	1.000
5°	steady	0.337	0.337	0.549	0.855	0.957	0.988
	peak	0.290	0.290	0.518	0.855	0.957	0.988

Table 2: Peak and steady values of horizontal cell responses for spot of increasing diameters at increasing distances. The cell potentials ranges from 1 (maximum depolarization) to 0 (maximum hyperpolarization).

Also, from a set of simulation results that ran with the coarse and dense dendritic kernels for horizontal cells, they were found to produce almost identical results. So, as in the retinal image formation case, the computationally efficient form will be used unless noted otherwise.

Discussion. From the simulation, the model suffers from the ease of saturation of horizontal cell potentials regarless of its neighbors' influence as compared to real retinal neurons. This is most evident in Figure 24 (b), where the response due to disc and annulus illumination isn't much different from that due to disc alone. Even though maximum hyperpolarization allows the horizontal cell to reach 0, the hyperpolarization almost never goes below 1/3. This is because the difference in the model single cone's peak and steady state potentials is 1/3 and the horizontal cells with their slow response towards external inputs together with gap junction propagation effect will average the spatial and temporal responses

in the horizontal cell layer.

For the model, (1) W_{hc} determines how fast horizontal cell responds including whether horizontal cell will have any transient peaks, (2) σ used to define its spatial kernel determines the degree to which horizontal cell respond to local single cones, (3) Connectivity W_{conn} determines how far a horizontal cell influences its neighbors and is influenced by them reciprocally. The value of W_{conn}, which for the current set of simulations ranges from 0.9 to 0.95, represents the propagation efficiency. The value of 0.9 is taken to mean that electrical coupling through the gap junction faces normalized 0.1 resistance for the signal to pass onto the next cell or the electric charge has 0.9 admittance. It appears to be a very economic way of communicating as well as a good way of averaging out local differences, although it takes some time to influence its far neighbors.

Naka [1972] shows that for small area effects follow the Naka-Rushton equation. It is rather obvious since we can think of the small area effect as arising from the direct connections from neighboring single cones to a given horizontal cell. The current model fails to explain the large area effect almost completely.

A recent model by Usui et al., [1983] reproduces the area effect for a set of stimulus with different sizes. It seems the major difference between the current model and Usui's appears to lie in the so-called cell unit. The model restricts its horizontal cell to communicate with its neighbors only with its nearest four neighbors which in turn seriously restricts the efficiency of the communication. In terms of CU, the model treats a single horizontal cell as a CU. So, it is strongly suggested that horizontal cells have gap-junction-like communications for much bigger areas, perhaps through dendritic junctions compared to current assumptions.

So, we tried a new set of simulations with a new hypothesis of gap junctions being located in dendrites. The preliminary results show that the propagation improves dramatically and so the transmission of signals to distant cells and faster averaging effect of horizontal cell potentials. But this still does not solve

the problem of horizontal cell saturation, which happens to horizontal cells under direct illumination without being affected by other cells. So, it appears that we have to modify our horizontal cell model to one which needs its inputs by both single cones and neighboring horizontal cells to saturate rather than the curent version where single cone is the dominating factor if the cell is under illumination.

Bipolar Cell Layers

Modelling of the Bipolar Cell Layers

Even though there are some well-founded cone pathway models which relate the physiological classes of bipolar cells to the synaptic contacts at the outer plexiform layer in cat's retina [Nelson et al., 1981] and in the catfish retina [Sakai and Naka, 1983], it is not at all sure that those same models are applicable to the amphibian retina. Lasansky [1978], for one, indicated that the same models do not hold in the case of the salamander retina. Figure 6 in chapter 2 showed some of the intracellular recordings from bipolar cells in a mudpuppy retina [Werblin and Dowling, 1969]. The present model assumes two subtypes of bipolar cells described by their characteristic pathways and signs as follows:

1. A hyperpolarizing bipolar cell with concentric center/surround receptive field (HBC) which receives sign-preserving inputs from the local cones[4] for the central portion of its receptive field (RF) and sign-reversing inputs from the less local horizontal cells for its overall RF, and

[4] Photoreceptors, in this case cones, depolarize during dark conditions outputting their synaptic transmitters, while they hyperpolarize under light illumination reducing the output synaptic transmitters. Horizontal cells output their transmitters in the same way, thus displaying the sign-preserving property of their receptors. Bipolar cells, on the other hand, vary in their receptor properties depending on their subtypes [Stell et al., 1977].

2. A depolarizing bipolar cell with concentric center/surround receptive field (DBC) which receives sign-reversing inputs from the local cones for the central portion of its RF and sign-preserving inputs from the less local horizontal cells for its overall RF.

Both HBCs and DBCs are thought to be morphologically the *outer* bipolar cells according to Cajal's [1893] classification. These lie in approximately the same level as the *inner* horizontal cells and are considered to be in contact with cones according to Cajal's [1893] description of amphibian retina. These characteristics are incorporated into the model: i.e., both HBCs and DBCs are represented as receiving inputs from the cones and from the *inner* horizontal cells, which receive their inputs from the cones. From pictures of flat mounts of various bipolar cells, the dendritic diameter for both HBC and DBC is considered to be 200 μm (approximately 3°) [Shantz, 1976]. The dendritic diameter for the central portions of the bipolar cells, where cones contribute to the center response, is taken to be about 70 μm (about 1.1°). This is based on the consideration that for bipolar cells to have sharp edge-detection capability at the bipolar cell level, the area for synaptic contacts with the cones have to be relatively small. For HBC and DBC, the overall connectivity for the cone-bipolar path is represented by a narrow two-dimensional Gaussian function, and that for the horizontal-bipolar path by a wider two dimensional Gaussian function. [Difference of Gaussian receptive field organization at the ganglion cell level in the cat retina: Rodieck, 1965]. Bipolar cells get their central input from the narrower range of photoreceptors, and their overall antagonistic input from wider range of horizontal cells.

Figure 27 shows the connectivity diagram and the kernels for the hyperpolarizing bipolar cell (HBC) model. The diagram for the depolarizing bipolar cell (DBC) would be exactly the same except the polarity of the synapses between single cone and bipolar cell and between horizontal cell and bipolar cell. The dynamics of the cell potential is modelled after a one-parameter leaky capacitor as in the horizontal cells, but with a much faster time constant. Miller [1979]

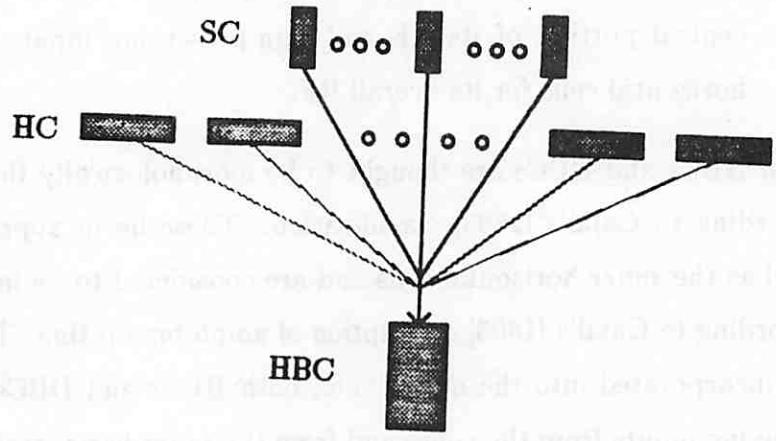

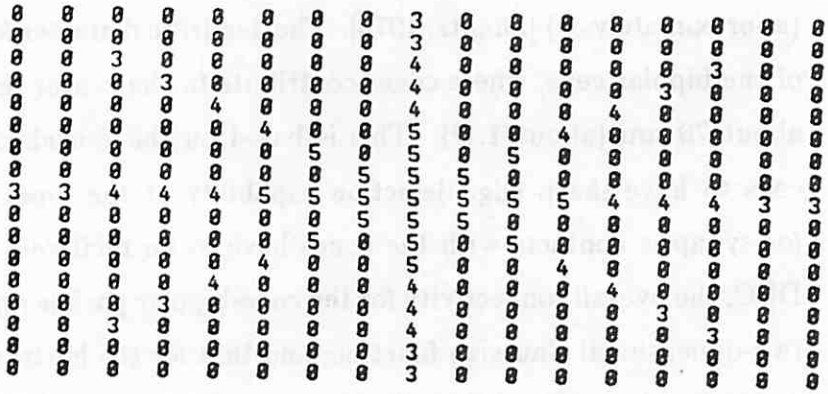

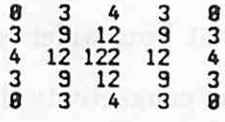

Figure 27: Connectivity diagram for the hyperpolarizing bipolar cell model with its spatial kernels.

suggests that the detection of transients at the IPL occurs due to different signal paths via hyperpolarizing and depolarizing bipolar cells and their respective delays. Siminoff [1986] modelled transient amacrine cells after this conceptual model, while the present model follows a more traditional view that both cells respond in exactly the same way except their polarities [Dowling, 1979; Sakuranaga and Naka, 1985b]. The detections of changing light intensity at the amacrine cell layer are performed by the presumed reciprocal synaptic junctions, which provide microcircuitry to perform the time differentiating function [Shepherd, 1978], between the transient amacrine cell dendrites and the bipolar cell axonal terminals. Followings are the algorithms for the two bipolar cells:

Algorithm

$$HBC_t = W_{hbc} \cdot HBC_{t-1} + W_{hbc}^{-} \cdot (K_{ch} * SC_{t-1} - \frac{1}{2} K_{sh} * HC_{t-1}^{-} + 1/2)$$

$$DBC_t = W_{dbc} \cdot DBC_{t-1} + W_{dbc}^{-} \cdot (K_{cd} * SC_{t-1}^{-} - \frac{1}{2} K_{sd} * HC_{t-1} + 1/2)$$

$$K_{ch} : Den(dia = 1°, \sigma = 1/4°) \quad K_{cd} : Den(dia = 1°, \sigma = 1/4°)$$
$$K_{sh} : Cor(dia = 3°, \sigma = 4/3°) \quad K_{sd} : Cor(dia = 3°, \sigma = 4/3°)$$

The present simulation used $dia = 1°$ for the center kernel K_{ch} and $dia = 3.5°$ for the surround kernel K_{sh} and the same values for the corresponding parameters for the hyperpolarizing and depolarizing bipolar cell. $W_{hbc} = 0.25$ and $W_{hbc} = 0.25$ are used for the fast response characteristic and bias potential of $1/2$ are used in both to normalize the bipolar cell responses.

Simulations of the Bipolar Cell Layers

Three simulations are performed for the bipolar cell layer. First, temporal response characteristics to the disc, annulus and disc-annulus stimulus patterns

are observed in comparison to responses of other neurons. This will show how individual bipolar cells respond to typical stimulus patterns, and provide us with the chance to compare our results with experimental data.

Second, spatial patterns of bipolar cell activities in response to a moving stimulus will be shown compared to other layers.

Third, we will provide the model with an edge stimulus and observe the spatial response pattern of bipolar cells around the border, testing the idea of *Mach Bands* at the bipolar cell level. If the OPL is the place for spatial discrimination enhancement within the retina as the model assumes, bipolar cells should show clear signs of spatial contrast enhancement through their center/surround receptive field organization.

Result of Simulations. Figure 28 (a) shows the simulated temporal responses for hyperpolarizing and depolarizing bipolar cells to stimulus patterns of disc, annulus and both illuminated simultaneously. As shown, the individual temporal response of a hyperpolarizing bipolar cell(depolarizing bipolar cell) closely follows that of a single cone. This can be compared to Figure 28 (b). By comparing the two, we can see that both produce comparable bipolar cell responses for the surround illumination, while they produce similar responses for the disc illumination except that the model produces a much sharper transient at the beginning. As for the disc-annulus type of illumination, there exists a big difference. This is due to the model's explicit attempt to include luminance information in the bipolar cell output as well as partial output range of the horizontal cells that supply bipolar cells surround inputs. Currently horizontal cells potentials range almost always between 0.3 and 1.0. It is suggested that we map this range into 0.0 to 1.0, so that in the next generation bipolar cell model surround influences from horizontal cells approximate those of central influences from single cones.

Figure 29 shows the spatial pattern of activity for a moving bar simulation for depolarizing/hyperpolarizing bipolar cell layers compared to retinal image at a given time. The bar is moving at a speed of 8.5°/sec from the left to the right

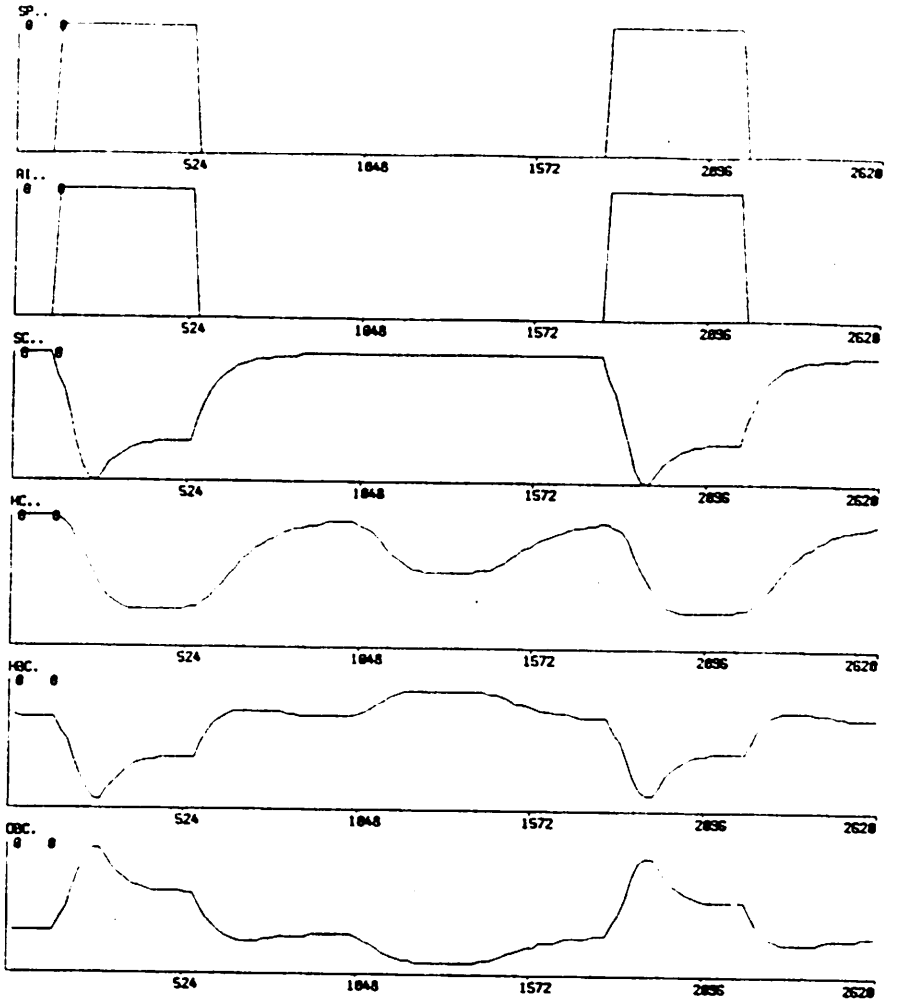

(a)

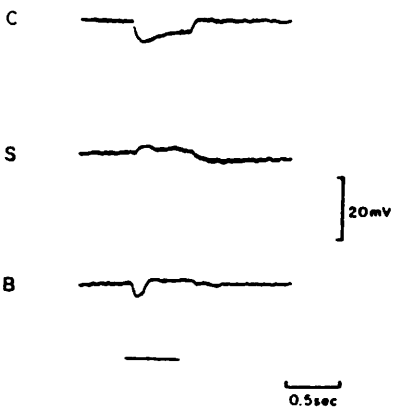

(b)

Figure 28: (a) Temporal activities for SP, RI, SC, HC and BCs. The unit in x-axis is millisecond. (b) Intracellular recordings from a hyperpolarizing bipolar cell of a frog. From Matsumoto and Naka [1972].

in the retinal layer.

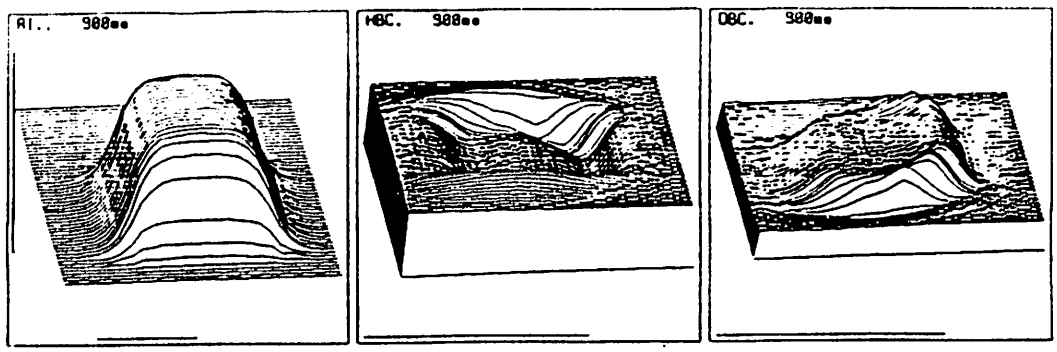

Figure 29: Spatial patterns of activities of bipolar cell layers compared to a retinal image at a sampled time step. Stimulus pattern is a moving bar of 4°x2° at a speed of 8.5°/sec from the left to the right.

Figure 30 shows what might be called a Mach Band [Ratliff and Hartline, 1959] phenomenon at the bipolar cell level of the retina. The stimulus pattern is

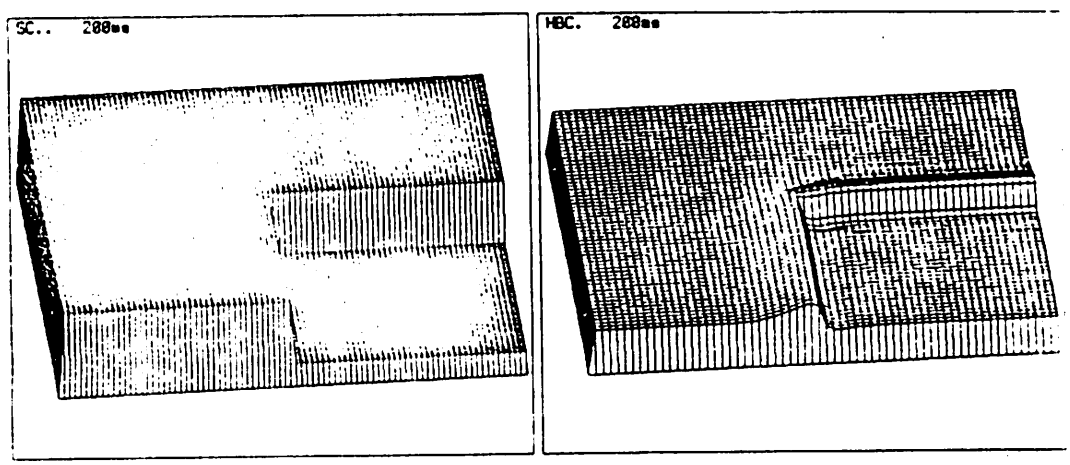

Figure 30: Mach Band simulation using a big bar stimulus.

a static square of 8°x8° projected to the lower right half of the simulated retinal patch. This essentially gives the retina a long edge between the dark and light

illuminations. Note that single cone layers display only two activities: uniform hyperpolarization for single cones under illumination and uniform depolarization for the others under dark condition. But for the hyperpolarizing bipolar cells, there is a gradual slope in potential between the cells close to the illumination border. Those which are not illuminated and near the illumination border are more depolarized than non-illuminated hyperpolarizing bipolar cells far from the border, and illuminated hyperpolarizing bipolar cells close to the illumination border are more hyperpolarized than those illuminated but further from the border. It is as expected since we know from the center/surround organization that the bipolar cell would carry out spatial contrast enhancement besides the temporal one. But the spatial contrast is not as dramatic as expected for the illuminated bipolar cells whereas those not illuminated and near the border are much depolarized, which represent a good spatial contrast enhancement. This is because the current model does not provide full range of horizontal cell inputs as mentioned.

Discussion. Werblin and Dowling [1969] showed in the mudpuppy that illuminating the surround RF alone does not evoke changes in the bipolar cell response, while Figure 28 (b) from Matsumoto and Naka [1972] shows that in *Rana* surround inputs alone do cause changes in the bipolar cell level. Theoretically this borders on the distinction between ***divisive*** inhibition and ***additive*** inhibition respectively. Currently the model adopts ***additive*** inhibition from horizontal cell to bipolar cell, i.e., modelled after frog retinal neurons, and as a result show inhibitory effects without the excitatory inputs as illustrated in Figure 28 (a).

The bipolar cell for the current conceptual model of the retina provides all the visual information to the IPL and ganglion cell layer, and the later stages of visual information processing appear to require at least spatial contrast, absolute luminance and temporal contrast information. Long-term luminance information is lost mostly through adaptational processes. Direct excitatory inputs from single cones compared to delayed inhibitory inputs through horizontal cells emphasize

the temporal contrast information. So, there are at least two possibilities within the current conceptual framework: Provide two separate channels for contrast information and for luminance information, or mix both types of information into one physical channel as in the current model. One way to handle this problem of mixing signals is adding the two with a constant ratio so that neurons in the later layers can recover selected informations as needed. These two are now mixed in a 2 to 1 ratio and the luminance information is recovered by the ***sustained*** type amacrine cells, while the temporal contrast information is recovered by the ***transient*** type amacrine cells as shown in the next chapter.

We can increase the weight of contrast information compared to that of luminance somewhat more since ganglion cell type 1 appears to require more of the contrast information than a short-term luminance information.

Also, the weights W_{hbc} or W_{dbc} and W_{hbc}^{-} or W_{dbc}^{-}[5] of the bipolar cells can be exaggerated to use the full range of numbers, i.e., a bipolar cell should be acting as a dynamic range ***enhancer*** rather than as a dynamic range ***compactor*** of the incoming visual information since that means increasing the S/N ratio which is desirable. For the present the relation $W_{hbc} + W_{hbc}^{-} = 1$ and overlapping dendritic fields (excitatory and inhibitory) prevents the bipolar cells from using their full dynamic range. The underlying reason being single cone carries only temporal information whereas the bipolar cell carries spatial as well as temporal information. For the future, it is suggested that we compute the difference between the weight under the central spatial kernel and that under the surround one and come up with a measure to maximize the contrast while still maintainning normalized range of output values for the cells involved. Of course, amacrine cells will extract some of the information, but the type 1 ganglion cell uses, at least in the model, bipolar cell information directly and it makes more sense to provide normalized

[5] W_{hbc} or W_{hbc} determines the degree to which the current cell potential depends on its cell potential at the previous time step, while W_{hbc}^{-} or W_{dbc}^{-} the degree the external input influences the current potential.

information because the neuron models in the later stages/layers can maximize the use of incoming information without relying on some arbitrary assumption on the range of input values.

If, as in the current model, there are two bipolar cells with exactly symmetrical functional properties, it appears to be a wasted design, which itself is highly improbable, and if so they probably wouldn't appear in every vertebrate retina. Nelson et al. [1979] point out the different speeds of signal flow through hyperpolarizing bipolar cells and depolarizing bipolar cells, and the resulting difference as a basis for transient amacrine cell to detect temporal contrast information of stimulus illumination intensities. But, it is not clear whether that is the general case, at least this does not need to be the case, for in our model the local reciprocal synapses of the transient type amacrine cells detect the temporal contrast information from the bipolar cells rather well.

CHAPTER VI

AMACRINE AND GANGLION CELL LAYERS

Amacrine Cell Layers

Modelling of the Amacrine Cell Layers

Based on the investigations of Chan and Naka [1976] and Miller [1979], amacrines are divided into five functional subtypes depending on whether they are *transient* type (T) or *sustained* type (S) and are receiving inputs from hyperpolarizing bipolar cells (H) or from depolarizing bipolar cells (D).

1. ACTHs are transient-type amacrine cells which get their input from hyperpolarizing bipolar cells (HBC) only and we see them as being mono-stratified.

2. ACTDs are transient-type amacrine cells which get their input from depolarizing bipolar cells (DBC) only and we see them as being mono-stratified.

3. ACTs are transient-type amacrine cells which get their input from both ACTH and ACTD and are seen as being bi-stratified in order to receive inputs from both ACTHs and ACTDS. They could be mapped to Cajal's [1893] *amacrines of the third level.*

4. ACSHs are sustained-type amacrine cells which get their input solely from the hyperpolarizing type bipolar cells (HBC) and which are seen to provide excitatory inputs to ganglion cell type 4 (GC4, to be discussed in the next section). We see them as Cajal's [1893] *amacrines of the second level.*

5. ACSDs are sustained-type amacrine cells which get their input solely from the depolarizing type bipolar cells (DBC) and are seen as providing excitatory inputs to ganglion cell type 0. These can be mapped to Cajal's [1893] *amacrines of the fourth level.*

The ACSHs are assumed to reside in the second sublayer, based upon the understanding that there are large monostratified ganglion cells with dendrites at the 2nd substratum, and the amacrine cells in the sublayer are likely to be related to the ganglion cell type 4, which would most likely receive their inputs from HBCs and/or ACSHs. It is likely then that ACTs, which share the same input bipolar cell type, resides in the adjacent sublayer: i.e. the first or the third sublayer. Since similar considerations suggest that ACSDs and ACTs lie in adjacent sublayers, we assume that they reside in the fourth and the third substrata respectively. These correlations of functional subtypes and their possible locations in the IPL are mentioned here as a plausible scheme and are not to be treated as a necessary condition for the model.

Transient Amacrine Cells

Figure 34 (b) shows some of the intracellular recordings of transient type amacrine cells from a mudpuppy retina [Werblin and Dowling, 1969]. The transient characteristic of ACTs is seen as coming from the reciprocal synapse between the bipolar cell processes and the amacrine cell processes. The *reciprocal* synapses consist of a bipolar cell axonal terminal and a process of a transient amacrine cell. An outflow of excitatory transmitter vesicles from the bipolar axonal terminal follwed by the uptake of the vesicles by the amacrine process will produce local excitatory post synaptic potential, which causes secretion of inhibitory transmitter vesicles to the synaptic junction. Uptake of these inhibitory vesicles by a bipolar cell axonal terminal will cause inhibitory synaptic potential at the bipolar cell axonal terminal which will in turn decrease the release of excitatory transmitter vesicles. It is a local phenomenon which does not affect the cell

potentials of the bipolar cells. Dowling [1968] suggested the existence of reciprocal synapses carrying out time-derivative-like functions in the frog retina. Rall and Shepherd [1968] formulated a model of reciprocal synapses in the olfactory bulb.

The dynamics of amacrine cell models are modelled after a leaky-capacitor with one parameter [Holden, 1976] like other neuron models. The synaptic contacts are assumed to contribute to the cell potential in one of the following three modes: providing a contribution of 1 if the bipolar cell making the contact depolarizes sufficiently during the short prior interval (the model uses the same fixed threshold for all dendritic synapses for a given transient amacrine cells), a contribution of 0 if the bipolar cells hyperpolarize, and a proportional contribution for in-between cases. A dendritic diameter of 0.8° is taken for all transient amacrine cells [Shantz, 1976]. Figure 31 shows the connectivity diagram and the spatial kernel for ACTH model.

Connectivity diagram and its spatial kernel for the ACTD model would be the same as Figure 31 except HBC would be substituted by DBC and the synaptic junction polarities would be reversed. Figure 32 shows the connectivity diagram and the spatial kernel for the ACT model.

Algorithm

$$ACTH_t = W_{acth} \cdot ACTH_{t-1} + W^-_{acth} \cdot (K_{acth} * (HBC_t - HBC_{t-1} - T_h)[^0_0|^1_0])$$

$$ACTD_t = W_{actd} \cdot ACTD_{t-1} + W^-_{actd} \cdot (K_{actd} * (DBC_t - DBC_{t-1} - T_d)[^0_0|^1_0])$$

$$ACT_t = W_{act} \cdot ACT_{t-1} + W^-_{act} \cdot (K_{act} * MAX$$

$$(HBC_t - HBC_{t-1} - T_h)[^0_0|^1_0], (DBC_t - DBC_{t-1} - T_d)[^0_0|^1_0]))$$

$$K_{acth} : Den(1.5°, 1/6°) \quad K_{actd} : Den(1.5°, 1/6°) \quad K_{act} : Den(1.5°, 1/6°)$$

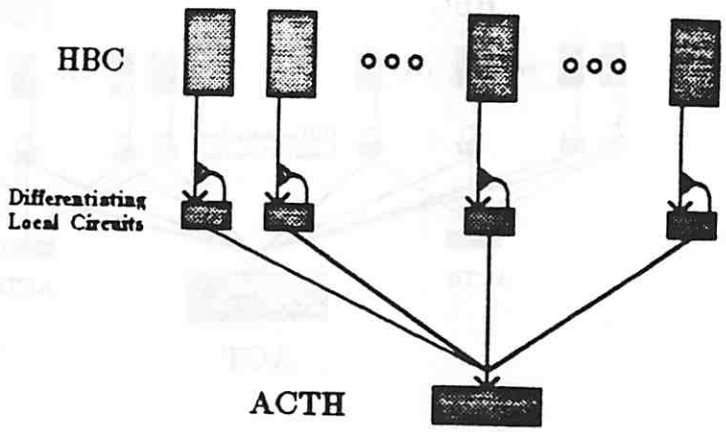

Figure 31: Connectivity diagram and the spatial kernel of the ACTH model.

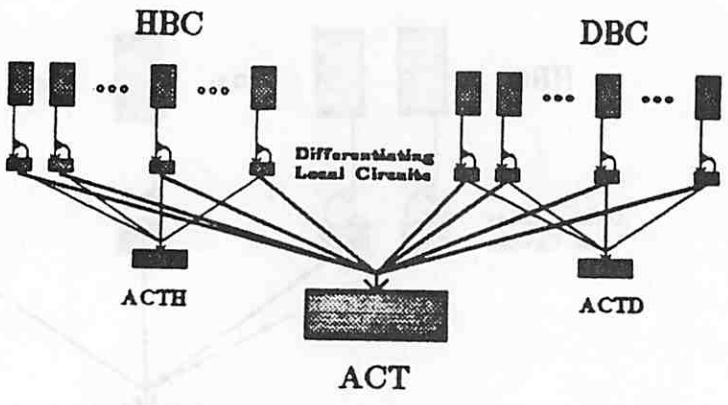

0	0	0	0	0	0	0	0	0
0	0	0	0	0	0	0	0	0
0	0	0	1	1	1	0	0	0
0	0	1	7	12	7	1	0	0
0	0	1	12	159	12	1	0	0
0	0	1	7	12	7	1	0	0
0	0	0	1	1	1	0	0	0
0	0	0	0	0	0	0	0	0
0	0	0	0	0	0	0	0	0

Figure 32: Connectivity diagram and the spatial kernel of the ACT model.

Currently $W_{acth} = 3/4$, $W_{actd} = 3/4$ and $W_{act} = 4/5$ are used. T_h and T_d are local dendritic thresholds for ACTH and ACTD models respectively. The difference between T_h and T_d arises because of the different rate of changes in bipolar cell's hyperpolarizing and depolarizing responses. This difference in responses is caused by the asymmetrical hyperpolarizing and depolarizing characteristics of single cones. Here threshold function is used to set the amacrine cell output potential to 1 for the cases when the difference between the current bipolar cell potential and the previous bipolar cell potential is bigger than the threshold value, and reset to 0 in the other cases for each amacrine cells.

Sustained Amacrine Cells

ACSH and ACSD cells are assumed to be synapsing to the previous cell types via non-reciprocal synapses with a threshold, which bypass input bipolar cell potentials if they are above certain threshold value. Short of a good terminolgy, we will call this type as *rectifying*[1] synaptic junction. Mathematical definition of this function is included in the algorithm. These synapses, in contrast to the well-known *reciprocal* ones, are seen as executing rectifying function, thus extracting *luminance* information form the bipolar cells outputs, which contain both *luminance* and *contras* informations. For the purpose of setting spatial kernel, a dendritic diameter of 1.5° is taken for both ACSHs and ACSDs based on their anatomy [Shantz, 1976].

Figure 33 shows the connectivity diagram and the spatial kernel for the ACSH model. The connectivity diagram for the ACSD model would be exactly the same except the bipolar cell would be DBC instead of HBC and the synaptic junction would be sign-conserving rather than sign-reversing. The dynamics of both ACSHs and ACSDs are modelled after a leaky capacitor.

Algorithm

[1] This does not rectify in reference to 0 millivolt, but rather to a potential level which is in the middle of the previous bipolar cell's dynamic range.

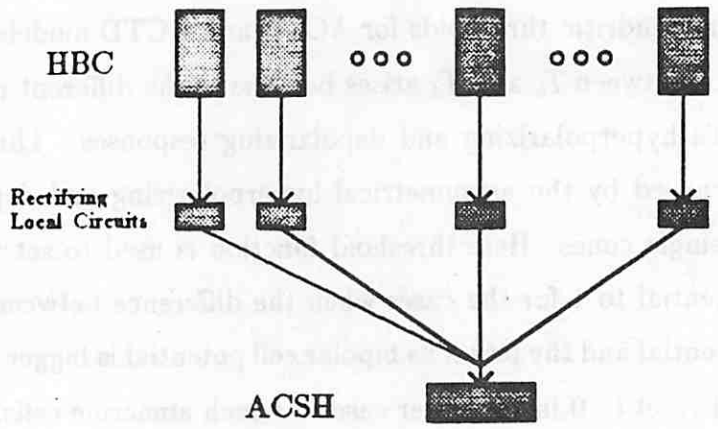


```
 0  0  6  0  0
 0 17 28 17  0
 6 28 46 28  6
 0 17 28 17  0
 0  0  6  0  0
```

Figure 33: Connectivity diagram and the spatial kernel of the ACSH model.

$$ACSH_t = W_{acsh} \cdot ACSH_{t-1} + W^-_{acsh} \cdot (K_{acsh} * (\frac{1}{T^-_h}(HBC_{t-1} - T_h)\lfloor 0 \mid 0 \rfloor)^-)$$

$$ACSD_t = W_{acsd} \cdot ACSD_{t-1} + W^-_{acsd} \cdot (K_{acsd} * (\frac{1}{T^-_d}(DBC_{t-1} - T_d)\lfloor 0 \mid 0 \rfloor))$$

$$K_{acsh} : Den(0.8°, 1/6°) \quad K_{acsd} : Den(0.8°, 1/6°)$$

Currently $W_{acsh} = 1/4$ and $W_{acsd} = 1/4$ are used. T_h and T_d represent the absolute threshold for ACSH and ACSD rectifying synapses and currently are 0.4 and 0.6 respectively. Mutipliers $\frac{1}{T^-_h}$ and $\frac{1}{T^-_d}$ to the difference term between the bipolar cell potential and the threshold are for the purpose of normalizing the range of external input values to the sustained amacrine cells. The threshold function (floor function in these cases) is used to reset the difference term to 0 if $DBC_{t-1} < T_d$ for the ACSD and if $HBC_{t-1} < T_h$ for the ACSH.

Simulation of the Amacrine Cell Layers

In this section, we want to show how reciprocal synapses acting like local feedback microcircuits work to detect the temporal light intensity changes from bipolar cell responses. Also, while doing this we want to find out whether this detection process is sensitive to the magnitude of local threshold. We also want to see how the sustained amacrine cells respond to typical stimulus patterns and how they can possibly be used in the later stages to aid in the visual information processing.

Result of Simulations. Figure 34 (a) show how transient amacrine cells react to the onset and offset of a static light illumination. Hyperpolarizing bipolar cells (BCH in the figure) detect the rising edge of hyperpolarizing bipolar cells potential through reciprocal dendritic depolarization when light illumination ceases, while transient amacrine cells (ACTD) receiving inputs from depolarizing bipolar cells (BCD in the figure) detect the rising edge of depolarizing bipolar cells potential depolarize when lights illuminates the local area. And since the third transient amacrine cell (ACT) combines the local ACTH and ACTD outputs, it reacts to both the onset and offset of the light illuminations as expected. But, as amacrine cells get their inputs from bipolar cells, depending on the sensitivity and the scope of their RF size they might get active when they are not directly illuminated upon as shown in the Figure 36. By changing the sensitivity of their local dendritic threshold we can adjust the sensitivity. This figure can be compared with Figure 34 (b). The simulation figure shows much sharper cell potentials compared to both experimental observations, also the former lacks the spikes. This can be modified by modelling the impulse acivities and the accompanying time constant for decay of the potential.

Figure 35 shows how an onset of disc illumination of 1° diameter evokes responses from a population of transient amacrine cells. Cells under the center and border of the illumination respond more compared to the in-between areas.

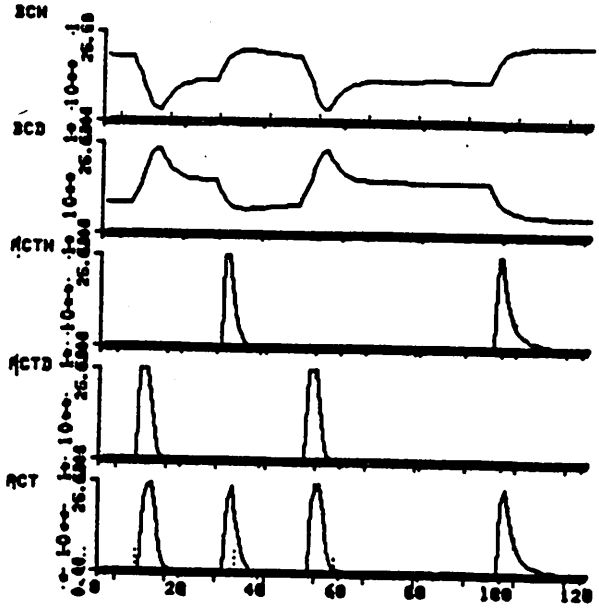

(a)

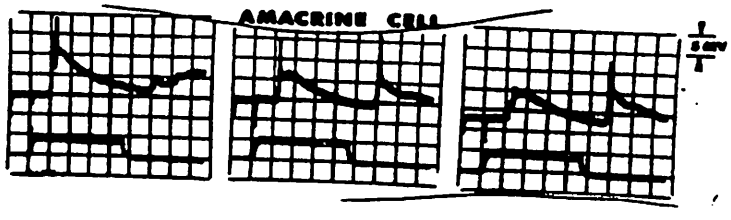

(b)

Figure 34: (a)Temporal responses of transient amacrine cell models. HBC and DBC are titled BCH and BCD respectively, and time unit is 20 msec. (b) Intracellular recordings from transient amacrine cells in a mudpuppy retina. From Werblin and Dowling [1969].

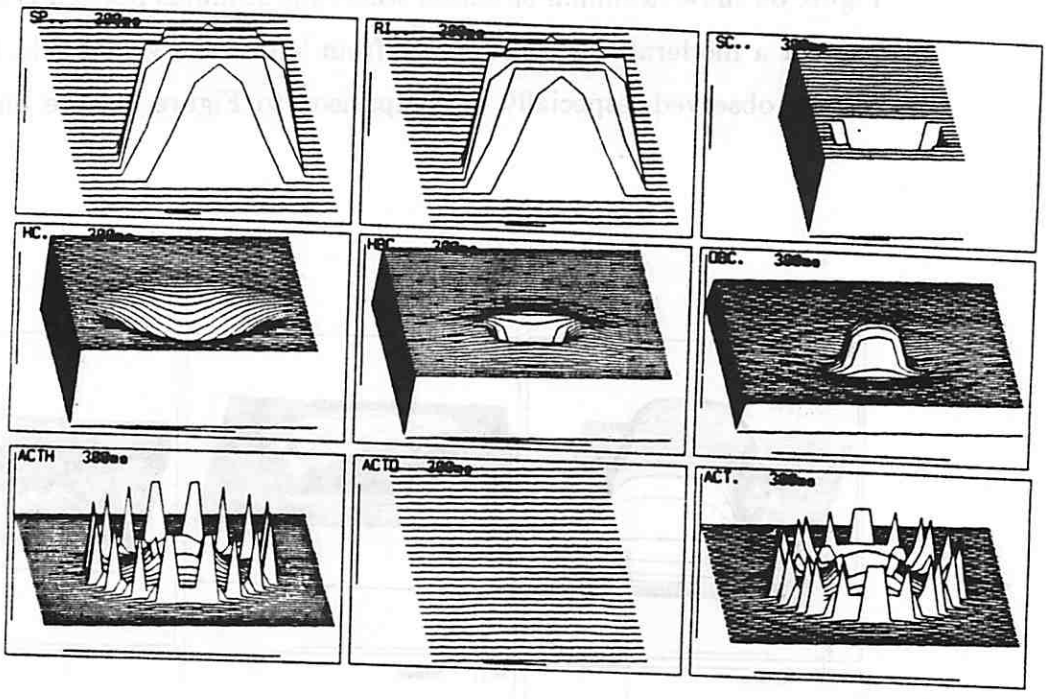

Figure 35: Spatial patterns of activities of transient amacrine cell models to a flash of spot illumination.

Even though the current figure does not depict it well, a flash of stimulus pattern gives the whole population of transient amacrine cells under the illumination to react/spike.

Figure 36 shows a similar situation where the stimulus pattern is a moving bar of 2°x2° at a moderate speed of 8°/sec from left of the visual field to the right. As can be observed, especially in comparison to Figure 35, the only amacrine

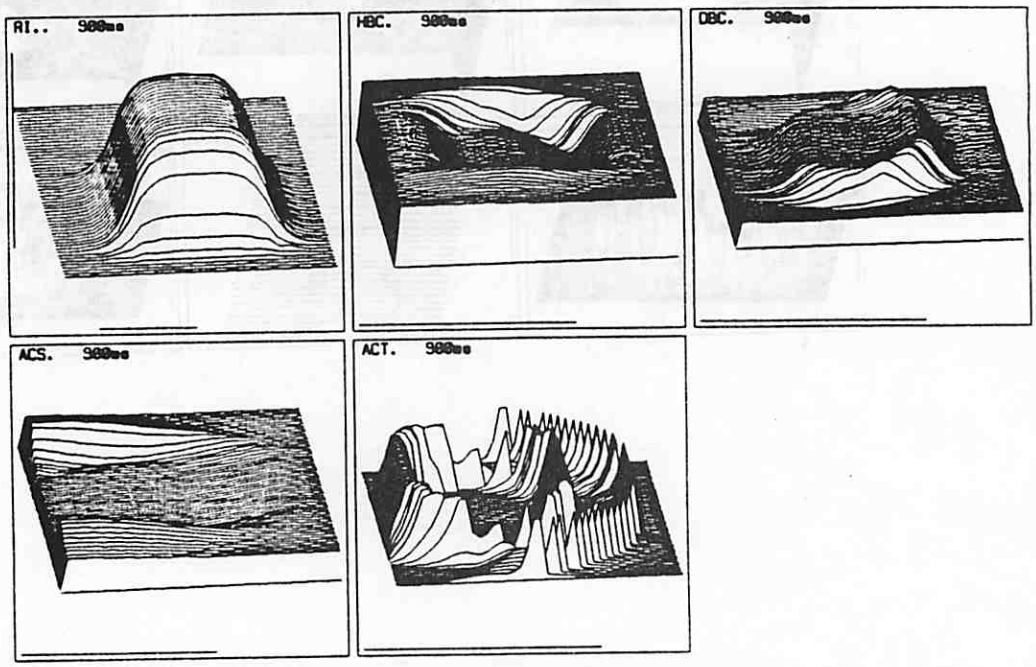

Figure 36: Spatial pattern of activities of transient amacrine cell models to a moving square of 2°x2° at 8°/sec speed.

cells firing are around the edge [2] of the square. Note that the activities inside of the edges are due to bipolar cell change from transient peak potential to the

[2]The peak to steady state change has caused enough change in the bipolar cell response for the sensitive amacrine cells to depolarize at these occcations.

steady state potential. It is because these are the only locations where the local illumination intensity changes, while in the previous figure in response to flash its all the cell under the stimulus pattern whose local illumination intensities has changed.

Figure 37 (a) show how *sustained* amacrine cell models depolarize in response to the different stimulus patterns of disc, annulus and both illuminated. They represent the existence or absence of illumination in the local area. This can be compared to Figure 37 (b) where response of the catfish *sustained* amacrine cell type has been recorded. Compared to the experimental data, the simulation result lack the high frequency impulses superimposed on top of the main sustaind potentials and the after-hyperpolarization after the cessation of the light illumination.

Discussion. The current model does not model the impulse generation of the transient amacrine cells. There are three well-defined types of amacrine cells – a *rising-edge detector/on* type, *falling-edge detector/off* type and a *change detector/on-off* type.

By adjusting the local thresholds at the reciprocal dendritic input, we can adjust the sensitivity to change of bipolar cell responses of each amacrine cells. Note that there is no reason why ACTH should detect the cessation of and ACTD the onset of light illumination. From the theoretical standpoint, as long as there are two bipolar cell types, it makes no difference which subtype performs which function.

Miller's [1979] idea of bi-modal functioning of transient amacrine cells is an interesting possibility of future investigation with the current model. Also, since there are many *serial* synapses between amacrine cells in the frog retina than those possibly accounted for by the synaptic junctions between ACTH, ACTD and ACT models, the idea of propagation of signals beween transient amacrine cells to facilitate the motion-detection function should be investigated in the future whose resulting responses could be fed to type 2 and type 3 ganglion cells among

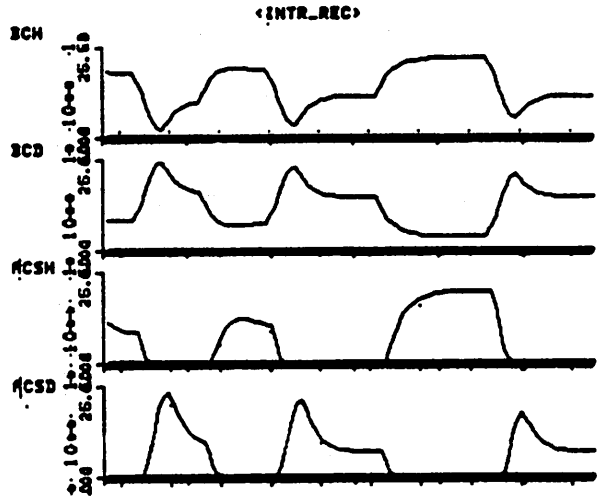

(a)

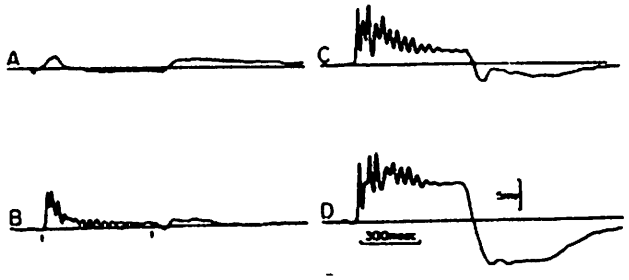

(b)

Figure 37: (a)Temporal responses of ACSH and ACSD models compared to those of HBC(BCH in the figure) and DBC(BCD in the figure). (b) Responses from a sustained neuron evoked by steps of increasingly bright lights (diffused illumination). From Chan and Naka [1976].

others. Even though there is a good model of how ganglion cell dendritic geometry might perform the direction selective movement detection in a cat retina [Koch et al., 1982], this still is a useful idea since the current transient amacrine cells detect essentially the change of light illumination which can be caused either by the illumination change or by the movements of the illuminated stimulus pattern, thereby creating functional specificity within the transient amacrine cells.

The *sustained* amacrine cells are not yet reported among the amphibian retinas as far as we know. But, after Naka's initial report on the class of *sustained* type amacrine cells in the fish retina , they have been reported in other species and it appears that they are general type that would be found in most vertebrate retinas [Grüsser, 79]. Obviously, type 0 and type 4 ganglion cells could extract necessary visual information directly from bipolar cells, but it would be much easier if there were some preprocessing done at the level of IPL. So, we suggested the two subtypes of *sustained* amacrine cells within the model, where ACSHs receive their input from hyperpolarizing bipolar cells and ACSDs from depolarizing bipolar cells. Another as yet unsubstantiated assumption about the amacrine cells are that they employ a type of input synapses called here as *rectifying* synapse.

There are three things that can change the sensitivity of evoking the response of the amacrine cells: dendritic threshold, size of dendritic tree and time-constant of amacrine cells. So it appears that the difference between flashing a stimulus pattern and a moving stimulus pattern is that spatial pattern of transient amacrine cells are very different even at the corresponding locations. This result can have some implications where the dendritic tree of certain ganglion cells are organized in a center/surround fashion so that different ganglion cells with same transient amacrine cell inputs might respond differently since ganglion cells with smaller dendritic organization will favor the moving stimulus pattern and biger ones will favor the flash of light instead of a moving stimulus pattern.

Ganglion Cell Layers

Modelling of the Ganglion Cell Layers

Figure 8 in chapter 2 shows Grüsser and Grüsser-Cornehls' [1976] scheme of the neuronal response type of four different classes of ganglion cells in frog retina. Besides integrating signals from the cells in other layers of the retina, the ganglion cells function as the output signal-encoding cells for the retina so that the signal can be properly transmitted to the higher visual brain areas.

Type 0 and type 4 ganglion cells

Large size monostratified ganglion cells, with their dendrites extending into the 4th substratum of the IPL are physiologically described as ganglion cell type 0 (GC0) [Grüsser and Grüsser-Cornehls, 1976; Shantz, 1976; Maturana et al., 1960]. The diameter of their dendritic tree is about 500 micron (7.5°) [Shantz, 1976].

GC0s get their inputs solely from ACSDs since it would be most economical to receive already processed information (in the sense that GC0 needs *luminance* information).

Figure 38 shows the connectivity diagram and the spatial kernel for the GC0 model.

Since the dendritic diameters of ganglion cells, together with dendrites of the overlapping previous stages, are relatively small in relation to their respective receptive field sizes, and since there are strong evidences that the amacrine cells inhibits, we hypothesize amacrine cells as being responsive to the surround receptive fields in general. Further, we hypothesize that GC0s gets their input, both at the center and at the surrounding, from ACSs because it will be more economical for cells with the task of relatively wide region detection to use smaller amount of informations of larger units (ACSs) than larger amount of smaller units (BCs),

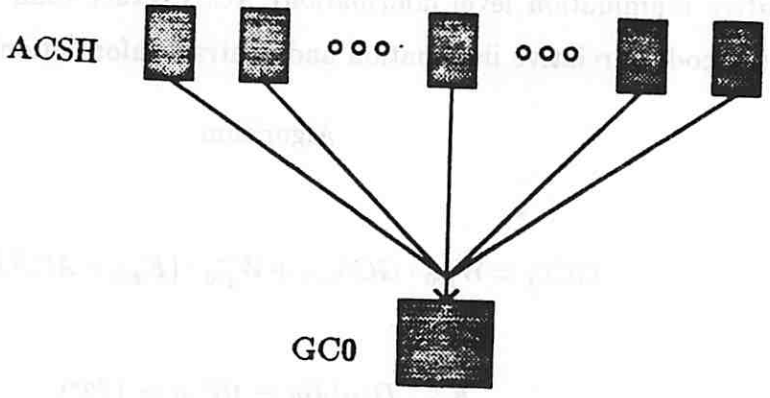

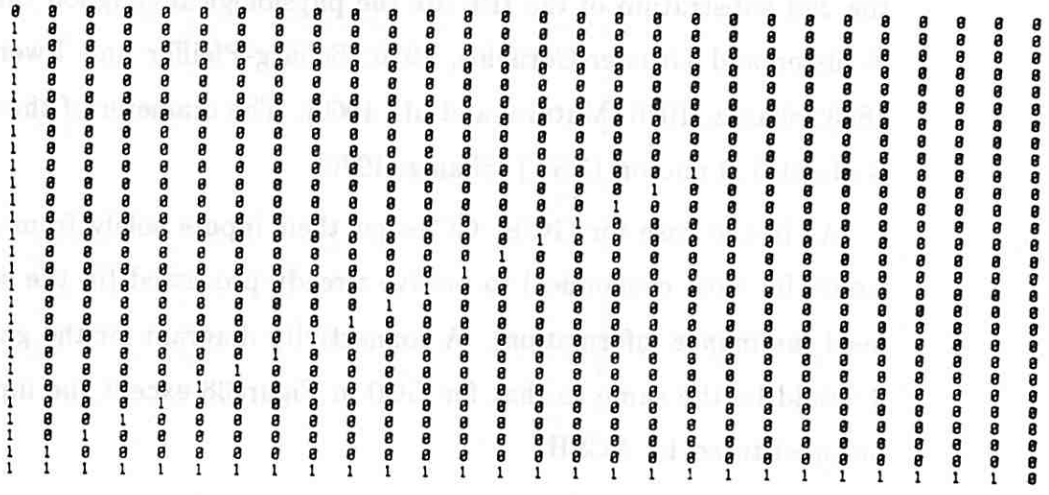

Figure 38: Connectivity diagram and spatial kernels for the GC0 model. Note the display of only the first quardrant of the spatial kernel due to its size.

thereby saving the number of synapses as well as size of the dendrites. At the same time, GC0 can just deal with center/surround contrast from singly coded (relative illumination level information) ACSs rather than level detection from doubly coded (relative ilumination and contrast information) BCs.

Algorithm

$$GC0_t = W_{gc0} \cdot GC0_{t-1} + W_{gc0}^{-} \cdot (K_{gc0} * ACSD_{t-1})$$

$$K_{c0} : Den(dia = 10°, \sigma = 1/2°)$$

Currently $W_{gc0} = 0.9$ is used.

Large size monostratified ganglion cells with their dendrites extending into the 2nd substratum of the IPL are the physiological ganglion cell type 4 (GC4) [Grüsser and Grüsser-Cornehls, 1976; Schürg-Pfeiffer and Ewert, 1981; Cajal, 1893; Shantz, 1976; Maturana et al., 1960]. The diameter of their dendritic tree is about 500 micron (7.5°) [Shantz, 1976].

As in the case for GC0s, GC4s get their inputs solely from ACSHs since it would be most economical to receive already processed (in the sense that GC4s need *luminance* information). A connectivity diagram for the ganglion cell type 4 would be the same as that for GC0 in Figure38 except the input layer ACSD be substituted by ACSH.

Algorithm

$$GC0_t = W_{gc4} \cdot GC0_{t-1} + W_{gc4}^{-} \cdot (K_{gc4} * ACSD_{t-1})$$

$$K_{c0} : Den(dia = 10°, \sigma = 1/2°)$$

Currently $W_{gc4} = 0.9$ is used.

Type 1 ganglion cell

The bistratified ganglion cells with small-size dendritic trees extending into the 2nd and the 4th substrata of the IPL are assumed to be the physiological type 1 ganglion cells (GC1) according to Grüsser and Grüsser-Cornehls [1976] physiological typology of ganglion cells.

GC1s are seen as being excited by signals from the local HBCs and DBCs, and inhibited by the less local ACSHs and ACSDs. The diameter of GC1s is taken to be between 150 to 200 microns (approximately 2° to 3°) [Shantz, 1976], and the excitatory/inhibitory connectivities from the local HBC and DBC are assumed to be distributed in the shape of a two-dimensional Gaussian function, with an excitatory receptive field (ERF) diameter between 2° and 3° and an inhibitory receptive field (IRF) diameter of 3° to 5° [Grüsser and Grüsser-Cornehls, 1976; Schrüger-Pfeiffer and Ewert, 1981]. GC1s get their central inputs solely from narrower range of both bipolar cells and their antagonistic surround/overall range of inputs the same cells. Figure 39 shows a connectivity diagram for the ganglion cell type 1.

The dynamics of GC1s is modelled after a two-parameter leaky capacitor model as in ACTs and ACTDs, but with a much faster cell-potential time-constant and a smaller absolute threshold potential (to initiate the initial firing), and with a very slow threshold time-constant, restraining additional firing once one has started. As mentioned before, the current simulation time step is too big to elaborate the spike generation properly. Therefore, for the time being, we skip the second step of encoding and regard GC1s' output as an encoding of the probability of the presence of the spike at the given time interval.

Algorithm

$$GC1_t = W_{gc1} \cdot GC1_{t-1} + W^-_{gc1} \cdot (\frac{1}{2} K_{c1} * HBC_{t-1} + \frac{1}{2} K_{c1} * DBC_{t-1}$$

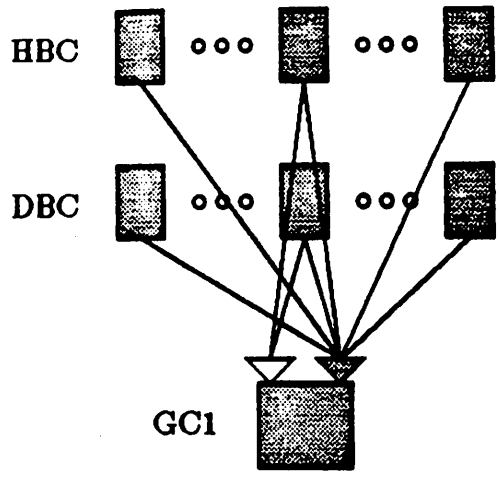

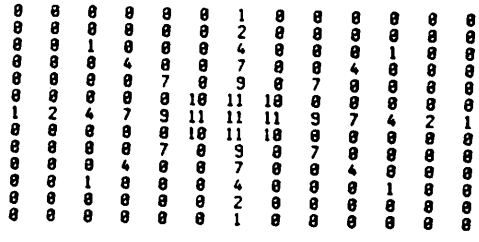

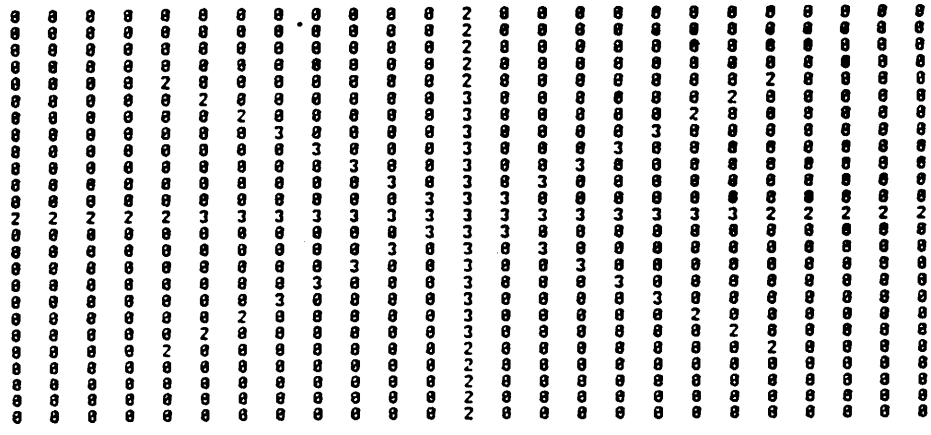

Figure 39: Connectivity diagram and the spatial kernels for the GC1 model. Filled arrowhead represents central connections, whereas unfilled one represents surround connections.

$$-\frac{1}{4}K_{s1} * ACSH_{t-1} + \frac{1}{4}K_{s1} * ACSD_{t-1})\lceil T1_{t-1} + Tab_{gc1} \mid 1\rceil$$

$$K_{c1} : Den(dia = 10°, \sigma = 1/2°) \quad K_{s1} : Den(dia = 28°, \sigma = 2°)$$

Currently $W_{gc1} = 0.9$ is used.

Type 2 and type 3 ganglion cells

The bistratified ganglion cells with medium-size dendritic trees extending into the 1st and the 3rd substrata of the IPL are the physiological type 2 ganglion cells (GC2) [Grüsser and Grüsser-Cornehls, 1976]. GC2 are excited by the signals from the local ACTs and ACTDs and inhibited by the less local ACTs and ACTDs. The diameter of GC2s is taken to be between 200 to 300 microns (approximately 3° to 4.5°) [Shantz, 1976], and the excitatory/inhibitory connectivities from the local ACTs and ACTDs are distributed in the shape of a two-dimensional Gaussian function, with an ERF diameter between 3° to 5° and an IRF diameter between 5° to 8° [Grüsser and Grüsser-Cornehls, 1976; Schrüger-Pfeiffer and Ewert, 1981]. GC2s get their central inputs solely from narrower range of both transient amcrine cells and their antagonistic surround/overall range of inputs the same cells. Figure 40 shows a connectivity diagram for the ganglion cell type 2.

The dynamics of GC2s is modelled after a two-parameter leaky capacitor model as in ACTs and ACTDs, but with a much faster cell-potential time-constant and a smaller absolute threshold potential with a very slow threshold time-constant.

Algorithm

$$GC2_t = W_{gc2} \cdot GC2_{t-1} + W_{gc2}^{-} \cdot (\frac{1}{2}K_{c2} * ACT_{t-1} + \frac{1}{2}K_{c2} * ACTD_{t-1}$$

$$-\frac{1}{4}K_{s2} * ACT_{t-1} + \frac{1}{4}K_{s2} * ACTD_{t-1})\lfloor 0 \mid 0\rfloor$$

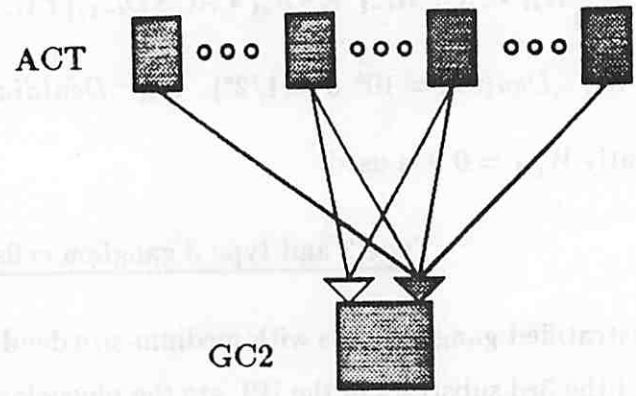

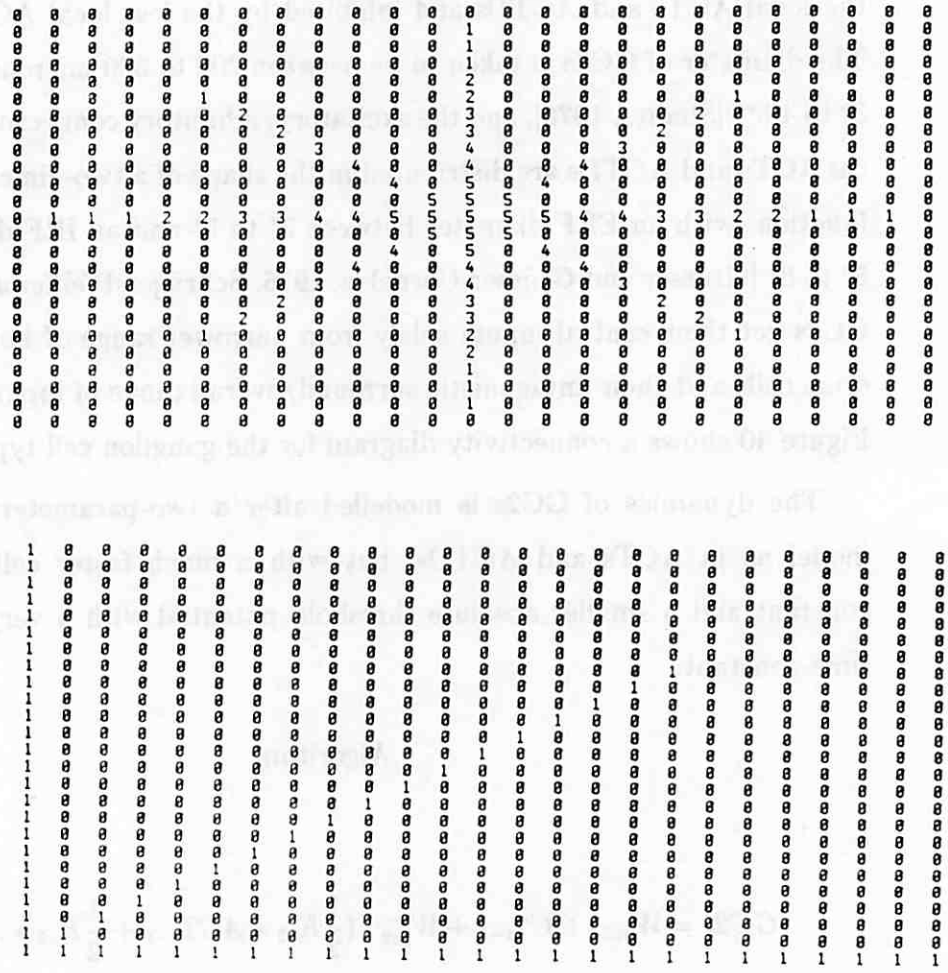

Figure 40: Connectivity diagram and the spatial kernels of GC2 model. Note the display of only the first quardrant of the surround spatial kernel due to its size.

$$K_{c2} : Den(dia = 10°, \sigma = 1/2°) \quad K_{s2} : Den(dia = 28°, \sigma = 2°)$$

Currently $W_{gc2} = 0.9$ is used.

The bistratified ganglion cells with medium-size dendritic trees extending into the 1st and the 3rd substrata of the IPL are the physiological type 3 ganglion cells (GC3) [Grüsser and Grüsser-Cornehls, 1976; Schrüger-Pfeiffer and Ewert, 1981]. GC3s are excited by the signals from the local ACTs and ACTDs and inhibited by the less local ACTs and ACTDs. The diameter of GC3s is taken to be between 200 to 300 microns (approximately 3° to 4.5°) [Shantz, 1976], and the excitatory/inhibitory connectivities from the local ACTs and ACTDs are distributed in the shape of a two-dimensional Gaussian function, with an ERF diameter between 3° to 5° and an IRF diameter between 5° to 8°.

GC3s get their central inputs solely from narrower range of both transient amcrine cells and their antagonistic surround/overall range of inputs the same cells. A connectivity diagram for the ganglion cell type 3 would be the same as ref 40 for ganglion cell type 2 except the size of the spatial kernels under the current model.

The dynamics of the GC3 is modelled after a two-parameter leaky capacitor model as in ACT and ACTD, but with a much faster cell-potential time-constant and a smaller absolute threshold potential with a very slow threshold time-constant.

Algorithm

$$GC3_t = W_{gc3} \cdot GC3_{t-1} + W_{gc3}^{-} \cdot (\frac{1}{2}K_{c2} * ACT_{t-1} + \frac{1}{2}K_{c3} * ACTD_{t-1}$$

$$-\frac{1}{4}K_{s3} * ACT_{t-1} + \frac{1}{4}K_{s3} * ACTD_{t-1})\lfloor 0 \mid 0 \rfloor$$

$$K_{c3} : Den(dia = 10°, \sigma = 1/2°) \quad K_{s3} : Den(dia = 28°, \sigma = 2°)$$

Currently $W_{gc3} = 0.9$ is used.

Preliminary Results of the Simulation of the Ganglion Cell Layers

Figure 41 shows the temporal response pattern for various ganglion cell types where a 2° x 2° bar stimulus is moved across the visual field at a speed of 8.5°/sec as in Figure 36. The responses of GC4 and GC0 shown in figure 41 are mostly active and inactive respectively for the whole temporal sequence of stimulus pattern of disc, annulus and both. It is because the the whole receptive fields for both subtypes are under dark condition except the relatively small part in the center.

Type 3 ganglion cells detect the activity of transient amacrine cell reasonably well as the change of illumination, while type 2 ganglion cell show more subdued response.

A different set of simulations were tried to see if the model would reproduce an *area* function [Grüsser and Grüsser-Cornehls, 1976]. Even with a different set of parameters from the current GC2 model, the model could not follow the activities predicted by the *area* function.

It is suggested further refinements in the neuronal models and their interconnections in the intermediate layers be pursued before any quantitative results can be compared.

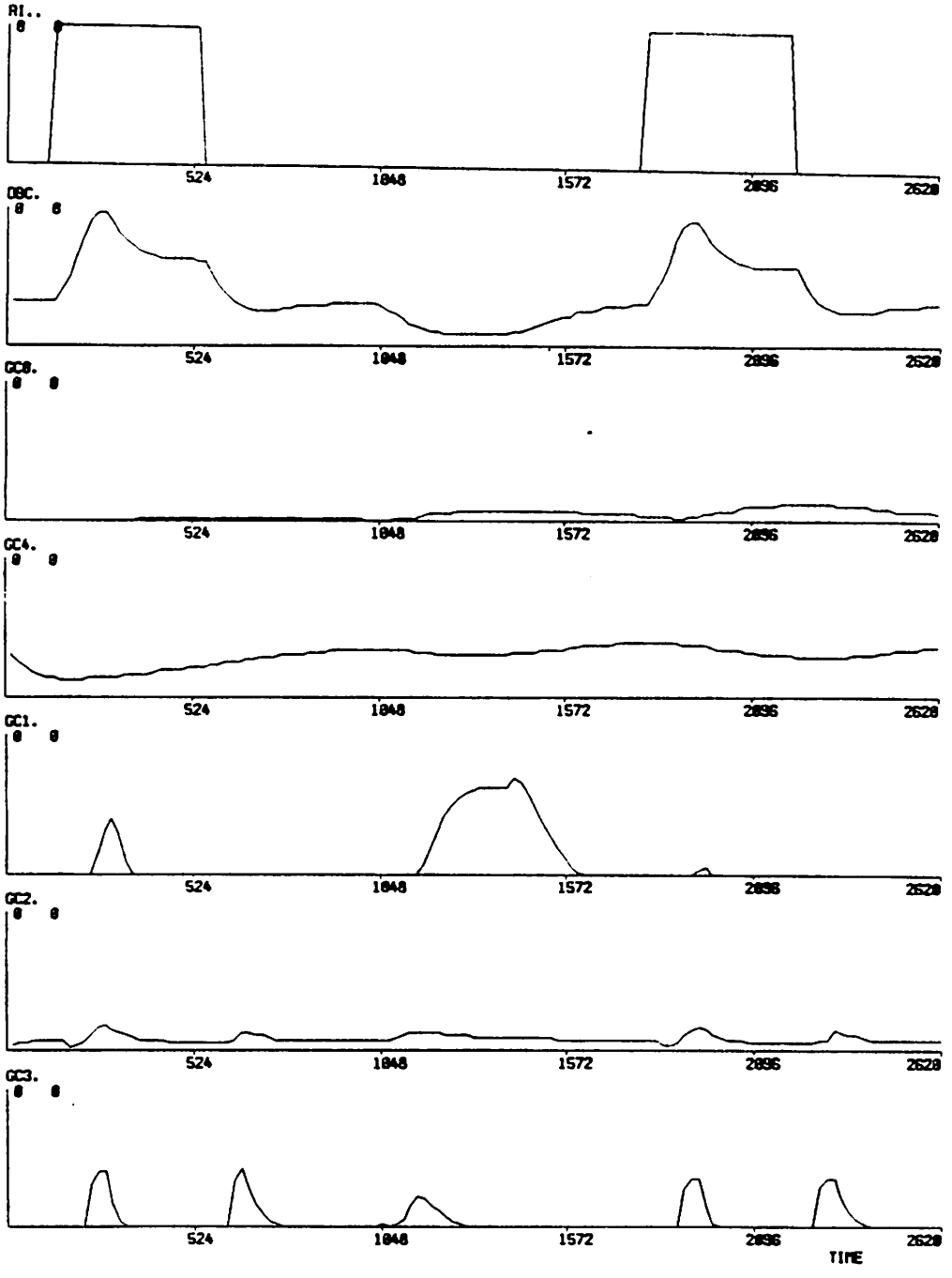

Figure 41: Preliminary simulation results of temporal response patterns of GC0, GC1, GC2, GC3 and GC4 compared to RI and ACT.

CHAPTER VII

CONCLUSIONS AND FUTURE RESEARCH

We said in the introduction that we start out with a *connectionist* paradigm and try to model temporal responses of individual neurons in the frog retina as well as to provide/predict the resulting spatio-temporal pattern of activities for the whole population of simulated neurons. In so doing, we learned how the current *neural network modelling* approach with *discrete space* and *time* representation applies to the study of frog retina and to nervous systems in general. In the first section of this chapter, we compare the initial hopes with the simulation results, and discuss the possible contributions of the approach. Then in the second section, we suggest fruitful ways in which the current modelling approach may be further extended in the future.

Conclusions

In the introduction, we mentioned that the rigorous nature of the computational model may provide us with a consistent and comprehensive framework. By now, we can say that at least we have a consistent testbed for different hypotheses about the frog/vertebrate retina. This has been well learned from the particular modelling/simulation cycles we went through for the horizontal cell layer where one change causes a chain of (unexpected) changes to be explained or accounted for. In general, the consistent nature of the computational model arises from the fact that its interrelated parts are affected automatically when

stimulated, without requiring conscious efforts by the modeller. The model provides a comprehensive framework since it begins to explain various phenomena occurring in different parts of the vertebrate retina observed in different experiments. Of course, these claims should not be interpreted as meaning the current modelling/simulation approach be substituted for any of the experiments or for any of the existing modelling methodology. Rather it should be interpreted as one more tool, but one that emphasizes/facilitates the consistent *synthesis* of the various results we get from anatomical, physiological and conceptual methods so that it aids the neuroscience community's understanding of the causal relationship between the nature of *intelligence* and the underlying *neural mechanisms.*

To achieve the above stated goal, we have to bridge a gap between the more traditional neuronal modelling where the main interest lies in understanding the behaviour/response of the single cell or the biophysics of the part thereof and the population modelling where the main interest lies in understanding the overall behavior of the population. The former approach does not provide any organizing theory of how connections, which are so abundant in the neural systems, computes [1] ; and the latter tends to overlook the importance of individual details within the regularity of a given population. But nervous systems are not unique structures with no repetition in design, nor are they uniform enough for us to ignore the individual variations with a few generalizations. There are many varieties of neurons and synaptic junction types and transmitters. As examplified by a vertebrate retina system, nervous systems can be generalized as a hierarchical structure where substructures of regular elements such as layers in the retina or clolumns in visual cortex subserve the function of the overall structure.

Our current modelling approach provides a way of displaying *spatio-temporal patterns of neural activities.* This lets us better study the local interactions which,

[1] As can be seen, there are connections of a type that can differentiate with respect to time or that can work as DOG operators; and connections that act as symmetrical i/o junctions besides the more traditional one-way gate type.

as mentioned in the introduction, play a crucial role in the central nervous system, bridging between individual neuronal representations and group/layer representations. Our ability to generate spatio-temporal patterns of activity furthermore encourages the testing of various neural phenomena of cooperation and competition that occur within and/or between substructures of any modelled systems, particularly those of the vertebrate retina. The model supports the general claim that there is a fundamental relationship between the structure and function of the vertebrate retina by representing the various *synaptic types* and spatial patterns of the *connections*, and by providing, at least in some cases, qualitatively correct results through computer simulations of the Model.

The current modelling approach is designed to model individual neurons in a population and then display any of them at any time. It does not require too sweeping assumptions for all neurons in the system, and allows to specify different cell types in a population. However, it fails to allow some details of single cell modelling, and does not allow the general analytical conclusions which are often achieved by population modelling approaches. The issue becomes a classical problem of the level of representations for modelling (a neural system). If the local interactions performed by the many connections and synapses are as important as the inner functions performed by an individual cells, then it can be argued favorably that the current approach of modelling neural network will contribute to the general neuroscience community by providing an approach of studying a neural system where both of these central concerns have to be compromised/ negotiated into a single consistent modelling framework and computer simulation environment.

We thought we could provide an organizing theory of how to make connections between individual neurons to produce *perceptual primitives* at least in the frog retina. The example of developing cycles of horizontal cell modelling and simulations show how the current modelling efforts can be used to formulate better theory. But our initial hope has to be tempered by the realization that we are still

far from achieving what we set out for, i.e., correlating the perceptual/cognitive primitives such as *bug detector* with the underlying neural machine, in part because of our insufficient knowledges about the subject such as various pathways in the IPL and in part because of the lack of better tools such as fast computers results in a rather long cycle of modelling and simulation for bigger simulations. The first problem of insufficient knowledge can be practically overcome if there are better interactions between experimentalists and the modellers. Here it seems inevitable that the modeller has to have at least a basic experimental trainning since it is his job to understand the wide varieties of experimental data and synthesize them into a consistent framework. The second problem is already attacked in that we are already beginning to use supercomputers to expedite the modelling and simulations cycles [Teeters and Lee, 1985; Teeters, Lee and Arbib, 1986]

The *connectionist* idea of simple elements doing information processing mainly in terms of their connections relates well with the current modelling approach and its assumed view on the nature of information processing in the vertebrate retina. The model and the accompanying simulations show that we can use the *connectionist* paradigm to model the behavior of neural network, and show an example of how different connection structures together with typified individual neurons might be working toward a common goal.

Also, it shows that where local interaction dominates as in the OPL or IPL, connectionist-like approach of neuromodelling can be quite successful in modelling the interactions or at least can provide useful insights through the modelling and simulation cycles.

Additionally, the current thesis offers connectionists an example where a challenging real world neural network problem is solved by essentially a connectionistic approach to modelling nervous systems, and is suggestive of the importance of varieties of basic connection types besides the traditional weighted/signed/one-way ones. The message is that the brain does not compute with only weighted/signed/one-way connections, but rather it combines several basic types

of connections to its advantage. A group of *connectionist* thinkers recently added non-traditional connection types such as *symmetrical* connections which represents the sort of computations performed by the gap-junctions of the horizontal cells in the vertebrate retina within the current connectionist framework [Tank, 1986; Koch, et al., 1986].

We have studied the kind of biological information processing performed in the vertebrate retina, using discrete space and time representation, and using both descriptive functions at an individual cell level, and connectivity characteristics at the local interaction level within individual layers and betwen layers in the network.

The current modelling approach with the accompanying simulation provides us with the power of replicating individual cell temporal responses and the power of predicting the spatial pattern of activities for the whole population of neurons. This provision of spatio-temporal pattern of activities will undoubtedly help in devising future experiments to test the basic ideas and also in verifying different conceptual models, and will aid in the progress of neuroscience in general by providing one more approach which is consistent and comprehensive, in the sense that it can serve as a basis to bulid upon.

Future Research

The current model of frog retina represents a very small part of a real frog retina, both in terms of its functional capability and its structural complexity. There are numerous limitations to the model. We think that the best way to extend the model is to provide the Model with the following structural or functional capabilities.

1. We want a detailed model of photoreceptor adaptation [Baylor, Hodgkin and Lamb, 1975; Carpenter and Grossberg, 1982], to account for the general ex-

perimental set-ups and different prepararations. A photoreceptor level adaptation model that includes adaptational effects due to pupil mechhanism [Grüsser and Grüsser-Cornehls, 1976], screening pigments movement [Fein and Szuts, 1982; Liebman et al., 1969], and photoreceptor cell movements and size changes [Daw and Pearlman, 1974; Ali, 1975].

2. Werblin [1976] and his colleages contend that the major information flow between photoreceptors and the bipolar cells are through synaptic junctions between them, modified through feedback pathways from the photoreceptors and the horizontal cells. They claim that the feedback pathways enhance bipolar cell sensitivity. Naka and his colleagues [Sakuranaga and Naka, 1984 a,b,c] also argue for feedback circuitry in the OPL, based on their white noise analysis utilizing the Wiener kernel. We would thus like to model the feedback circuitry in the OPL.

3. Modify the current model of transient amacrine cells following Miller's [1979] conceptual model, where once fired the cell potential retrogressively propagates up its dendrites.

4. Add ganglion cell impulse generations for a more realistic study of ganglion cell response characteristics.

5. Modelling different connections in the IPL to account for the various GC response characteristics, and at the same time suggest to the experimentalists which structural pathways to look for.

6. Incorporate feedback between the two plexiform layers to account for the control of sensitivities such as suggested to exist within the OPL by Werblin [1976], where interplexiform cells might play such a role.

APPENDIX

SOFTWARE FOR THE MODELLING AND SIMULATION

There are two major types of software that have been developed: One for the setting up the model and the other for the simulation. We will discuss these in separate sections, but they are used together to form a complete modelling/simulation cycle. All of this software was developed under the VAX[2]/780 VMS environment of the Research Computing Facility within the Department of Computer and Information Science at the University of Massachussetts, which supports various graphics devices including a GRINNEL color graphics display device and a SYMBOLICS laser graphics printer. The majority of the software including all model-related software was written in VAX PASCAL, while a part of the graphics routines was written in VAX FORTRAN.

Setting up the Model

The software for the Model consists of 8 modules: MRET.pas, MSP.pas, MRI.pas, MSC.pas, MHC.pas, MBC.pas, MAC.pas and MGC.pas. The main module *MRET.pas* provides the necessary data structures to represent all the major cell type data and the corresponding layers. It also provides to other modules basic system routines such as ***spatial kernel initialization***, ***simulation initialization***, ***output data compaction***, ***simulation diagnostics*** and various supporting functions.

[2]VAX and VMS are trademarks of Digital Equipment Corporation.

The other seven modules inherit the *MRET.pas* data structures and subroutines, and provide ***initialization*** and ***updating*** of the corresponding cell types and their layers. Implementing the whole model into these logical modules helps to keep the relavant details in small codes where they logically belong, and to save substantial amount of compilation time by allowing us to separately compile only those codes where we made changes.

Making the executable model code requires three steps: (1) *Modify* source code to include the desired changes in the submodel by making changes in the corresponding module(s) using an editor, (2) *compile* the changed source code file(s), and then (3) *link* compiled object code files to get *MRET.exe*.

Simulation Phase

Once we have a desired model in the form of an executable *MRET.exe*, we can proceed to the simulation phase as shown in the Figure 42 in the following three steps: (1) *Specify* simulation setups and stimulus in the input file *IRET.DAT*[3], (2) ***run*** the simulation program *MRET.exe* with the prepared input file, (3) ***display*** the simulation output data file *DRET.DAT* with the graphics driver program *GRAPHIT.exe*, and (4) ***analyse*** the output data/graphs.

Graphics Display Drivers

Initially, a simulation graphics driver to use the GRINNELL color graphics display device was developed to view the simulation output data both in the form of 2-D intensity maps and for any combination of individual cell location and layer. But, later the device independent graphics driver called *GRAPHIT*

[3]The more usual approach has been to create a set of input data files representing various simulation set ups with different names, and just *logicaly assign* one of these file as *IRET.dat*.

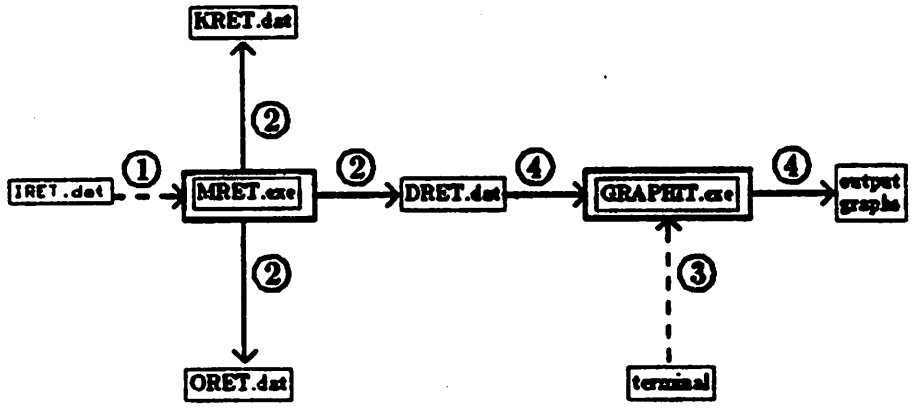

Figure 42: Simulation phase diagram

was developed by J. Teeters utilizing the locally developed GUS package for the simulation.

BIBLIOGRAPHY

Arbib, M. A. (1982) Rana computatrix: An evolving model of visuomotor coordination in frog and toad. *Machine Intelligence*, 10: 501-517.

Baylor, D. A., Fuortes, M. G. F. (1970) Electrical responses of single cones in the retina of the turtle. *J. Physiol.*, 207: 77-92.

Baylor, D. A., Fuortes, M. G. F., O'Brian, P. M. (1971) Receptive fields of cones in the retina of the turtle. *J. Physiol.*, 214: 265-294.

Baylor, D. A., Hodgkin, A. L. (1974) Changes in time scale and sensitivity in turtle photoreceptors. *J. Physiol.*, 242: 729-758.

Baylor, D. A., Hodgkin, A. L., Lamb, T. D. (1974a) The electrical response of turtle cones to flashes and steps of light. *J. Physiol.*, 242: 685-727.

Baylor, D. A., Hodgkin, A. L., Lamb, T. D. (1974b) Reconstruction of the electrical responses of turtle cones to flashes and steps of light. *J. Physiol.*, 42: 759-791.

Bäckström, A., Reuter, T. (1975) Receptive field organization of ganglion cells in the frog retina: Contributions from Cones, green rods and red rods. *J. Physiol.*, 246: 79-107.

Boycott, B. B., Dowling, J. E. (1969) Organization of the primate retina : Light microscopy. *Philos. Trans. R. Soc. Lond.* B 255: 109-184.

Butenandt, E. (1975) A theoretical model for movement-specific neurons of the frog's retina. IBM Research RJ1598, IBM Research Laboratory, San Jose, California.

Butenandt, E., Grüsser, O.-J. (1968) The effect of stimulus area on the response of movement detecting neurons in the frog's retina. *Pflügers Archiv.*, 298: 283-293.

Cajal, R. (1893) The vertebrate retina (English translation of Cajal's *La retine des vertebres*, which was published in *La Cellule* in 1893, translated by D. Maguire and R. W. Rodieck, and included in the appendix of Rodieck's 'The vertebrate retina', 1973).

Carey, R. G. (1975) A quantitative analysis of the distribution of the retinal elements in frogs and toads withh special emphasis on the *Areae retinalis.* M.S. Thesis, University of Massachusetts, Amherst, Massachusetts.

Carpenter, G. A., Grossberg, S. (1981) Adaptation and transmitter gating in vertebrate photoreceptors. *J. Theoret. Neurobiol.*, 11: 1-42.

Cervantes, F. (1985) Modelling and analysis of neural networks in the visuomotor system of anuran amphibian. Ph. D. Dissertation, University of Massachusetts, Amherst, Massachusetts.

Cervetto, L. (1976) Interactions between cones and second-order neurons in the turtle retina. In F. Zettler and R. Weiler eds., *Neural Priniciples in Vision.* New York: Springer-Verlag, pp. 131-142.

Chan, R. Y., Naka, K.-I. (1976) The amacrine cell. *Vision Res.*, 16: 1119-1129.

Donner, K. O., Reuter, T. (1976) Visual pigments and photoreceptor function. In R. Llinas and W. Precht eds., *Frog Neurobiology.* New York: Springer, pp. 251-277.

Dowling, J. E. (1968) Synaptic organization of the frog retina: An electron microscopic analysis comparing the retinas of frogs and primates. *Proc. R. Soc. Lond.* B 170: 205-227.

Dowling, J. E. (1970) Organization of vertebrate retinas. *Invest. Ophthal.*, 19: 655-680.

Dowling, J. E. (1976) Physiology and morphology of the retina. In R. Llinas and W. Precht eds., *Frog Neurobiology.* New York: Springer-Verlag, pp. 278-296.

Dowling, J. E. (1979) Information processing by local circuits: The vertebrate retina as a model system. In F. O. Schmitt and F. G. Worden eds., *The Neurosciences: Fourth Study Program.* Cambridge, Massachusetts: M.I.T. Press, pp. 163-181.

Dowling, J. E., Boycott, B. B. (1966) Organization of the primate retina: electron microscopy. *Proc. R. Soc. Lond.* B 166:80-111.

Dowling, J. E., Werblin, F. S. (1969) Organization of the retina of the mudpuppy, *Necturus maculosus*: I. Synaptic Structure. *J. Neurophy.*, 32: 315-338.

Dubin, M. W. (1970) The inner plexiform layer of the vertebrate retina: A quantitative and comparative electron microscopic analysis. *J. Comp. Neur.*, 140: 479-506.

Duda, R., and Hart, P. (1973) *Pattern Classification and Scene Analysis.* New York: John Wiley and Sons, Inc.

Du Pont, J. S., de Groot, P. J. (1976a) A schematic dioptric apparatus for the frog's eye, *Rana esculenta. Vision Res.*, 16: 803-810.

Du Pont, J. S., de Groot, P. J. (1976b) The quality of the optic system of the frog's eye *Rana esculenta. Vision Res.*, 16: 1179-1181.

Ewert, J.-P. (1976) The visual system of the toad: Behavioral and physiological studies on a pattern recognition system. In K. Fite ed., *The Amphibian Visual System.* New York: Academic Press, pp. 142-202.

Ewert, J.-P. (1980) *Neuroethology.* Berlin: Springer-Verlag, pp. 69-76.

Fain, G. L. (1975) Interactions of rod and cone signals in the mudpuppy retina. *J. Physiol.*, 252: 735-769.

Fain, G. L., Gold, G. H., Dowling, J. E. (1976) Receptor coupling in the toad retina. *Cold Spring Harbor Symp. Quant. Biol.*, 40: 547-561.

Famiglietti, E. V. Jr., Kaneko, A., Tachibana, M. (1977) Neuronal architecture of on and off pathways to ganglion cells in carp retina. *Science*, 23: 1267-1269.

Fein, Szuts (1982) *Photoreceptors: Their Role in Vision.* Cambridge, Massachusetts: Cambridge University Press.

Finkelstein, D., Grüsser, O.-J. (1965) Frog retina: Detection of movement. *Science*, 150: 1050-1051.

Fite, K. V. (1973) The visual fields of the frog and toad: A comparative study. *Behavioral Biology*, 9: 707-718.

Gaze, R. M. (1958) The representation of the retina on the optic lobe of the frog. *Q. J. Exp. Physiol.*, 43: 209.

Gaze, R. M., Jacobson, M. (1963) Convexity detectors in the frog's visual system. From the Proceedings of the Physiological Society, Edinburgh Meeting, July 12-13, 1963.

Gordon, J., Graham, N. (1973) Early light and dark adaptation in frog on-off retinal ganglion cells. *Vision Res.*, 13: 647-659.

Grüsser, O.-J. (1979) Cat ganglion-cell receptive fields and the role of horizontal cells in their generation. In F. O. Schmitt and F. G. Worden eds., *The Neurosciences: Fourth Study Program.* Cambridge, Massachusetts: M.I.T. Press.

Grüsser, O.-J., Grüsser-Cornehls, U. (1976) Neurophysiology of the anuran visual system. In R. Llinas and W. Precht eds., *Frog Neurobiology.* New York: Springer-Verlag, pp. 297-385.

Grüsser-Cornehls, U., Saunders, R. McD. (1975) The spectral properties of class 1, 2, 3, and 4 neurons of the frog's optic tectum. *Europ. J. Physiol.*, 359(Suppl. R): 101.

Grüsser-Cornehls, U., Saunders, R. McD. (1981a) Chromatic subclasses of frog retinal ganglion cells: studies using black stimuli moving on a monochromatic background. *Vision Res.*, 21: 469-478.

Grüsser-Cornehls, U., Saunders, R. McD. (1981b) Response of frog retina ganglion cells to moving monochromatic spots under photopic conditions. *Vision Res.*, 21: 1617-1620.

Hartine, H. K. (1938) The response of single optic nerve fibers of the vertebrate eye to illumination of the retina. *Amer. J. Physiol.*, 121: 400-415.

an der Heiden, U. (1980) *Analysis of Neural Networks.* New York: Springer-Verlag.

an der Heiden, U., Roth, G. (1983) A mathematical network model for retino-tectal prey recognition in amphibians. In *Proceedings of the Second Workshop on Visuomotor Coordination in Frog and Toad: Models and Experiments*, Technical Report 83-19, Computer and Information Science Dept., University of Massachusetts, Amherst, Massachusetts.

Holden, A. V. (1976) *Models of the Stochastic Activity of Neurones.* New York: Springer-Verlag.

Hood, D. C., Grover, B. G. (1974) Temporal summation of light by a vertebrate visual receptor. *Science*, 184: 1003-1005.

House, D. H. (1984) Neural models of depth perception in frogs and toads. Technical Report 84-16, Computer and Information Science Dept., University of Massachusetts, Amherst, Massachusetts.

Kandel, E. R., Schwartz, J. H. (1981) *Principles of Neural Science.* Amsterdam: Elsevier/North-Holland.

Keating, M. J., Gaze, R. M. (1970) Observations on the 'surround' properties of the receptive fields of frog retinal ganglion cells. *Q. J. Exp. Physiol.*, 55: 129-142.

Koch, C., Poggio, T., Torre, V. (1982) Retinal ganglion cells: a functional interpretation of dendritic morphology. *Phil. Trans. R. Soc. Lond.* B 298: 227-264.

Kolb, H. (1979) The inner plexiform layer in the retina of the cat: electron microscopic observations. *J. Neurocytol.*, 8: 295-329.

Krüger, H., Moser, E. A. (1972) The influence of the modulation transfer function of the dioptric apparatus on the acuity and contrast of the retinal image in *rana esculenta. Vision Res.*, 12: 1281-1289.

Krüger, H., Moser, E. A. (1973) On the approximation of the optical modulation transfer function (MTF) by analytical fuctions. *Vision Res.*, 13: 493-494.

Lara, R., Carmona, M., Daza, F., Cruz, A. (1983) A global model of the neural mechanisms responsible for visuomotor coordination in toads. In *Proceedings of the Second Workshop on Visuomotor Coordination in Frog and Toad: Models and Experiments*, Technical Report 83-19, Computer and Information Science Dept., University of Massachusetts, Amherst, Massachusetts.

Lasansky, A. (1978) Contacts between receptors and electrophysiologically identified neurones in the retina of the larval tiger salamander. *J. Physiol.*, 285: 531-542.

Lettvin, J. Y., Maturana, H. R., McCulloch, W. S., Pitts, W. H. (1959) What the frog's eye tells the frog's brain. *Proc. Instn. Elect. Engrs.*, 47: 1940-1951.

Lettvin, J. Y., Maturana, H. R., Pitts, W. H., McCulloch, W. S. (1961) Two remarks on the visual system of the frog. In W. A. Rosenblith ed., *Sensory Communication*. Cambridge, Massachusetts: M.I.T. Press, pp. 757-776.

Liebman, P. A., Carroll, S., Laties, A. (1969) Spectral sensitivity of retinal screening pigment migration in the frog. *Vision Res.*, 9: 377-384.

Matsumoto, N., Naka, K.-I. (1972) Identification of intracellular responses in the frog retina. *Brain Research*, 42: 59-71.

Maturana, H. R., Lettvin, J. Y., McCulloch, W. S., Pitts, W. H. (1960) Anatomy and physiology of vision in the frog *Rana Pipiens*. *Jour. Gen. Physiol.*, 43, Suppl 2: 129-175.

McCulloch, W. S., Pitts, W. H. (1943) A logical calculus of ideas immanent in nervous activity. *Bulletin of Mathematical Biophysics*, 5: 115-133.

Miller, R. F. (1979) The neuronal basis of ganglion-cell receptive-field organization and the physiology of amacrine cells. In F. O. Schmitt and F. G. Worden eds., *The Neurosciences: Fourth Study Program*. Cambridge, Massachusetts: M.I.T. Press, pp. 227-245.

Moreno-Diaz, R. (1965) An analytical model of the group 2 ganglion cell in the frog's retina. Instrumentation Laboratory (E-1858), M.I.T., Cambridge, Massachusetts.

Moreno-Diaz, R. (1977) Models of retinal processes. *Brain Theory Newsletter*, 3: 7-10.

Moreno-Diaz, R., Royo, F. R., Rubio, E. (1980) A theoretical proposal to account for visual computation in a frog's retina. *Int. J. Bio-Medical Computing*, 11: 415-426.

Moreno-Diaz, R., Rubio, E. (1979) A theoretical model for layered visual processing. *Int. J. Bio-Medical Computing*, 10: 231-243.

Moreno-Diaz, R., Rubio, E., Nunez, A. (1980) A Layered model for visual processing in avian retina. *Biol. Cybernetics*, 38: 85-89.

Morrison, J. D. (1975) The responses of the retinal ganglion cells of the frog. *Vision Res.*, 15: 1339-1344.

Naka, K.-I. (1972) The horizontal cells. *Vision Res.*, 12: 573-588.

Naka, K.-I, Rushton, W. A. H. (1966) S-potentials from luminosity units in the retina of fish *Cyprindiae*. *J. Physio.*, 185: 587-599.

Nelson, R., Kolb, H., Robinson, M. M., Mariani, A. P. (1981) Neural circuitry of the cat retina: Cone pathways to ganglion cells. *Vision Res.*, 21: 1527-1536.

Nye, P. W., Naka, K.-I. (1971) The dynamics of inhibitory interaction in a frog receptive field: A paradigm of paracontrast. *Vision Res.*, 11: 377-392.

Pask, C., Barrell, K. F. (1980) Photoreceptor optics I: Introduction to formalism and excitation in a lens-photoreceptor system. *Biol. Cybernetics*, 36: 1-8.

Pickering, S. G. (1968) The extremely long latency response from on-off retinal ganglion cells: Relationship to dark adaptation. *Vision Res.*, 8: 383-387.

Pomeranz, B. (1972) Metamorphosis of frog vision: Changes in ganglion cell physiology and anatomy. *Exp. Neurol.*, 34: 187-199.

Rall, W., Shepherd, G. M. (1968) Theoretical reconstruction of field potentials and dendrodendritic synaptic interactions in olfactory bulb. *J. Neurophysiol.*, 31: 884-915.

Ratliff, F., Hartline, H. K. (1959) The responses of Limulus optic nerve fibres to pattern of illumination on the receptor mosaic. *J. Gen. Physiol.*, 42: 1241-1255.

Richards, W. (1979) Why rods and cones? *Biol. Cybernetics*, 33: 125-135.

Richter, J., Ullman, S. (1982) A model for the temporal organization of X- and Y-type receptive fields in the primate retina. *Biol. Cybern.*, 143: 127-145.

Rodieck, R. W. (1965) Quantitative analysis of cat retinal ganglion cell response to visual stimuli. *Vision Res.*, 5: 583-601.

Rodieck, R. W. (1973) *The Vertebrate Retina.* San Francisco, California: W. H. Freeman and Co.

Sakai, H., Naka, K.-I. (1983) Synaptic organization involving receptor, horizontal and on- and off-center bipolar cells in the catfish retina. *Vision Res.*, 23: 339-351.

Sakuranaga, M., Naka, K.-I. (1985a) Signal transmission in the catfish retina: II. Transmission to type-N cell. *J. Neurophysiol.*, 53(2): 390-410.

Sakuranaga, M., Naka, K.-I. (1985b) Signal transmission in the catfish retina: III. Transmission to type-C cell. *J. Neurophysiol.*, 53(2): 411-428.

Scalia, F., Arango, V. (1983) Ganglion cell morphology observed by retrograde HRP-filling in flat mounted retina. *Abstract of the Society for Neuroscience*, Part 2: 803.

Schürg-Pfeiffer, E., Ewert, J.-P. (1981) Inverstigation of neurons involved in the analysis of Gestalt prey features in the frog, *Rana temporaria*. *J. Comp. Physiol.*, 141: 139-152.

Shantz, M. (1976) Description and classification of neuronal structure in the frog retina. Ph. D. Dissertation, California Institute of Technology, Pasadena, California.

Shepherd, G. M. (1978) Microcircuits in the nervous-system. *Scientific American* 238(2): 92-103.

Shepherd, G. M. (1979) *The Synaptic Organization of the Brain* (2nd Ed.) Oxford: Oxford University Press.

Siminoff, R. (1981) A cybernetic model of the vertebrate cone retina. *Vision Res.*, 21: 1537-1539.

Siminoff, R. (1983) An analogue model of the luminosity-channel in the vertebrate retina. *Biol. Cybernetics*, 46: 101-110.

Siminoff, R. (1986) Personal communications.

Stell, W. K., Ishida, A. T., Lightfoot, D. O. (1977) Structural basis for on- and off-center responses in retinal bipolar cells. *Science*, 198: 1269-1271

Svaetichin, G., MacNicholl, E. F. (1958) Retinal mechanisms for chromatic and achromatic vision. *Ann. N.Y. Acad. Sci.*, 74:385-404.

Teeters, J., Lee, Y., Arbib, M. A. (1986) Supercomputer simulation of of frog retina. Unpublished manuscript, University of Massachusetts, Amherst, Massachusetts.

Tomita, T. (1970) Electrical activity of vertebrate photoreceptors. *Q. Rev. of Biophysics*, 3(2): 179-222.

Toyoda, J., Nosaki, H., Tomita, T. (1969) Light-induced resistance changes in single photoreceptors of *Necturus* and *Gekko*. *Vision Res.*, 9: 453-463.

Usui, S., Mitarai, G., Sakakibara, M. (1983) Discrete nonlinear reduction model for horizontal cell response in the carp retina. *Vision Res.*, 23: 413-420.

Walls, G. L. (1942) *The Vertebrate Eye and Its Adaptive Radiation.* Michigan: Cranbrook Press.

Werblin, F. S. (1972) Lateral interactions at the inner plexiform layer of vertebrate retina: Antagonistic responses to change. *Science*, 175: 1008-1010.

Werblin, F. S., Dowling, J. E. (1969) Organization of the retina of the mudpuppy, *Necturus maculosus*: II. Intracellular recording. *J. Neurophysiol.*, 32: 339-355.

Wilson, M., Attwell, D., Wu, S. M. (1983) Measurement of electrical coupling between receptors of the salamander retina. *Abstract of the Society for Neuroscience*, 9: 685.

Yellott, J. I., Wandell, B. A., Cornsweet, T. N. (1984) The beginning of visual perception: The retinal image and its initial encoding. In I. Darian-Smith ed., *Sensory processes*, Baltimore, Maryland: American Physiological Society.